RECONFIGURABLE MIMO ANTENNA ARRAY BASED METAMATERIALS FOR 5G AND OTHER MODERN WIRELESS COMMUNICATION NETWORKS

2024
PhD THESIS
COMPUTER ENGINEERING

Humam Neamah Hussein HUSSEIN

Thesis Advisors
Assist. Prof. Dr. Ferhat ATASOY
Prof. Dr. Taha A. ELWI

RECONFIGURABLE MIMO ANTENNA ARRAY BASED METAMATERIALS FOR 5G AND OTHER MODERN WIRELESS COMMUNICATION NETWORKS

Humam Neamah Hussein HUSSEIN

T.C.
Karabuk University
Institute of Graduate Programs
Department of Computer Engineering
Prepared as
PhD Thesis

Thesis Advisors
Assist. Prof. Dr. Ferhat ATASOY
Prof. Dr. Taha A. ELWI

KARABUK
July 2024

I certify that in my opinion the thesis submitted by Humam Neamah Hussein HUSSEIN titled "RECONFIGURABLE MIMO ANTENNA ARRAY BASED METAMATERIALS FOR 5G AND OTHER MODERN WIRELESS COMMUNICATION NETWORKS" is fully adequate in scope and in quality as a thesis for the degree of PhD.

Assist. Prof. Dr. Ferhat ATASOY ....
Thesis Advisor, Department of Computer Engineering

Prof. Dr. Taha A. ELWI ....
Thesis Co-Advisor, Iraqi Ministry of Higher Education and Scientific Research/Office of the Deputy Minister for Scientific Research Affairs

This thesis is accepted by the examining committee with a unanimous vote in the Department of Computer Engineering as a PhD thesis. July 22, 2024

Examining Committee Members (Institutions)   Signature
Chairman   : Prof. Dr. Baha ŞEN (YBU)   ....

Member   : Assoc. Prof. Dr. Caner ÖZCAN (KBU)   ....

Member   : Assoc. Prof. Dr. Turgut ÖZTÜRK (KBU) ....

Member   : Assist. Prof. Dr. Ferhat ATASOY (KBU) ....

Member   : Assist. Prof. Dr. Cihat ŞEKER (IBU)   ....

The degree of PhD by the thesis submitted is approved by the Administrative Board of the Institute of Graduate Programs, Karabuk University.

Assoc. Prof. Dr. Zeynep ÖZCAN ....
Director of the Institute of Graduate Programs

"I declare that all the information within this thesis has been gathered and presented in accordance with academic regulations and ethical principles and I have according to the requirements of these regulations and principles cited all those which do not originate in this work as well."

Humam Neamah Hussein HUSSEIN

ABSTRACT

Ph.D. Thesis

RECONFIGURABLE MIMO ANTENNA ARRAY BASED METAMATERIALS FOR 5G AND OTHER MODERN WIRELESS COMMUNICATION NETWORKS

Humam Neamah Hussein HUSSEIN

Karabük University
Institute of Graduate Programs
Department of Computer Engineering

Thesis Advisors:
Assist. Prof. Dr. Ferhat ATASOY
Prof. Dr. Taha A. ELWI
July 2024, 102 pages

Multi-input multi-output (MIMO) is a pivotal wireless technique extensively employed in contemporary communication networks due to its ability to enhance spectral efficiency, increase data throughput, and improve system reliability. By utilizing multiple antennas at both the transmitter and receiver ends, MIMO systems exploit spatial diversity and multiplexing, allowing for the simultaneous transmission of multiple data streams within the same frequency band. This not only improves coverage and extends the range of wireless networks but also mitigates the effects of fading and interference, resulting in higher data rates and improved signal quality. MIMO technology is integral to various wireless standards such as LTE, Wi-Fi, and 5G, playing a crucial role in meeting the ever-growing demands for faster, more

reliable wireless communication. In this work, four designs have been introduced in this thesis. The initial design was a printed monopole antenna array that is suggested for MIMO applications over 5G subs-6GHz bands. It has a good gain and an outstanding matching impedance bandwidth, $|S_{11}|$ <-10, at 3.45GHz and 5.8GHz. The antenna element is installed on a 1.5mm FR4 Epoxy substrate in the shape of historical Iraqi locations. With a 50Ω SMA port, the maximum antenna dimensions are 33.6×20mm^2. With a $|S_{11}|$ of -20dB and -31dB, respectively, the suggested antenna design achieves an impedance bandwidth of approximately 130MHz and 380MHz at 3.45GHz and 5.8GHz. At 3.45GHz and 5.8GHz, the antenna gain is determined to be 1.5dBi and 3.6dBi, respectively. It is discovered that the intended designed antenna array coupling is inside the relevant frequency spectrum by roughly -15dB. The second design, an origami antenna, a relatively new technique designed to address many related problems such as visual pollution and antenna embedding inside structures. At 2.45GHz, the suggested antenna array is made up of two 2D array components with a separation distance of λ/10. Through the use of CST Microwave Studio, we conducted multiple parametric simulations until we arrived at the best possible performance for the suggested design. Three frequency bands with matching $|S_{11}|$ ≤-6dB, 1.7GHz-2.7GHz, 3.1GHz-3.8GHz, and 4.5GHz-5.1GHz are observed in the proposed antenna array, with gains of 5.2dBi, 6.8dBi, and 8.1dBi, respectively. The third concept was for multiple inputs multiple outputs (MIMO) application systems operating at Sub-6GHz frequency ranges, is a highly downsized two-element microstrip antenna array. When activated through the monopole basic antenna, the antenna is structured from a meander line in conjugate with an interdigital capacitor. When printed on FR-4 substrate, the suggested antenna elements are separated using a Minkowski factor-shaped metamaterial (MTM) column to obtain a separation distance (D) of 0.08λ at 3GHz. Later, optical switches based on light-dependent resistance (LDR) terminals are used to adjust the antenna performance in terms of gain and bandwidth. As a result, biasing circuits are not necessary when using such a strategy to reduce reconfiguration complexity. The computation of Channel Capacity (CC) and Bit Error Rate (BER) was done with the assumption that the antenna should be set up as an array of 64 by 64 elements. Improving 5G communication networks' energy efficiency is the main goal of the fourth design. The technique seeks to minimize energy usage and operating expenses

by incorporating solar panels and reducing dependency on traditional grid power sources. On the other hand, combining solar panels and antennas may seriously impair the performance of the antennas. As a result, it was recommended that the planned work include MIMO antenna design. Regarding $|S_{11}|$, it is obtained three bands at 2.5 GHz, 3.6 GHz, and 5.5 GHz, where S_{12}, S_{13}, and S_{14} were below -20 dB throughout all bands of interest.

Keywords: Sub-6GHz, 5G, MIMO, Reconfigurable, MTM, Solar panel, BER, CC, Wireless communication, Antenna.

Science Code : 92407

ÖZET

Doktora Tezi

5G VE DİĞER MODERN KABLOSUZ İLETİŞİM AĞLARI İÇİN YENİDEN YAPILANDIRILABİLİR MIMO ANTEN DİZİSİ TABANLI METAMATERYALLER

Humam Neamah Hussein HUSSEIN

Karabük Üniversitesi
Lisansüstü Eğitim Enstitüsü
Bilgisayar Mühendisliği Anabilim Dalı

Tez Danışmanları:
Doç. Dr. Ferhat ATASOY
Prof. Dr. Taha A. ELWI
Temmuz 2024, 102 sayfa

Çok girişli çok çıkışlı (MIMO), spektral verimliliği artırma, veri verimini artırma ve sistem güvenilirliğini artırma yeteneği nedeniyle çağdaş iletişim ağlarında yaygın olarak kullanılan önemli bir kablosuz tekniktir. MIMO sistemleri, hem verici hem de alıcı uçlarında birden fazla anten kullanarak, uzamsal çeşitlilik ve çoğullamadan yararlanarak aynı frekans bandında birden fazla veri akışının eşzamanlı iletilmesine olanak tanır. Bu yalnızca kapsama alanını iyileştirmekle ve kablosuz ağların menzilini genişletmekle kalmaz, aynı zamanda solma ve parazitin etkilerini de azaltarak daha yüksek veri hızları ve gelişmiş sinyal kalitesi sağlar. MIMO teknolojisi LTE, Wi-Fi ve 5G gibi çeşitli kablosuz standartların ayrılmaz bir parçasıdır ve daha hızlı, daha güvenilir kablosuz iletişim için sürekli artan talebin

karşılanmasında önemli bir rol oynar. Bu çalışmada, bu tezde dört tasarım tanıtılmıştır. İlk tasarım, 5G alt 6GHz bantları üzerindeki MIMO uygulamaları için önerilen baskılı tek kutuplu anten dizisiydi. İyi bir kazanıma ve olağanüstü bir eşleşen empedans bant genişliğine sahiptir, $|S_{11}|$ <-10, 3,45 GHz ve 5,8 GHz'de. Anten elemanı, tarihi Irak konumları şeklinde 1,5 mm FR4 Epoksi alt tabaka üzerine monte edilmiştir. 50Ω SMA bağlantı noktasıyla maksimum anten boyutları $33,6{\times}20mm^2$ 'dir. $|S_{11}|$ ile Sırasıyla -20dB ve -31dB'lik önerilen anten tasarımı, 3,45GHz ve 5,8GHz'de yaklaşık 130MHz ve 380MHz'lik bir empedans bant genişliğine ulaşır. 3,45GHz ve 5,8GHz'de anten kazancının sırasıyla 1,5dBi ve 3,6dBi olduğu belirlendi. Amaçlanan tasarlanan anten dizisi bağlantısının ilgili frekans spektrumunun kabaca -15dB içinde olduğu keşfedilmiştir. İkinci tasarım, nispeten yeni bir teknik olan origami anteni, görsel kirlilik ve antenlerin yapıların içine yerleştirilmesi gibi birçok ilgili sorunu çözmek için tasarlandı. 2,45 GHz'de önerilen anten dizisi, ayırma mesafesi λ/10 olan iki 2 boyutlu dizi bileşeninden oluşur. CST Microwave Studio'yu kullanarak, önerilen tasarım için mümkün olan en iyi performansa ulaşana kadar çok sayıda parametrik simülasyon gerçekleştirdik. $|S_{11}|$ ile eşleşen üç frekans bandı Önerilen anten dizisinde sırasıyla 5.2dBi, 6.8dBi ve 8.1dBi kazançlarla ≤-6dB, 1.7GHz-2.7GHz, 3.1GHz-3.8GHz ve 4.5GHz-5.1GHz gözlemlenmektedir. Üçüncü konsept, 6GHz'in altındaki frekans aralıklarında çalışan çok girişli çoklu çıkış (MIMO) uygulama sistemlerine yönelikti ve oldukça küçültülmüş iki elemanlı bir mikroşerit anten dizisidir. Tek kutuplu temel anten yoluyla etkinleştirildiğinde anten, dijital bir kapasitörle eşlenik olarak kıvrımlı bir çizgiden yapılandırılmıştır. FR-4 alt katmanına yazdırıldığında önerilen anten elemanları, 3 GHz'de 0,08λ'lik bir ayırma mesafesi (D) elde etmek için Minkowski faktör şekilli meta malzeme (MTM) sütunu kullanılarak ayrılır. Daha sonra anten performansını kazanç ve bant genişliği açısından ayarlamak için ışığa bağımlı direnç (LDR) terminallerine dayalı optik anahtarlar kullanılır. Sonuç olarak, yeniden yapılandırma karmaşıklığını azaltmak için böyle bir strateji kullanıldığında öngerilim devreleri gerekli değildir. Kanal Kapasitesi (CC) ve Bit Hata Oranı (BER) hesaplaması, antenin 64'e 64 elemandan oluşan bir dizi olarak kurulması gerektiği varsayımıyla yapıldı. 5G iletişim ağlarının enerji verimliliğinin artırılması dördüncü tasarımın ana hedefidir. Teknik, güneş panellerini dahil ederek ve geleneksel şebeke güç kaynaklarına bağımlılığı azaltarak enerji kullanımını ve işletme giderlerini en

aza indirmeyi amaçlıyor. Öte yandan güneş panelleri ile antenlerin birleştirilmesi antenlerin performansını ciddi şekilde bozabilir. Sonuç olarak planlanan çalışmanın MIMO anten tasarımını da içermesi önerildi. $|S_{11}|$ ile ilgili olarak 2,5 GHz, 3,6 GHz ve 5,5 GHz'de üç bant elde edildi; burada S_{12}, S_{13} ve S_{14}, tüm ilgili bantlarda -20 dB'nin altındaydı.

Anahtar Kelimeler : 6GHz altı, 5G, MIMO, Yeniden yapılandırılabilir, MTM, Güneş paneli, BER, CC, Kablosuz iletişim, Anten.

Bilim Kodu : 92407

ACKNOWLEDGMENT

First of all, I would like to give thanks to my advisor, Assist. Prof. Dr. Ferhat ATASOY, and my Co-advisor Prof. Dr. Taha A. ELWI for their great interest and assistance in preparation of this thesis.

CONTENTS

LIST OF FIGURES

LIST OF TABLES

SYMBOLS AND ABBREVITIONS INDEX

SYMBOLS

λ : Wavelength

εr : Permittivity

μr : Permeability

dB : Decibel

mm : Millimeter

X_g : Separation-distance

Y_g : Ground-plane length

X_m : Monopole-width

φ_T : Latitude

λ_T : Longitude

h_t : Height of Transmitter

P_t : Transmitted Power

P_r : Received Power

d_i : Separation-distance

γ : Path Loss Exponent

X_σ : Fading Characterized

η : Amplifier Efficiency

γ : Path Loss

ABBREVITIONS

MIMO : Multi-Input Multi-Output

4G : Fourth Generation

5G : Fifth Generation

FR : Flame Retardant

SMA : SubMiniature version A

MTM : Metamaterial

LDR   : Light Dependent Resistance

CC   : Channel Capacity

BER   : Bit Error Rate

D   : Dimensions

GHz   : Gigahertz

Sub-6GHz : Frequency range below 6 GHz in the radio spectrum

OFDM   : Orthogonal Frequency Division Multiplexing

RF   : Radio Frequency

IoT   : Internet of Things

SRR   : Split-Ring Resonator

EBG   : Electromagnetic Band Gap

FSS   : Frequency Selective Surface

TM   : Transverse Magnetic

TE   : Transverse Electric

EM   : Electromagnetic

RH   : Right Hand

LH   : Left Hand

CRLH   : Composite Right/Left-Handed

MICs   : Microwave Integrated Circuits

MMW   : Millimeter Waves

BPFs   : Bandpass Filters

MICs   : Microwave Integrated Circuits

MMW   : Millimeter Waves

CPW   : Coplanar Waveguide

ADS   : Advanced Devices Simulator

RLH   : Resistance of the left hand

RRH   : Resistance of the right hand

GLH   : Conductance of the left hand

GRH   : Conductance of the right hand

CLH   : Capacitance of the left hand

CRH   : Capacitance of the right hand

LLH   : Inductance of the left hand

LRH   : Inductance of the right hand

IDC	:	Interdigital Capacitor
LTE	:	Long Term Evaluation
GSM	:	Global System for Mobile
PMC	:	Perfect Electric Conductors
PMC	:	Perfect Magnetic Conductors
ECC	:	Envelop Correlation Coefficient
DG	:	Diversity Gain
CCL	:	Channel Capacity Loss
TARC	:	Total active reflection coefficient
SNR	:	Signal-to-Noise-Ratio
ECC	:	Envelope Correlation Coefficient
RL	:	Load Resistance
SNR	:	Signal-to-Noise Ratio
AI	:	Artificial Intelligent
QoS	:	Quality of Service
MSE	:	Mean Square Error
NOMA	:	Non-Orthogonal Multiple Access
ERP	:	Effective Receive Power

PART 1

INTRODUCTION

1.1. BACKGROUND

By reason of the urgent need to design a mobile microchip antenna that is suitable for modern system applications, metamaterials (MTM) have been suggested for such deployment [1]. MTM structures have been applied to microchip antenna engineering, mainly, in three different categories: (1D, 2D, and 3D array). The bulk of the attractive MTM research has been in their applications with MIMO systems to minimize the effects of the mutual coupling within the antenna elements.

MIMO system has been considered as a one of the most urgently needed technologies to increment the channel capacity (CC) in an environment of multipath reflection [2]; the MIMO concept is being applied in congested areas [3]. However, the OFDM introduction was theoretical before the invention of system with MIMO antenna [4]. So, after MIMO technologies invention, the OFDM system has been actualized in contemporary mobile communication gadgets like both networks 4th Generation and 5th Generation. Conversely, though the green energy consider as an important require in this century. This is consequent to the problem of power resources into many low-power devices that consume a small amount of energy usage [5]. For that reason, the solar panel and radio frequency (RF) harvesting introduction, for instance, has a major impact on deployment of low-power devices such as phones and new wireless devices.

These days, many countries are implementing 5G due to its enhanced performance including CC which supports various applications including IT care systems, IoT, and AI [6]. So, this development has started as an urgent generation to provide support for those application types using sub-6 GHz and millimeter bands. The connection between the mobile network and the subscriber using sub-6GHz

band. Nevertheless, millimeter waves are used for the connection between 5G-networks parts. This is for the reason that the propagation reality is usually hard to apply between the network and subscriber due to obstacles of the environment. Nonetheless, the use of millimeter waves between the parts of the network is usually applied in a free space environment where there are no effects of obstacles.

Since many systems nowadays utilize 5G technology, various limitations are still affecting the antenna [4]. That is why many researchers are today applying the utilization of antenna reconfiguration [4]. Utilizing smart devices (SD) based on high speed electronics systems (HSES) such as varactor diodes, pin diodes and etc. [7]. When this technology is applied to antenna systems, a notable improvement in antenna performance is achieved to making the antenna more adaptable regarding the environment and multipath-reflection characteristics and a smarter terminal [8]. Moreover, this technology, in particular, is highly demanded in OFDM and mMIMO systems, for instance, in 5th Generation networks [9]. The antenna features should be manufactured sufficiently to fit 5G applications, and therefore, a massive antenna array is applied to create this technology viable [10]. For this, a various methods have been applied by many researchers in terms of reducing the size of antenna to suit more elements of antenna into array structure to validate MIMO system benefits.

1.2. PROBLEM STATEMENT

As mentioned beforehand, the integration of the circuit with the antennae strategies is considered in unlike technologies and investigate parts, hence, this investigate is invoked to realize the possibility of the integration of the active adjustments with MlM0 antennae array and education the belongings on the antennae array recital and vice versa. In such investigate, the problematic of the exteriors wave that is produced among the antennae basics and the corners of the antennae array is mostly a significant issue in exact after the active adjustments introductory. Hence, the possibility of reducing the belongings of such integration among the array basics would be the most challenging part. This is to maintain the antennae recital.

1.3. RESEARCH OBJECTIVES

The purposes of this work, design micro strip antennae arrays with the following characteristics:

- ✓ Design a micro strip antenna with a miniaturized size to fit the 5G applications.
- ✓ The proposed antenna must be resonant within sub-6 GHz bands with a frequency range of (1GHz to 6GHz).
- ✓ The performance of the antenna elements will be configured using a pin-diode to control its performance within multipath reflection environments.

1.4. SCOPES OF PROJECT

Nowadays, wireless strategies based modern tenders have been geared toward green real-power collecting with a new investigate philosophy [7]. This is by reason of the fact that most modern wireless schemes rely on batteries, which are susceptible to overheating and significant charging loss, resulting in short charge and discharge cycle life [11]. As a result, integrating wireless communication schemes with solar photovoltaic schemes widely employed to intelligently provide such strategies with real-power storage [12]. As instance, the investigate ers in [5] employed solarpanels and supercharging capacitors to real-power wireless sensors. But, So of the antennae basics, merging solarpanels with wireless communication schemes has severe consequences [13]. As mentioned in [6] integrating a solarcell directly on a top of the radiating basics greatly Condenses EM leakage. Later, a parabolic reflector antennae was added to solarpanels to provide external real-power support [3]. A patch element including a solar cell was presented, and the belongings of conductor component shadowing on solarpanel recital were examined [2]. The solar cell was then fitted with a ground plane antennae equivalent, although this had a considerable detrimental influence on the antennae band-width [4]. For wireless communication schemes, a whole solarpanel assembly was integrated into an antennae array, although the antennae array's efficiency was Condensed [9]. Another antennae design had been integrated into solarpanels in an attempt to Condense antennae size;

3

nevertheless, by reason of metallization bus-bar belongings, the antennae gain was drastically Condensed [14]. For GSM tenders, inverted-F antennae had been integrated to an a-Si solar cell in [10], but the antennae had a considerable gain loss [8]. For satellite communication schemes, a circularly polarized micro_strip antennae had been conjunctly merged with solarpanels [1], but the design was bulky and heavy. To Condense shadowing belongings, another antennaee design was installed vertically on a solarpanel; nevertheless, the antennae size was large [15]. In [16], a low-gain patch slot antennae was installed on a solarpanel, with light passing directly through the patch slots to the solarpanel.

1.5. CONTRIBUTION OF THE RESEARCH

By reason of the rewards of microstrip-antennaes knowledge including low weight, low-profile, and low size easy to manufacture and easy to be integrated with portable-circuit strategies; the author is motivated to design of miniaturize microstrip-antennaes that are applicable to the 5Gnecessities at Sub6GHz. Moreover, such antennae can be integrated into active adjustments to control the recital that is suiTablefor numerous modern tenders including the 5Gnet-work. They are applicable to unlike high-speed antennae strategies including pin diode characters that may be used later to re-conFigurethe antennae recital. Their assembly can be engineer by via MTM to realize unusual possessions of Augmentd been and frequency band-width.

1.6. SIGNIFICATION OF THE RESEARCH

First of all the antenna design would be developed to operate within frequency bandwidth on 1GHz to 6GHz to suit the application of the 5G system. Improve antenna performance including bandwidth, efficiency and gain. Antenna elements should be of a class 3D array to suit to the MIMO system. This is an effort to ensure that antenna elements are covered in all guidance as well as to minimize mutual-coupling within antenna elements. So, the MTMs is a split ring resonator (SRR) based design that can be implemented to minimize the mutual coupling. This is taken into account because (SRR) leads to high-impedance due to (-µr) which realizes Vincent modes. Integrating antenna design with an (SRR) at a given frequency range

4

within elements of antenna in a single array structure expands the benefits of minimizing mutual coupling. Minimizing the effects of mutual-coupling at a given range meets the requirements of 5G Network system. The antenna array will be integrated into the active switches. Test the performance of the antenna array after inserting the active switches. Minimize the negative impact from the antenna to the active switches and from active switches to the antenna. All this can be summarized as the following:

- ✓ Design novel recon-figurable antennaes for modern wireless communication schemes.
- ✓ Augment the recital of the wireless communication schemes through inventing novel antennae arrays.
- ✓ Merge all these purposes in one integrated scheme to gratify the current state-of-arts.
- ✓ Condense the antennae array size.
- ✓ Augment the antennae gain band-width product.
- ✓ Condense the mutual correlation among the antennae basics.
- ✓ Condense the belongings of integration the antennae array to the active adjustments.

1.7. THESIS OUTLINES

This thesis is divided into six chapters, each of which will focus on a distinct aspects of this thesis. The dissertation outlines for each of the five chapters are grouped as follows.

- ✓ Part 1: Introduction including background, problem statement, research objectives, scopes of project, contribution of the research, signification of the research and thesis outlines.
- ✓ Part 2: Including a literature review, MTM theory and classification, mtms and LH-MTM definitions, the difference among backward waves and LH-MTM, composite right/left-hand (CRLH) MTMs, the implementation of CRLH-MTM via LC net-work, MTM tenders, aim and contribution of this

work, micro_strip antennae operation and theory and comparision and investigate gap.

- ✓ Part 3: Focuses on Theoretical and design methodology, the project process and design steps. The steps of the fabrication process as well as the measuring technique are also depicted.

- ✓ Part 4: Shows the results of simulated and measured microstrip antenna array designs. The figure is used to show discussions regarding comparisons between simulated and measured results.

- ✓ Part 5: Focuses on thesis conclusion, future work and recommendations.

PART 2

LITERATURE REVIEW

2.1. INTRODUCTORY

Over the last three decades, there an increase in scientific interest in the concept of EM Band Gap (EBG) assemblyas photonic band gaps. Recent work have focused on the belongings of joining EBG assemblyto antennae recital for the purpose of improving their recital [7]. As a MTM category, EBG assemblyare periodic-like layers with outstanding surface wave concealing features, one of which is not observed in nature [11]. EBG equivalents were characterized as near zero refractive index [12], soft and hard surfaces [5], (high-impedance) surfaces [13], and artificial magnetic conductors [6] based on their unconventional EM possessions. A few of these assemblyhave relative EM possessions [3], which is worth noting. As a result, EBG assemblycan be thought of as a unique kind of MTM [2], [4], [9], and [14], having frequency stop bands, passbands, and band gaps as a result of their interaction with EM waves.

Another kind of EBG assembly is the Frequency Selective Surface (FSS), which is stacked as dielectric and/or metallic unit cells in various ways [10]. [10]. Such assemblyare often high-resonant assemblythat are heavily influenced by the macroscopic and microscopic periodicity resonances [8]. The macroscopic resonance is sometimes denoted to as Bragg resonance So it is related to the unit cell periodicity, but the microscopic resonance is denoted to as Mie resonance So it is related to the lattice resonance [1]. Furthermore, having two resonances may increase the operational band gap width or cause one of the stop bands to dominate the other [15]. The stop band rejects all incident waves in this scenario, but the other band may be allowed to pass through the middle [16].

FSS classifications have recently been established as filters [17], (artificial magnetic conductors) [18], (photonic crystals) [19], and (photonic band gaps) [20] based on their applications. Furthermore, these structures can be employed as artificial periodic and non-periodic layers to prevent and/or aid the propagation of incident waves [21]. As in mushroom-like structures [22], the structures have high impedance in both TE and TM modes, allowing for the creation of an in-phase reflection coefficient [23]. Furthermore, soft and hard surfaces function as FSS structures [24], which are used in a wide range of antenna engineering research and industry applications.

2.2. MTM THEORY AND CLASSIFICATION

MTM has properties that goes beyond those of natural material. Their name have been derived from Greek-word [meta], that mean as beyond the nature. For that, these materials are artificially constructed with specific specifications in order to achieve the desired performance, and their features are because their structural-composition rather than their physical-compositions [7]. MTM could be known as materials that derive their electromagnetic features from the structure of the materials rather than materials themselves. In condition the structure is carefully designed, a refractive index with negative sign could be obtained at specific frequencies. Stated differently, this material do not obey the right-hand RH rule, hence name "left-hand LH MTMs" [11]. A negative-refractive index doesn't mean a constant motion of the signals, but rather bend EM waves in vs direction when they pass from a (RH)-middle to (LH)-middle as publicized in Figure 1.1 [12].
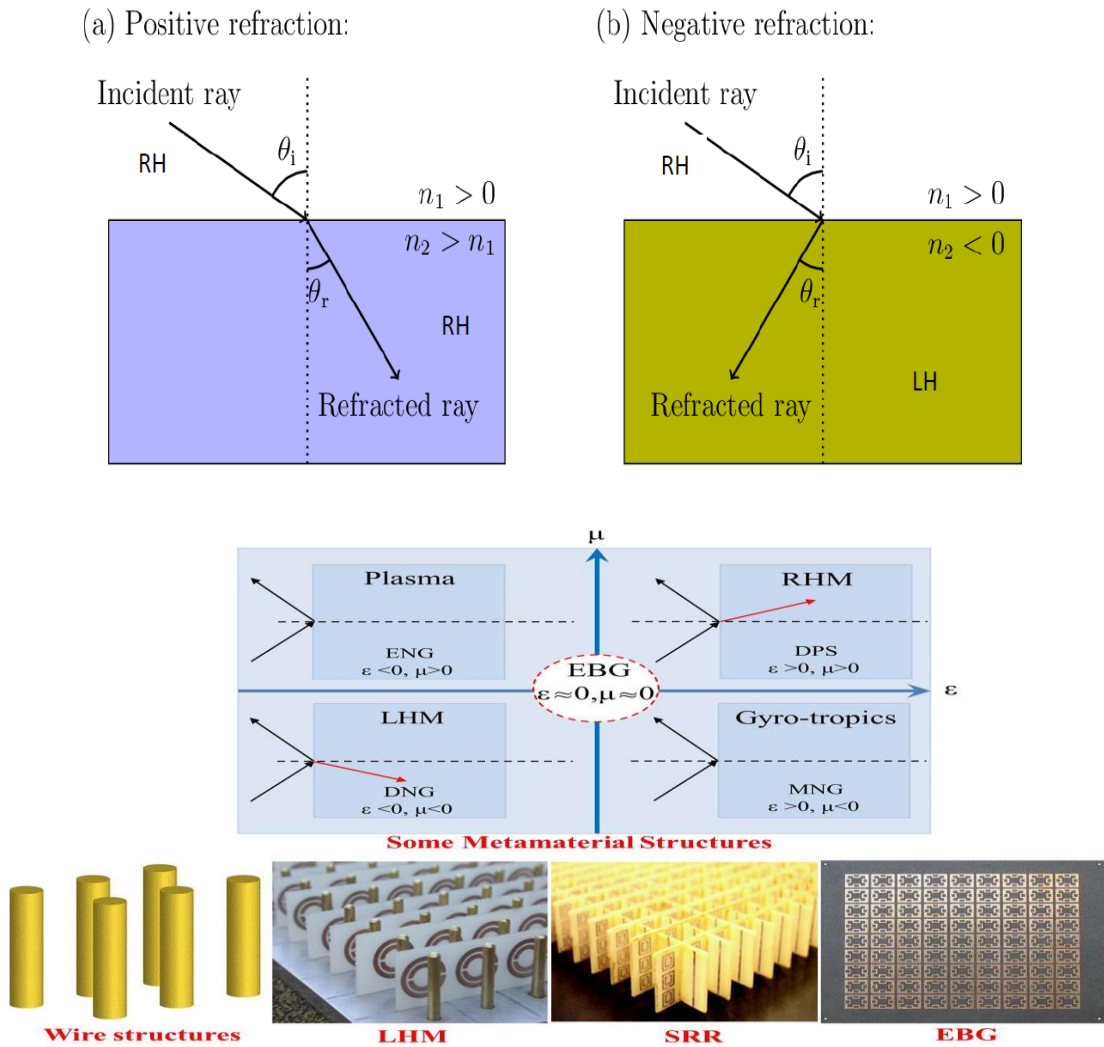
Figure 2.1. Refraction of electromagnetic waves at the contact between media. (a) Two mediums with similar handedness "positive refraction", (b) oppositely handedness "negative refraction" are the two scenarios that can occur.

MTM is a rich subject for scientific research and researchers to cover an extensive frequencies range from the radio waves (RW) to visible range (VR) [5]. In the last few years, the utilize of these materials has been extended to the microwave frequency range (1GHz to 100 GHz), and more details will be given in the section 1.8 on the applications of metamaterials.

2.3. LH-MTM AND MTMS DEFINITIIONS

The MTMs can be known as an actual standardized reproduction middle with possessions and distinctives not initiate in nature [13]. An efficient structure as homogeneous is considered as a material whose cell size of (p) is an extremely tiny compared with wavelength of (λg). For this objective, the average cell size should be shorter than a quarter of the wavelength (p < λg/4). To make certain that the refraction-phenomenon dominates over the diffraction/scattering phenomenon during the propagation of EM waves in the medium of MTMs. The circumstances (p = λg/4) are considered as events of the homogeneity effective [6]. The both parameter (μr εr) depends on the unit cell characteristics, where the structure becomes a real-material in case of homogeneity effective, as a result of which the structure is considered electromagnetically uniform in the direction of propagation. The refractive-index (n) can be determined from the constituent parameters of the structure namely the permittivity (ε) and the permeability (μ), where showed by the following relation:-

$$n = \pm\sqrt{\varepsilon r\ \mu r}\ \ldots\ldots\ldots\ldots\ldots.(1.1)$$

Where μr and εr are free space relative permeability and permittivity, given by ($\mu_0 = \mu/\mu r = 4\pi * 10^{-7}$), ($\varepsilon_0 = \varepsilon/\varepsilon r = 8.854 * 10^{-12}$).

Figure 1.2 represents the diagram of ($\varepsilon - \mu$) showing the signal sets for the pair (ε, μ). These are (-,-), (-,+), (+,-), and (+,+), where the last three sets are defined in conventional materials, while the first set is the new type, which is indicated to as left hand (LH) materials [3]. Due to the constitutive parameters' negative sign, left-hand metamaterials have group velocities and antiparallel phases. As indicated in the previous definition, left-hand materials have been considered MTM due to they are synthetic (man-made) add to effectively homogeneous (p < λg/4), besides possessing special qualities (εr, μr < 0). The MTM term has been utilized to indicate to LH materials in the literature, nevertheless, it covers a higher broader range. LH materials are perhaps the widely common type of MTM because of their distinctive features with "negative-refractive index". Within this chapter, the type of MTM will be discusses in particular composite right/left-handed (CRLH) MTM.
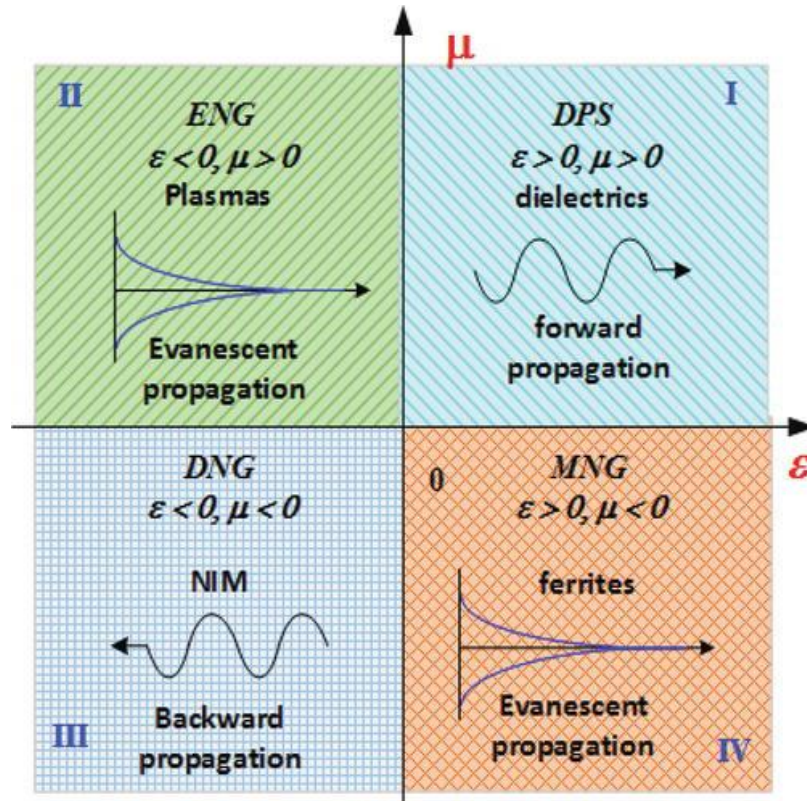
Figure 2.2. The (μ : ε) diagram [2].

2.4. THE DIFFERENCE BETWEEN BACKWARD WAVES AND LH-MTM

The propagation of the opposite phase and the group velocity has been defined for a long period in diverse domains and is not a new theory. Figure 2.3 shows the circuit model used by "Brillouin and Pierce" to represent (CRLH) model and its many utilizes and is utilized especially to explain this kind of propagation, and signals with these properties is known "backward waves" [9].
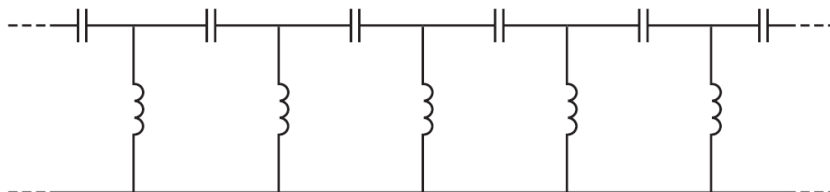
Figure 2.3. Backward wave line circuit model

There are numerous references that provide a detailed explanation of backward-waves. All cases of background wave phenomenon, with the exception of magnetostatic backward-volume waves, occur at higher modes or space harmonics. Backward-waves have been linked to phenomenon of reverse amplification in travel wave tubes. For that, in structures where such kind of waves propagate, the cell size needs to be multiple (p = nλg/2) at the higher modes or equivalent to an half of the wavelength (p $\approx$ λg/2). Consequently, Therefore, the parameters μ and ε can not adequately dominate the structures by which these waves propagate because diffraction and scattering phenomena predominate [14]. As a result, it will not exhibit the EM behavior of the real structures, for instance, the refractive property subject to Snell's law. Conversely, the LH-MTM functions in the mode of fundamental, which is an effective homogeneous structure where cell size is less than (λg/4), so the constitutive-parameters may be determined and the structure behaves like the real material. In fact, there is just a quantitative variation between left-hand structures and dielectric materials as long since the size of the cell is less than a quarter wavelength (p < λg/4).

In natural dielectric-materials, the structural units that given a specific permittivity value are component particles of the order of Angstroms; while in modern left-handed materials, they are centimeters in size in the microwave range. In the (L-X) microwave region, the unitary structure's electrical volume is around (p/λg $\approx$ 10−9) in the first case and (10−1) – (10−2) in the second. However, LH-MTM displays refractive phenomena that are qualitatively identical to conventional dielectrics. Herein lies the fundamental uniqueness of LH MTM. The term LH MTM refers to artificial structures that behave as well as dielectrics, hence the name MTM, but with negative attributes. Due to their effective homogeneity, LH-MTM can include both two and three-dimensional structures.

2.5. COMPOSITE RIGHT/LEFT-HAND (CRLH) MTMs

Calloz introduced the CRLH-MTMs concept, which summarises the broader case of LH-MTM and provides a concise explanation of their essence. The model of TL is shown in Figure 2.4 consists series of interdigital capacitors CL and short (shunt) inductors LL, that are intended to provide the left-hand of the explanations in the previous section. Nevertheless, as currents and voltages flow through the material, they cause parasitic effects [8]. When the current passes through the capacitor CL, producing a magnetic field, which results in a series inductance LR; Additionally, a voltage gradient occurs between the ground plane and the upper conductors, which results in a shunt capacitance CR. Consequently, even in the limit frequency spectrum, the pure LH structure (PLH) does not exist at all, due to the true LH structure should include reactance's (LR, CR) and (LL, CL). This finding is the foundation for using the term CRLH to describe the characteristics and nature of the actual LH-MTM [1]. The basic attributes of the CRLH can be inferred from examining the analog model that shown in Figure 2.9. (a), LR and CR are shorted and opened in the low-frequency spectrum, so the circuit becomes a pure of LH structure because it has phase velocities and parallel combinations, which LH structure is a high-pass circuit, thus there is an LH stopband below a certain cutoff limit. While in the high-frequency range, LL and CL are shorted and open. The circuit becomes a pure RH structure with phase velocities and parallel combinations, and this RH structure is low-pass circuit, so there is RH stopband above a certain cutoff limit. In general, when the shunt resonances and series are not equal, there is often a gap between the RH and LH structures.
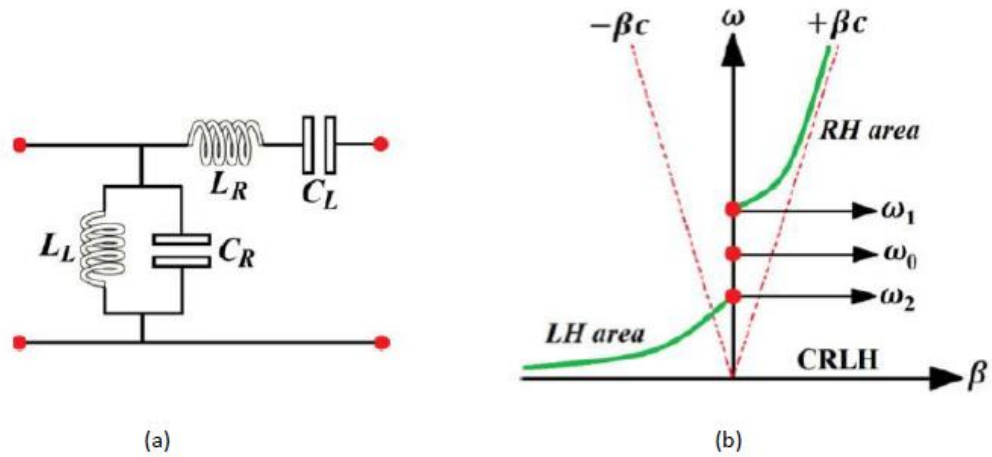
Figure 2.4. Properties of CRLH-MTM. (a) The structure of unit cell (b) The dispersion diagram. (At LH circuit LR = CR = 0), (At RH circuit LL = CL =∞) are given for comparison purposes.

Within this diagram (ωse < ωsh), the converse could also have done depends on LC values. When the resonances be in balance, the gap completely-disappears, as well as endless wavelength propagation [λg = 2π/|β|] is obtained at the transition frequency ω_0. Despite the advantage of the filter. The CRLH only works at the frequency of transition frequency where the requirement of the effective homogeneity is satisfied [p < λg/4], and never works at the Brillouin zone boundary, where [p ≈ λg/2]. The CRLH dispersion curve contains both RH and LH effects is fairly different from that of pure RH/LH structures because the merge effect of the structures on all frequencies.

2.6. THE IMPLEMENTATION OF CRLH- MTM USING LC NETWORK

As mentioned earlier, a pure LH structure should not exists even within a circuit contains only shunt-inductance and series-capacitance , that because the parasitic effects of series inductance and shunt capacitance resulting from the current flowing through the metals and voltages generated within the metals and ground [15], [16]. Thus, the generic form of this kind is represented by the CRLH structure. As shown in Figure 2.5 the structure of a lossless CRLH. The model is consist of the impedance Z(Ω/m) represented through LR[H/m] in series with CL[F·m], plus an admittance

14

Y[S/m] represented through CR[F/m] in parallel with LL[H.m], all parameters per a unit length [17].
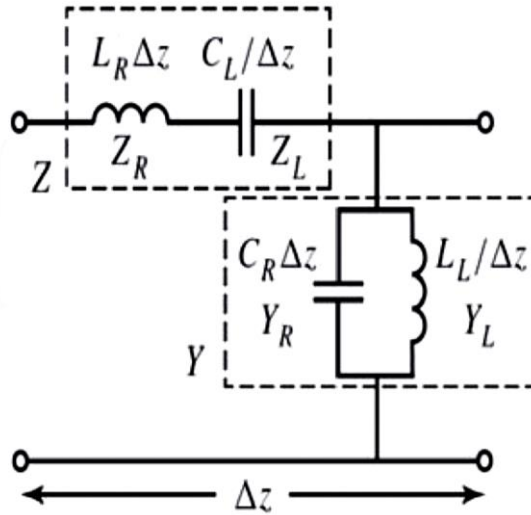
Figure 2.5 The Equivalent circuit model of ideal (CRLH TL).

The previous impressionl of CRLH assembly are not actually feasible, but a homogeneous-structure can be effectively built within a given frequency range based on a ladder network [18]. This network could be gained by the connecting of cell that shown in Figure 2.6 in series to generate the ladder-network that is shown in Figure 2.7. The structure of unit cell structure has impedance (Z=LR+CL) in a series with an admittance (Y=1/CR+1/LL). In the balanced scenario, there is no gap within the RH and LH regions of the CRLH TL line that is because made equal the series and shunt resonances. When (p=$\Delta z \to 0$), the permeability per a unit length becomes (Z/p $\to$ Z), (Y/p $\to$ Y), and thus the L-C circuit illustrated in Figure (2.6/a) becomes the same as the circuit in Figure 2.6.
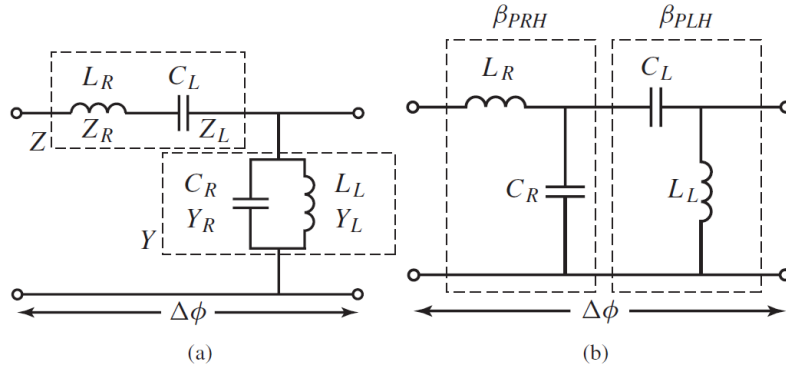
Figure 2.6. Unit cell structure LC CRLH TL. Cases that are (a) unbalanced and (b) balanced (LRCL = LLCR).

Figure 2.7 shows a subsection of a transmission-line of length (Δz), and a practical transmission-line of length (*l*) could be formed by copying this section, where (*l*= N*Δz). By unit cells connecting sequentially as illustrated in Figure 2.7 and under the state (p $\rightarrow$ 0), an identical to the ideal CRLH transmission line can be provided with a total length that equivalent to (*l*).
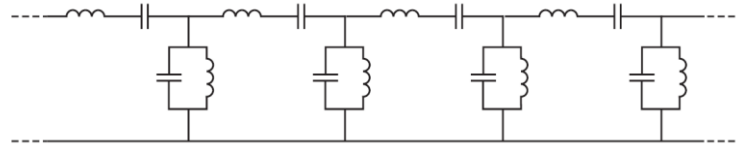
Fig. 2.7. Construction of a periodic ladder networks based on unbalanced (LC CRLH-TL).

As shown in Figure 2.8, where an artificial transmission line equals the lossless homogeneous line a condition known as the homogeneity condition occurs. In fact, this condition actually can be translated into a condition of effective homogeneity, (p < λg/4) where resonances along line discontinuities are prevented [19]. Since it combines the behavior of the (RH) and (LH) filters described in the previous section with that of represent CRLH through the propagation constant (β) and the characteristic-impedance (Zc) in its passband, the (LC) construction of (CRLH TL) represents the band-pass filter.
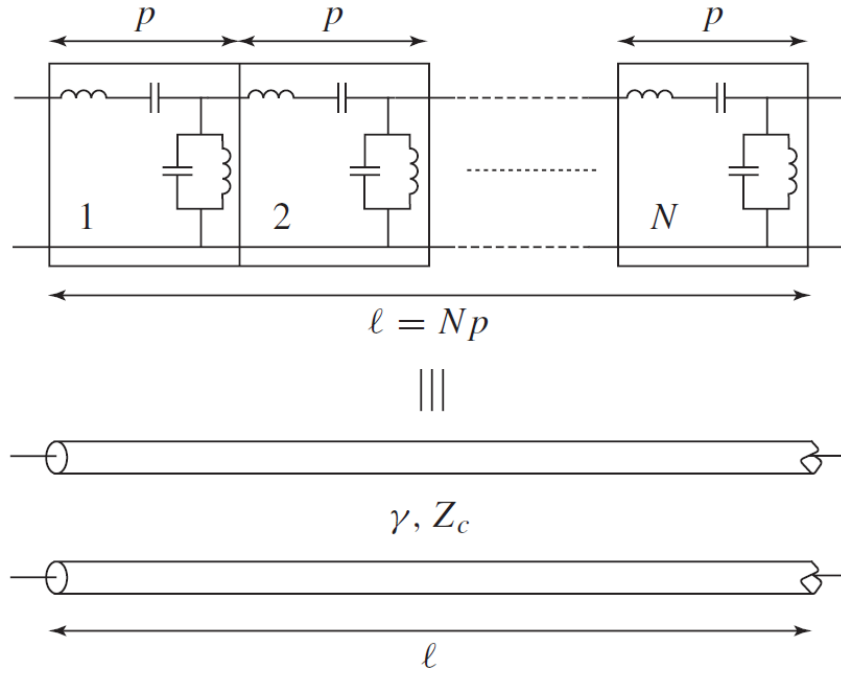
Figure 2.7 A periodic ladder network is equivalent to the ideal transmission line under the state (p = Δz → 0), when (p < λg/4) the network structure in a limited frequency range provides a good approximation to the ideal transmission line (TL).

2.7. METAMATERIAL APPLICATIONS

MTMs have provided alternative and unexplored perspectives due to their unnatural interactions with electromagnetic waves, overcoming the inherent limitations of conventional and advanced technology. Consequently, they have been able to revisit the principles of EM from a different perspective, leading to:

✓ **Discovery of new properties of EM materials.**

It is increasingly common to consider MTMs as materials with negative-refractive index, negative-permittivity, and negative-permeability, with very-high or very-low values of permeability and permittivity [20].

✓ **Utilize of MTMs in implementation of radio frequency components.**

MTM has the potential to significantly impact sensor technology. These components mainly consist of power dividers, bandpass filters as passive circuits, active power amplifiers, and couplers. [21].

✓ **Overcoming the limitations inherent in traditional materials.**

MTM-TL is artificial line containing a reactive material that has greater degrees of freedom than conventional lines and adjusts both dispersion and characteristic-impedance properties [22].

✓ **Enhance the capabilities of existing devices.**

MTMs have been successfully applied to create potentially new devices like electromagnetic transformation devices, invisibility cloaks, and optical Nano circuits, or to improve the performance of already-existing parts (e.g., in microwave designs) [23].

2.8. AIM AND CONTRIBUTION OF THIS WORK

There are various contributions to this work that should be mentioned:

✓ A new microstrip antenna design is presented for the modern wireless communication networks tenders.

✓ The basic element of the proposed antennas would have constructed from metamaterial arrays.

✓ Extensive numerical investigations would be reported to illustrate the design methodology and performance of the proposed antenna arrays.

✓ The fabricated prototype on an FR4 substrate would be constructed and tested experimentally to be compared against their simulated results.

✓ The antenna profile would be relatively miniaturized with small dimensions.

✓ The proposed antennas would utilize an excellent gain bandwidth product over the wide range of frequencies for modern applications.

✓ The antenna would show a distortion less feature that is very suitable for modern applications in terms of receiving and transmitting in low energy devices.

✓ The antenna structure would be structured in 3D profile arrays.

2.9. MICROSTRIP ANTENNA OPERATION AND THEORY

The micro strip antenna consists of two narrow metallic layers (t<< $\lambda_\circ$, where λ is the wavelength in the free space), one as a radiating patch and the other as a ground plane, sandwiched between them as a dielectric substrate. As illustrated in Figure 2.9, the conductor patches are placed on the dielectric substrate and used as a radiating element. The conductive layer serves as a ground plane on the other side of the substrate. As a metallic coating, copper and gold are commonly employed. Radiating patches could be of any shape, although simple designs are commonly utilized since basic shapes are easy to analyse using theoretical models and forecast performance. Basic forms are square, rectangular, dipole, triangular, elliptical, and circular. Because of their ease of analysis and production, the most commonly used shapes are circular, rectangular, and dipole. For the substrate, a variety of dielectric materials with dielectric constants of $2.2 \leq \varepsilon_r \leq 12$ [2] are available. The antenna properties are influenced by the height of the substrate, which is typically in the range of $0.003 \leq h \leq 0.05$.
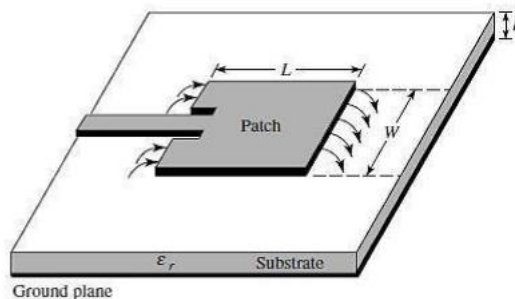
Figure 2.8: A microstrip antenna structure.

The frequency band-width of a micro_strip antennae is quite limited. Micro_strip antennaes, on the other hand, are beneficial in some tenders where restricted band-width is essential, such as government security schemes. The height of the substrate is directly proportional to the band-width of the micro_strip antennae. Two basic ways exist to increase band-width: one is circuit theory, and the other is operational. The possessions of an antennae are influenceed not only by the antennae element, but also by the TX-line and antennae mergation. The input impedance of a micro strip

19

antenna is typically complicated, whereas the TX-distinctive line impedance is actual and typically 50 ohm. Poor impedance band-width and a voltage standing wave pattern on the transmission line are the results of impedance mismatching. The use of impedance matching net-works among the antennae and the transmission line is one technique to solve this problem. Impedance matching routines are accessible in a variety of forms, and circuit theory is concerned with them.

The operational approach is used to change substrate restrictions like height and dielectric constant. It is possible to improve the band-width by raising the height. But, it will introduce surface waves, which will increase real-power loss and degrade recital and distinctives. Investigate ers have projected a variety of approaches, including parasitic patches, defective ground planes, stacking and improving the band-width of micro_strip antennaes, which remains an intriguing issue for investigate. An antennae with the desired resonant frequency EM pattern and polarization can be simply designed by selecting a particular shape. By adding loads such as PIN diodes and Varactor diodes, making a tiny micro strip antennae is easy with recon-figurable resonance frequency, polarization and EM patterns.

A. EM mechanism

Designers discovered in 1969 that if the micro_strip line is left open ended on one end and fed on the other, some of the real-power is radiated in space as of both ends as EMwaves by reason of the discontinuity formed. Designers also discovered that the quantity of real-power radiated in space is greatest when both discontinuities are separated by half a wavelength or a multiple of half a wavelength [6]. The designers concluded that EMs occurred as of the open end as a result of the discontinuity's surrounding fields. Consider a rectangular antennae with a half wavelength long radiating patch fed through a micro_strip feed line to better understand the mechanics underlying micro_strip antennae EM. Some rectangular antennae can be thought of as an open-ended micro_strip line with real-power fed as of the differing end. So the patch is half wavelength long and open ended on the other side, the current should be zero at the patch's corners "at beginning and end" and maximal at the patch's center. As seen in Figure10, current and voltage will be 90 degrees out of

20

phase. The voltage will be at its maximum positive at the beginning of the patch and at its maximum negative at the end [4].
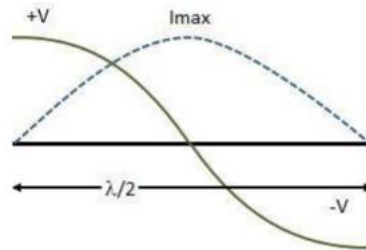
Figure 2.9: Current and voltage variation.

B. Rewards and Disrewards:

Micro_strip antennaes are light-weight, low-profile and simple to install antennaes that are widely used in handheld wireless strategies such as pagers and cell-phone phones, as well as in high-recital communication schemes such as spacecraft, satellites, missiles, and airplanes. The following are some of the primary aids of micro_strip antennaes as stated by Randy Bancroft [12] and Garg [9]:

- ✓ Inexpensive and simple to make.
- ✓ Simply, can be planted at every surface.
- ✓ Recon-figurable distinctives are simple to obtain.
- ✓ It's simple to create an antennae with the polarization you want.
- ✓ Suitable for microwave integrated circuits (MICs).
- ✓ Mechanically resistant, robust to vibration and shock.
- ✓ It's simple to create an antennae array.

Micro_strip antennaes, on the other hand, have a amount of drawbacks and restrictions when compared to other antennaes. The following are some of the primary drawbacks of micro_strip antennaes:

- ✓ Factor of high quality.
- ✓ A Cross polarization.
- ✓ There is a lack of polarization efficiency.

- ✓ Experiencing spurious feed EM.
- ✓ Narrow band-width impedance (5 percent to 10 percent without either technique)
- ✓ High conductor and dielectric losses.
- ✓ Sensitive to changes in the situation, such as temperature and humidity.
- ✓ When a factual with a high dielectric-constant is utilized, it suffers as of surface waves.
- ✓ Low gain with a lot of real-power handling capacity.

There are several approaches to avoid this constraint; for example, "defective ground plane" strategy, "stacked patches", "slotted patches", and "parasitic patch" can all be used to increase the band-width of a micro_strip antennae. Making an antennae array helps to improve the antennae's gain and real-power handling ability. The use of a MTM and EM Band Gap "EBG" assembly improves antennae possessions as well [20].

C. Tenders

After overcoming a amount of constraints, micro_strip antennaes have proven to be quite actual in a variety of tenders. Micro_strip antennaes are commonly utilized in defense scheme such as missiles, satellites, aircraft and rockets. Micro_strip antennaes are now widely utilized in commercial tenders by reason of their low cost and ease of fabrication, which is aided by modern printed circuit knowledge. So of the advancements and continuous investigate in the field of micro_strip antennaes, it is projected that most "conventional antennaes" will be replaced with "micro_strip antennaes" in the future. Micro_strip antennaes are utilized in a variety of tenders, including:

- ✓ Satellite Communication.
- ✓ Cell-phone Communication.
- ✓ Global Positioning Scheme.
- ✓ Direct Broadcast Satellite Scheme.
- ✓ Antennae for Pedestrian.
- ✓ In Radar Tenders.

✓ Tender in Medical Science.

2.10. COMPARISION AND RESEARCH GAP

In this section, several comparisons are introduced in different aspects of this study as shown following:

A- *Antenna types for 5G and modern applications*

In this section, a comparison study is discussed in Table1. Hence, for this comparison a call is invoked to compare among the antennae kinds for the 5Gand modern tenders. As well as, the comparison is extended to discuss the antennae size in terms of wavelength, configuration whither it is single element or array, and antennae recital in terms of: Frequency, gain, and band-width. Nevertheless, a comparison among the ability of integration with small circuit strategies and the design complexity is comprised. Telecommunication providers have already been investment in cell-phone net-works to increase coverage, improve services, and attract more users since the first cell-phone phones were introduced in the 1980s. Cell-phone phone calls were supported on first-generation net-works, although coverage and capacity were limited. Providers built and deployed 2G cell-phone net-works, followed then 3G and 4G net-works to solve these restrictions [7]. Each group brought faster speeds, more capacity, and newer topographies and facilities. But, Telecommunications corporations started installing 5Gnet-works in 2018 to billet mounting data stresses as of clients and trades. 5Gnet-works are likely to agree earners to swell user services (such as video flooding and virtual reality tenders), care the rising total of joined strategies: medical strategies, IOT, smart homes, care new trade uses: engineering sensors and monitoring schemes, accomplish innovative data investigation, pluse permit the usage of technical progresses e.g., independent vehicles, smart city tenders. 5G is another element driving 5Grollout. The EM is used by all wireless technologies to communicate [7]. The radio frequencies utilized to communicate across the airways are denoted to as . Multiple bands are used in 5G. Low-band (below 1GHz), mid-band (1GHz-6GHz), and high-band (MMW) are all used in 5G. 5Gessentials the disposition of 5Gknowledge in the high band (MMW) to provide ultra-fast services to densely populated areas. Existing consumers

advantagous as of 5Gtechnologies implemented in the mid-band, which provide increased capacity and coverage, faster service, and additional features. Numerous IoT tenders essential widespread coverage, which 5Gknowledge deployed in a low-band can transport. Besides, the most cell-phone strategies are usage frequencies below sub6-GHz So the frequencies inside that subdivision of the are very suiTablein wireless communications. Let's say, frequencies private this section of the might very well to portable long reserves providing attention over big areas, and it can effortlessly arrive edifices and fences But, as more persons use cell-phone strategies for a broader range of tenders [7],[12]. All gatherings involved in emerging of 5Gtechnologies accept that 5Gessentials in 3 main main frequency ranges to meaning properly:

1- Sub-1GHz for comprehensive coverage in metropolitan, suburbia, and rural settings, as well as in-building coverage for IoT strategies and services.
2- 1-6GHz for increased band-width, including the 3.3-3.8GHz band that is expected to also be the initiate ation for numerous earliest 5Gservices.
3- Above 6GHz, which comprise MMW, to focus on providing Ultra-high wideband speeds.

Table 2.1 shows a comparison between the antenna types that are used for 5G and modern applications in advantages and disadvantages as listed below.

Table 2.1. A comparison table between the antenna types that are used for 5G and modern applications in its advantages and disadvantages [25].

Antenna Type	Advantages	Disadvantages
Monopole	• Simple to design and fabricate • In multi-element monopole antenna design, it can be easily rotated in any direction.	• Less gain • Requires large area of ground • Gives poor response in bad weather condition
Dipole	• Simple to design and fabricate • Receives balanced signal	• Less gain • Cannot be used for long range communication • Low bandwidth
Magneto-Electric (ME) Dipole	• High front to back ratio • Low side lobe and back lobe level • Wide bandwidth • Low cross polarization	• Design and fabrication is complex • Costly
Loop	• Easy to design • Provides good channel capacity	• As single element loop antenna cannot meet the 5G requirements, multi-element loop antenna is required. • Low gain
Antipodal Vivaldi Antenna (AVA)	• Enhances the gain • Provides wider bandwidth • Gives stable radiation pattern	• Requires more space • Low gain at lower frequencies
Fractal	• It helps to miniaturize antenna size. • Provides wider bandwidth • Good impedance matching • Provides consistent antenna performance over the operating range.	• Design is complex • Limitation on repetition of fractal design
Inverted F Antenna (IFA)	• Smaller in size • Good impedance matching due to intermediate feeding	• Narrow bandwidth • Low gain
Planar Inverted F Antenna (PIFA)	• Low profile • Good impedance matching • Enhances front to back ratio	• Narrow bandwidth • Low gain

B- Antenna reconfiguration comparison

In this comparison, the author listed in table 2.2, a study to classify the type of reconfiguration whether it is: frequency, gain, beam forming, or polarization. As well as, the applied technique is listed in this work and the complexity of the realization. Reconfigurable-antennas could be categories into four class that's based on the reconfiguration methods features as it is simplify in Figure 2.11.
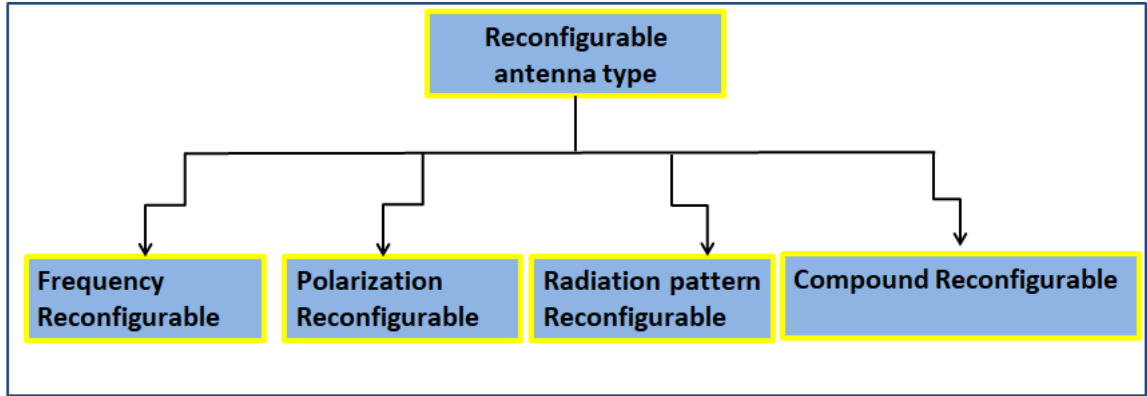
Figure 2.10. Classification of reconfigurable antennas.

Table 2.2. A comparison table between the reconfiguration techniques [26].

Reconfiguration Technique	Advantages	Disadvantages
Electrical Reconfiguration	• Ease of implementation • Low-cost	• Complex structure • Requires biasing systems
Optical Reconfiguration	• No need the use of bias lines • No intermodulation distortion	• Lossy behavior • Complex activation mechanism
Mechanical Reconfiguration	• No need of active elements • No need of biasing systems	• Slow response • Requires power source
Smart-Materials-Based Reconfiguration	• Low-profile • Lighter weight	• Low efficiency • Limited application

The easy selection of a reconfiguration technique that consistently yields the intended function or property is necessary to obtain the desired reconfiguration function. In order to acquire reconfiguration and enable the antenna to be used for actual wireless communication activities requiring an adjustable radio frequency front end, four universal techniques have been applied to reconfigurable antennas. Figure 2.12 provides an illustration of these four methods.
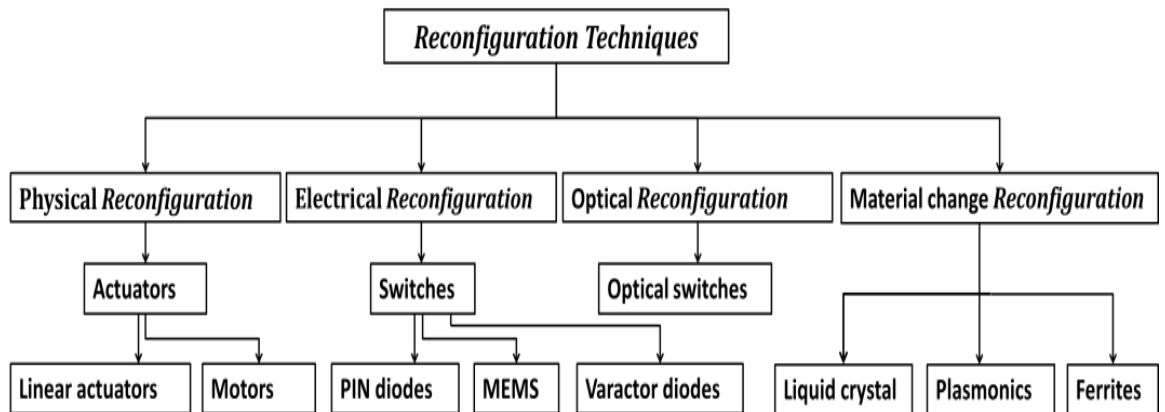
Figure 2.11. The reconfiguration techniques used in reconfigurable antennas.

C- *Antenna feeding techniques comparison*

In this section, the most important consideration is the efficient transfer of real-power among the radiating assembly and the feed assembly , also recognized as impedance matching are listed in Table2.3. Stepped impedance transformers, bends, stubs, junctions, transitions, and so on are all associated with impedance matching and introduce discontinuities, resulting in spurious EM and surface wave loss. Unwanted EM may raise the side lobe level and cross-polar amplitude of the EM pattern. One of the most important factors in evaluating a feed is the decrease of spurious EM and its resulton the EM pattern.

Table 2.3. Comparison between different feeding techniques.

Feeding technique	Radiation leakage	Matching process	Fabrication complexity	Reliability	Bandwidth
Microstrip line	More	Easy	Easy	Better	2-5 %
Coaxial	More	Easy	Need drilling and soldering	Poor	2-5 %
Proximity Coupled	Minimum	Easy	Need Alignment	Good	13 %
Aperture Coupled	Less	Easy	Need Alignment	Good	21 %

D- General comparison

In this part, a comparison of different antennas for modern applications was introduced in the literature from various perspectives, as follows:

Table 2.4. General comparison.

Ref.	Antenna Size (mm²)	Substrate ε_r/ Thickness (mm)	BW (GHz)	No. of Ports	Gain (dBi)/ Efficiency (%)	Isolation (dB)	ECC	Reconfig-urable
[27]	50 × 100	FR4 4.4/4.5	2.7–3.6	4	3/85	25	-	No
[28]	180 × 180	RT Duroid3/1.52	0.7–1, 2.6–7.2	4	5/70	>13	<0.5	Yes
[29]	120 × 65	FR4 4.4/1.6	3.3–5	4	2/40	18.8	<0.018	No
[30]	70 × 145	polyamide 3.5/0.2	2.37–5.85	4	5/85	17.5	<0.05	Yes
[31]	150 × 73	FR4 4.4//0.8	3.4–3.6	4	51/74	20	<0.06	No
[32]	88 × 88	Polyimide3.5/0.05	2.38–2.52	4	4/80	>15	-	Yes
[33]	71 × 49	DAK-3.52.7/0.3	2.30–2.60	1	1.4/60	-	-	Yes
[34]	66 × 66	ROGERS3003/0.13	3–4.12	4	4/84	>20	<0.005	Yes

Research gap:

It is clear as of the projected comparison, to the best of the author knowledge, the current state of the art did not consider the tenders of a recon-figurable antennae array design with solarpanel integration for smart self-real-powered 3D antennae arrays for MlM0 schemes in the modern cell-phone communication net-works. On the other hand, the projected design could be subjected for RF collecting specifically, by integrating the rectifier circuit inside the antennae array scheme.

PART 3

THEORETICAL AND DESIGN METHODOLOGY PART

3.1. A PRINTED MONOPOLE ANTENNA ARRAY INSPIRED BY HISTORICAL CITIES IN IRAQ.

3.1.2. Antenna Design And Geometrical Details

In this reserch, the antenna array based on two antenna elements is shown in Figure 1(a). In this section, the antenna array operation and geometrical details are discussed. The antenna is structured a printed monopole that is shaped as hunchback structure-shaped as seen in Figure 3.1(b). The antennas are separated with a transformer impedance of Malwiya minaret-shaped, see Figure 3.1(c), as a twisted geometry. Next, to ensure good diversity, Ishtar Gate structure, see Fig. 3.1(d), is introduced to reflect the antenna radiation away from the array center. Later, the antenna array ground plane is introduced in the back panel partially to realize bandwidth enhancement. The width of feeding line is fixed to 2mm to ensure characteristic impedance of 50Ω.
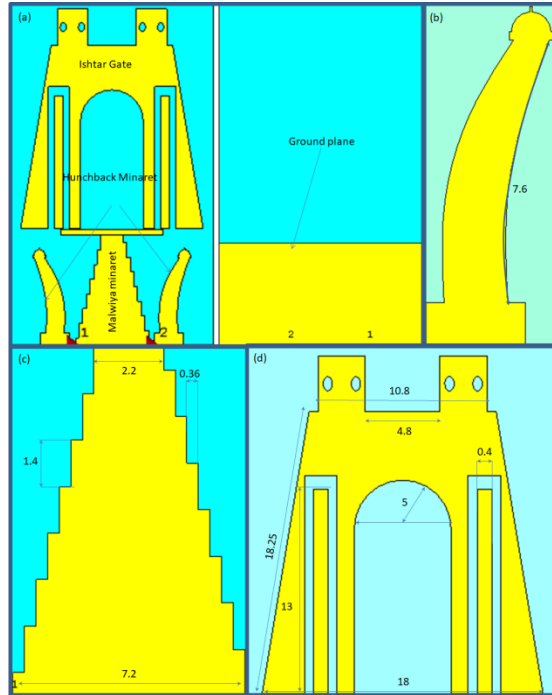
Figure 3.1. The proposed antenna geometry: (a) Antenna geometry, (b) Monopole structure, (c) transformer twisted, and (d) Ishtar Gate.

3.1.2. Design Methodology

In this section, a parametric study based on CST MWS simulation analysis is applied on this geometry. In this analysis, the proposed antenna performance evaluation is taken and the effects of each part introduction on antenna performance in terms of S_{11} and gain spectra are taken in the consideration. The authors focused in this work on achieving multi frequency bands within the sub-6GHz ranges. The simulation process is gone through the following:

3.1.2.1. Monopole Structure

The study is started by applying a monopole with a hunchback-shaped structure. The parametric analysis study begins with changing the curve size from 100mm to 300mm of the hunch back curve radius with respect to S11 and gain spectra. As seen in Figure 3.2, various radiuses are considered to conclude that the antenna shows two frequency bands at 3.2GHz and 5.5GHz with return loss below -10dB; when the radius is 300mm. Therefore, the authors decided to choose 300mm is the optimal

value. The achieved results are compared to those obtained from strait monopole. The researchers suggested the optimal dimensions according to the monopole radiation limitations in [12] to fix them to 2mm in width and 7.6mm in length. The proposed antenna array is feed with 50Ω SMA ports. The main advantage of introducing the curve hunchback-shaped geometry is to insure electric field fringing toward the first element. The antenna hunchback is changed from strait structure to curved structure with a reduce of 100mm to 300mm. The obtained results are shown in Figure 3.2.
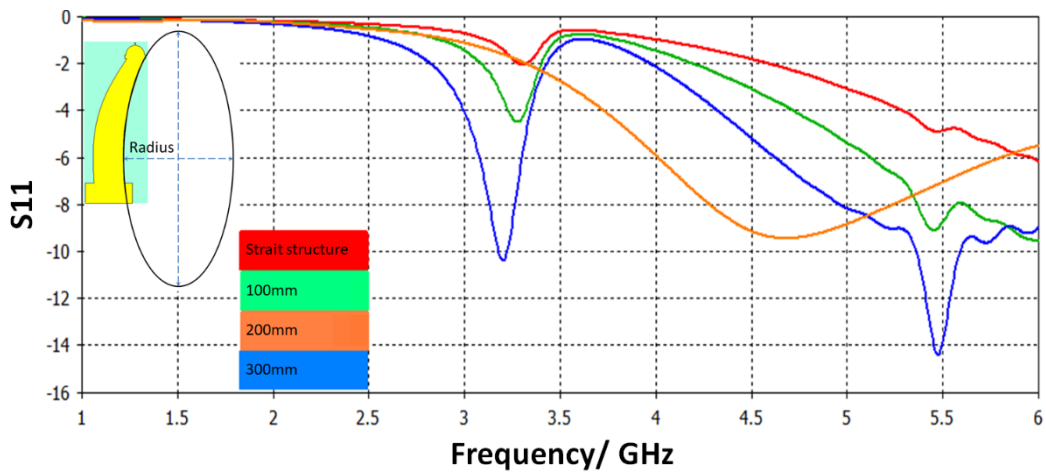
Figure 3.2. Effect of hunch back radius of the proposed monopole on S_{11} spectra.

3.1.2.2. Transformer twisted steps

In this study, increasing the step order on the antenna performance in terms of S_{12} is discussed in this section. So, to analysis the effects of their addition to the antenna characteristics, the researchers utilized different orders to investigate the effect of adding a step order as seen in Figure 3.3 on antenna performance based on CST MWS results. The order is changed from 4 stages to 12 stages with a step of 4 stages. It is found that the proposed antenna mutual coupling is reduced significantly with 8 stages. Therefore, it is concluded to consider 8 stages is the best option to the next design step.
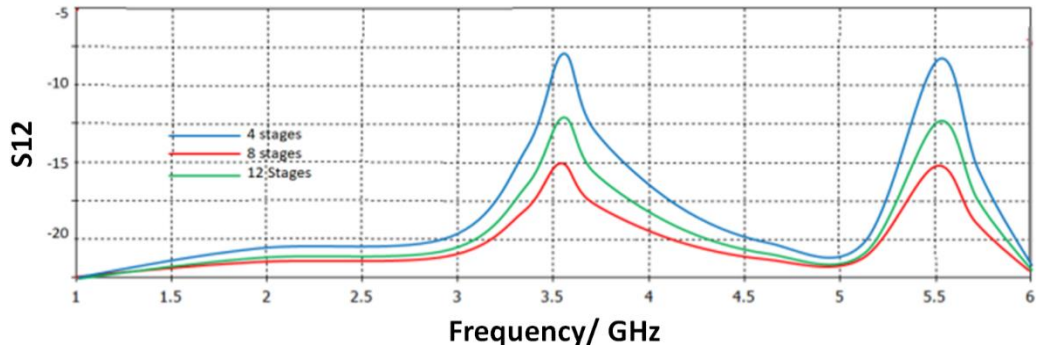
Figure 3.3. S_{12} spectra variation with changing stage number.

3.1.2.3. Ishtar Gate

This study applied two cases on the proposed antenna structure. Later, the antenna performance is compared the realized results of the two cases with and without Ishtar gate structure. The first case when one-unit cell is added to the design structure as shown in Figure 3.4. In this study, it is found that the introduction of the Ishtar get, a significant enhancement in the antenna bandwidth can be realized for two frequency bands at 3.25GHz and 5.65GHz. Nevertheless, we noted that the maximum coupling in terms of S_{12} is below -15dB after Ishtar gate introduction as seen in S_{12} spectra.
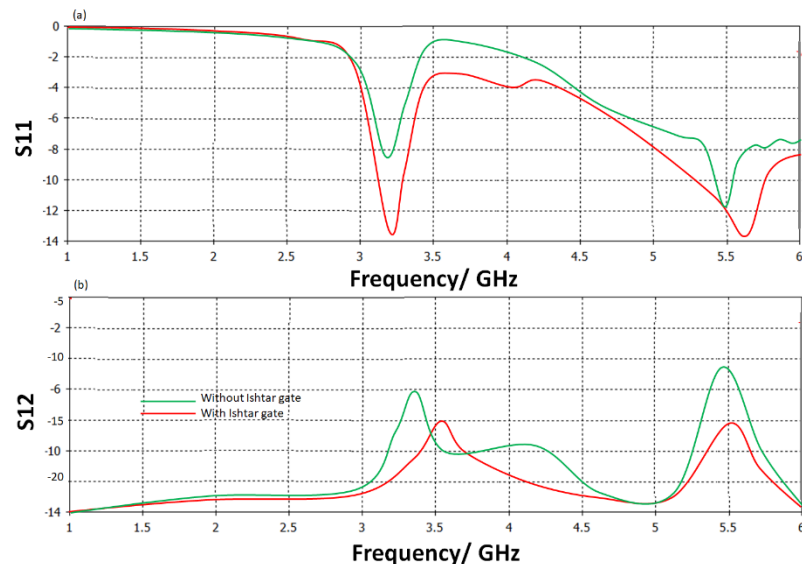
Figure 3.4. Antenna array performance after Ishtar gate introduction; (a) S_{11} and (b) S_{12} spectra.

3.1.2.4. Ground plane

The proposed antenna ground plane length is changed from 6mm to 8mm. The effects of changing the ground plane length are found to be very effective on the antenna bandwidth and gain spectra. However, the coupling effects are found not significantly changed with the ground plane length change. The obtained results are shown in Figure 3.5.
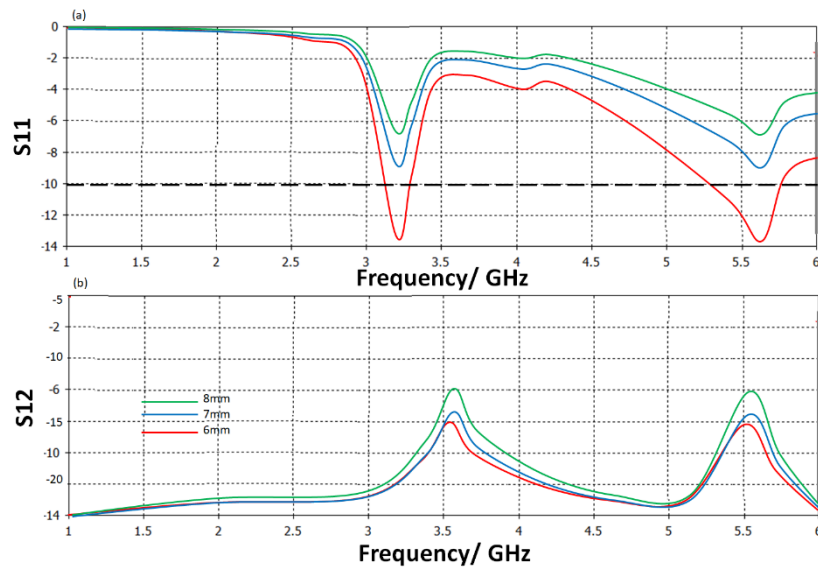
Figure 3.5. Antenna array performance with the ground plane length variation; (a) S_{11} and (b) S_{12} spectra.

3.2. ORIGAMI ANTENNA ARRAY IN THE SHAPED MOSQUE OF MUHAMMED AL-FATIH FOR VISUAL SIGHT ENHANCEMENT IN MODERN MIMO 5G NETWORKS

3.2.1. Antenna Geometrical Details

The design specifications of a sub-6GHz 5G antenna will depend on the specific application and use case, but there are some general design considerations that are important to keep in mind. Some of the key design specifications of a sub-6GHz 5G antenna include:

3.2.1.1 Frequency Range

Sub-6GHz 5G operates in the frequency range of 600 MHz to 6 GHz, so the antenna must be designed to operate within this range.

3.2.1.2 Bandwidth

5G networks require antennas with a wide bandwidth to support high data rates. The antenna should have a bandwidth of at least several hundred megahertz to support the wide range of frequencies used in 5G networks.

3.2.1.3 Gain

The antenna gain determines the strength of the signal that can be transmitted and received. Higher gain antennas can transmit and receive signals over longer distances. The gain of the antenna will depend on the specific application and use case, but typically sub-6GHz 5G antennas will have a gain of around 5-7 dBi.

3.2.1.4 Polarization:

The polarization of the antenna determines the orientation of the electric field of the transmitted and received signal. The most common polarization used for sub-6GHz 5G antennas is linear polarization, which can be either vertical or horizontal.

3.2.1.5 Beam Width

The beam width of the antenna determines the angle over which the antenna can transmit and receive signals. For sub-6GHz 5G antennas, the beam width should typically be wider than for higher frequency antennas, to accommodate the larger wavelengths of sub-6GHz signals.

3.2.1.6 Radiation Pattern

The radiation pattern of the antenna determines the direction and strength of the signal transmitted and received. The antenna should be designed to have a uniform radiation pattern over the desired coverage area.

3.2.1.7 Size And Shape

The size and shape of the antenna will depend on the specific application and use case, but generally sub-6GHz 5G antennas should be designed to be compact and lightweight to enable easy integration into devices and infrastructure.

These are some of the key design specifications to consider when designing a sub-6GHz 5G antenna, but there may be other factors that are specific to the application or use case that need to be taken into account.

In this research, the antenna design is fixed to $60\times136\times1$ mm^3, the MIMO design (two antennas with MTM in between) is shown in the top left of the Figure 3.6, also Figure 3.6(a) shows domes with radiation element printed on an FR-4 substrate with permittivity of 4.6 and losses about 0.00178. The antenna ground plane is introduced as a coplanar waveguide (CPW) conductive plate as shown in Figure 3.6(b). The antenna array is organized on 2D configuration that is separated with metamaterial (MTM) spacer of hexagonal shape. The proposed MTM spacer is organized as a 1D array configuration of 5 unit cells as seen in Figure 3.6(c).
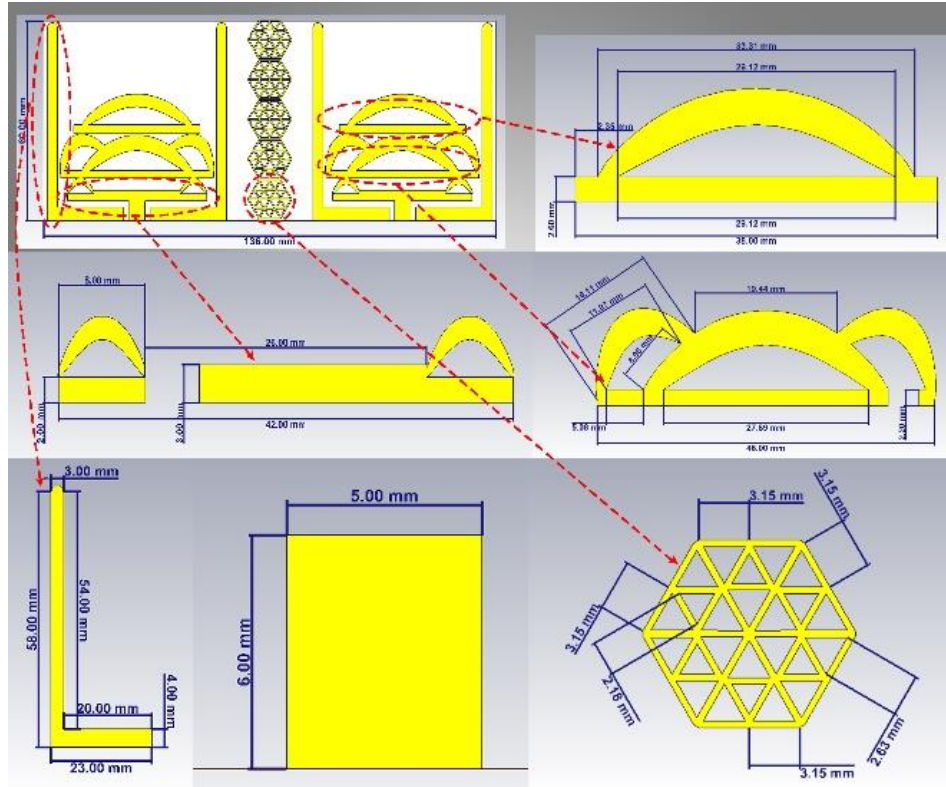
Figure 3.6. Antenna array design: (a) front view, (b) CPW view, and (c) MTM unit cell.

3.2.2. Design Methodology

At beginning, it is considered several parameters during this section without affecting the original shape of the mosque. Therefore, they are satisfied with the following parameters:

3.2.2.1 Effects Of Changing L-Shaped Stub Length:

The effects of changing the L-shaped stub length on the proposed antenna array performance in terms of S11 and S12 spectra are shown in Figure 3.7. It is found from the obtained results; the antenna matching impedance bandwidth is enhanced significantly with changing the proposed L-Shaped stub length. This realizes a fact that such structure shows an effect of a matching circuit that is very useful for the proposed antenna performance. However, the antenna coupling effects is found to be significantly decade with increasing the proposed L-Shaped stub length.

37
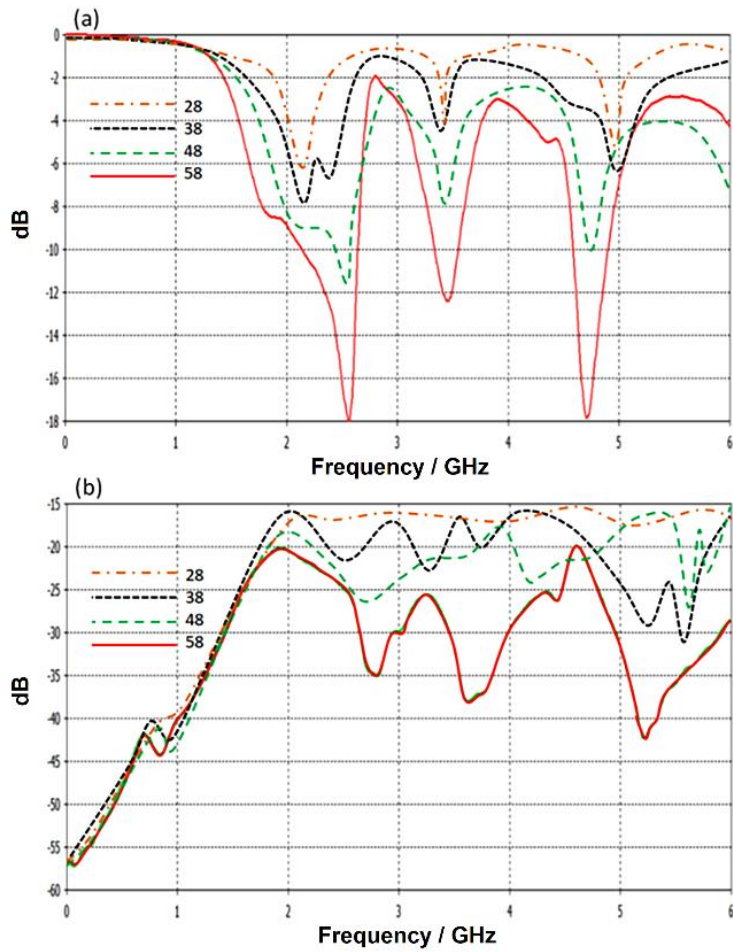
Figure 3.7. Antenna S-parameters the proposed L-shaped length: (a) S_{11} and (b) S_{12} spectra.

3.2.2.2 Effects Of Changing CPW Gap:

Next, to explore the effects of varying, the proposed CPW on the proposed antenna performance, the gap space is changed between of the proposed CPW from 1mm to 2.5mm with a step of 0.5mm. It is found after reaching the distance of 2.5mm, the antenna realizes an excellent bandwidth with low coupling effects as seen in Figure 3.8.
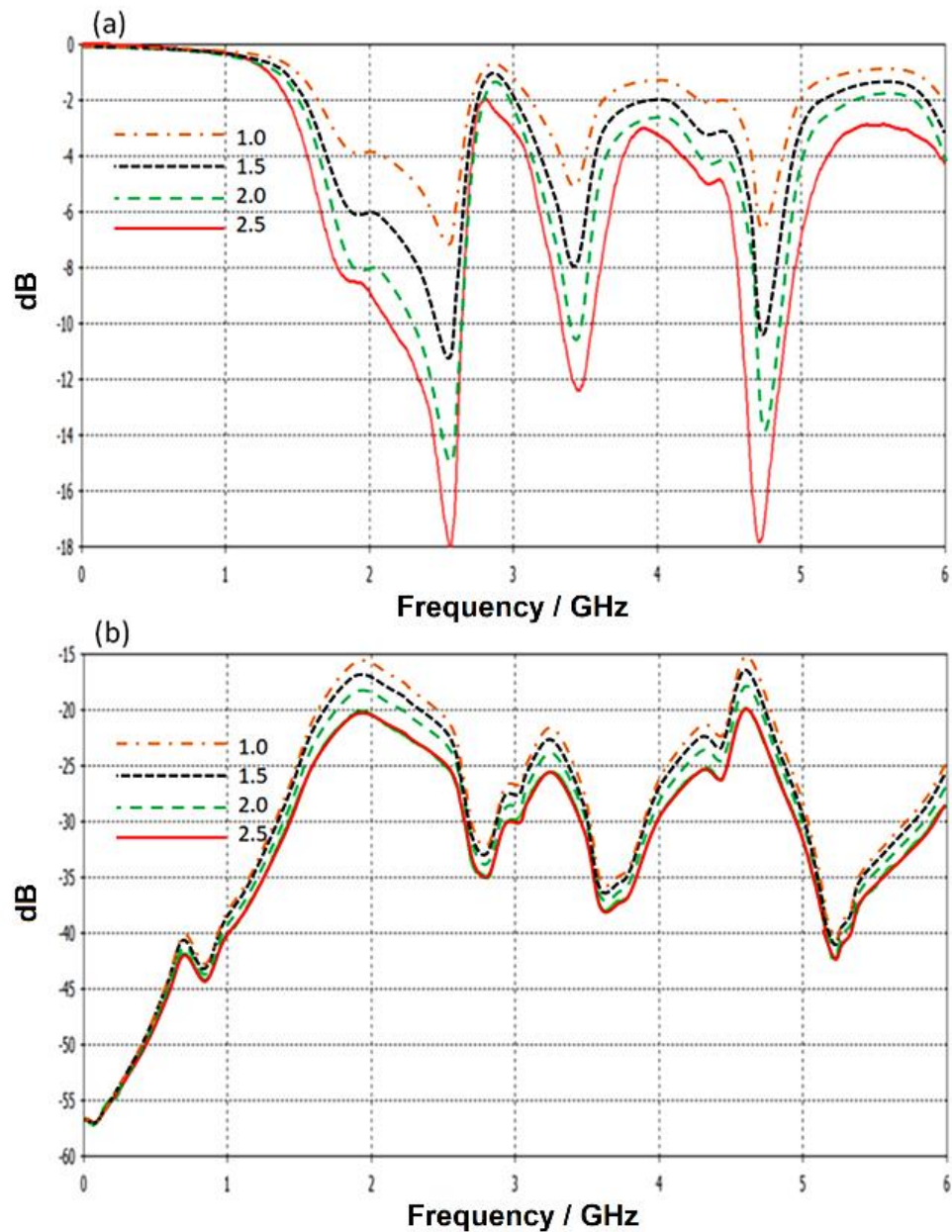
Figure 3.8. Antenna S-parameters with varying the gap distance of the proposed CPW structure: (a) S_{11} and (b) S_{12} spectra.

3.2.2.3 Effects Of Introducing MTM Unit Cells:

Now, to realize the effects of the proposed MTM unit cells number on the proposed antenna performance, the authors conducted a simulation study by varying the unit cells number from 0 to 5 unit cells with a step of 1-unit cell. It is observed a significant enhancement could be achieved by increasing the unit cell number with

an obvious reduction in the mutual coupling can be achieved with increasing the unit cell number. As seen in Figure 3.9, the proposed antenna performance shows an excellent enhancement with increasing the proposed unit cell number to 5. It is good to mention that the proposed antenna may not cover the entire frequency bands within sub-6GHz, but shows some resonance within sub-6GHz to be very suitable enough for such applications [35].
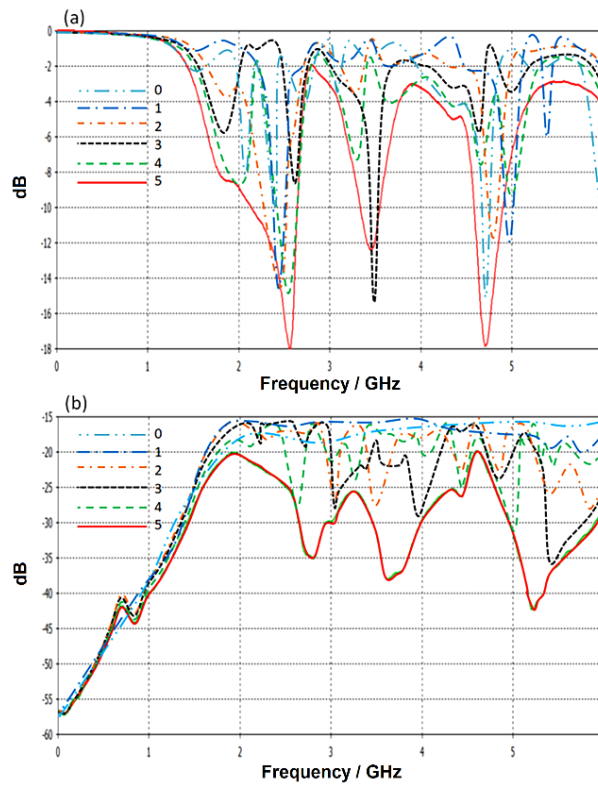
Figure 3.9. Antenna S-parameters with varying the proposed unit cell number: (a) S_{11} and (b) S_{12} spectra.

It is found that the proposed antenna array mutual coupling with is reduced significantly with increasing the number of unit cell because the increase of the surface impedance as series connection facts [36].

3.3. MINIATURIZED ANTENNA ARRAY BASED NOVEL METAMATERIAL TECHNOLOGY FOR RECONFIGURABLE MIMO SYSTEMS

3.3.1. Antenna Array Design Details

The proposed antenna is designed from two antenna elements printed on the same substrate for MIMO system design. Each antenna element is structured from three main parts: Printed monopole, interdigital capacitor array, and meander line. The proposed antenna is fed with CPW to eliminate the ground plane on the same patch side as well as ensure harmonics generation by accumulating the electrical charge on the ground plane [37]. Therefore, the proposed meander line is fetched to the ground plane of the proposed CPW structure. In such a structure, the effects of field gradients can be enhanced altimetry to realize bandwidth enhancements [38]. For this, the antenna gain bandwidth would be enhanced to realize the desired frequency resonances with maximum size reduction [39]. Nevertheless, the proposed antenna performance can be controlled by switching the connections between the antenna meander line and the ground plane through four LDR resistors. The proposed antenna array is found to occupy an area of 50×30mm^2 when printed on FR4 substrate of 1mm thickness.

For MIMO configuration, the authors applied the design of two elements that are mounted on the same substrate with the same direction as shown in Figure 3.10. The antenna array is defective with an MTM structure at the center position between the antenna elements to ensure surface wave sprucing at the desired frequency bands [40]. The proposed MTM structure is constructed from Minkowski fractal design with the third iteration. In such a structure, a high capacitive load is coupled near the edges of the proposed monopoles; in which most fringing effects are initiated [38]. Logically, positioning such MTM at the center of the proposed array would be an excellent option. In another aspect, the proposed MTM is structured to provide a single negative performance in which a high coupling redaction can be achieved [41]. Therefore, the surface wave mitigation between the antenna elements would be vanished smoothly without significant phase reflections [42]. Simultaneously, a high diversity can be achieved by directing most antenna radiation away from the array

center through the inductive imposing effect from the proposed MTM fractal structure [43].

It is good to mention that the effect of introducing the meander line can be summarized by generating a frequency band different from the band is generated that is generated by the monopole, as will be seen later. However, the proposed meander line is connected through LDR switches to control the antenna surface current motion by shorting that with the antenna ground plane. The main advantage of proposing the interdigital capacitor to the design is to match the electromagnetic aperture coupling to the free space impedance by equalizing the induction effect of the monopole antenna structure. Therefore, the antenna radiation efficiency would be significantly improved as will be seen later [44]. Finally, the proposed antenna is printed on an RF-4 substrate with 1mm thickness and 4.4 dielectric constants. The rest of the proposed array geometrical details are listed in table 3.1

Table 3.1. Antenna geometrical details.

Symbol	Value	Abbreviation
X_g	3	Separation distance
Y_g	3	Ground plane length
X_m	4	Monopole width
D	12	Separation distance between antenna elements
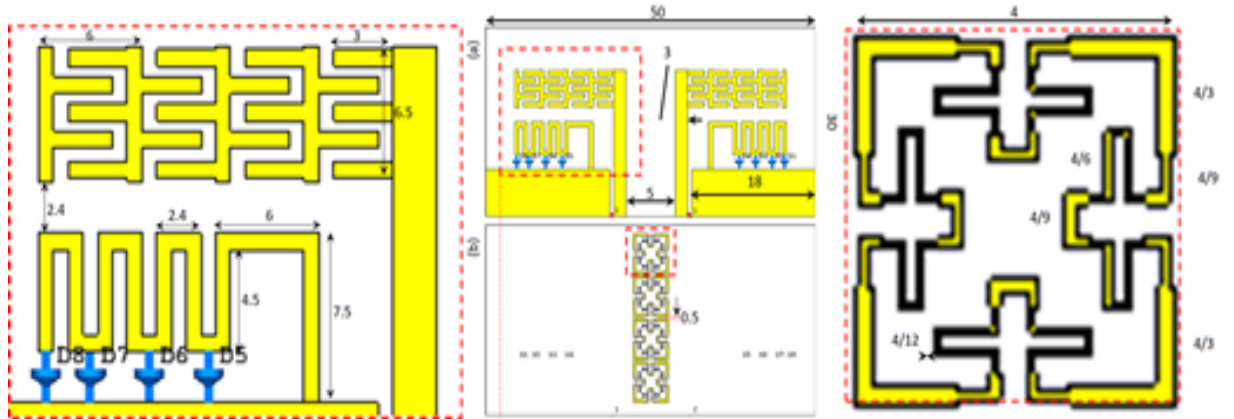
Figure 3.10. Antenna geometrical details in (mm) scale: (a) Front view and (b) back view.

3.3.2. MTM Analysis and Discussion

The proposed MTM structure is constructed from a 1D array with four unit cells as seen in Figure 3.10(b). The individual unit cell is shaped as the Minkowski fractal of the third iteration. To investigate the proposed unit cell properties, a circuit model is derived to explain the performance based on a transmission line theory. Basically, such a unit cell can be translated to a circuit model of a combination of right and left-hand branches as shown in Figure 3.11(a).

Numerically, the proposed unit cell is investigated from different orientation directions at normal and tangential electric field incidence. Nevertheless, in such investigation, the proposed unit cell iteration is increased from 1st to 4th with 1 step increase. This is applied to ensure the effects of the iteration increase on the proposed unit cell performance. Therefore, the proposed unit cell is located inside a virtual waveguide to monitor the S-parameters spectra at the frequency band of interest. In such a simulation process, the effective medium theory is invoked by applying two electrical and two magnetic walls to the virtual waveguide. Such a process is applied to mimic the transverse electromagnetic mode generations in the form of a plane wave [45].

Now, after inserting the proposed unit cell with different orientations and different iterations, the calculated S-parameters, in terms of S_{12} spectra, are shown in Figure

43

3.11(b). It is found that the proposed unit cell provides a cut-off frequency at the frequency bands from 3GHz up 5.3GHz. Therefore, such achievement nominated the proposed unit cell to be an excellent candidate for coupling reduction in MIMO array systems. The proposed sensor design based on an equivalent circuit model is derived analytically using an analogous circuit model based on the created RLC network, which is generally constructed as an IDC in series connection with a CSI and the Hilbert fractal. The proposed structure equivalent circuit model is generated using the lumped elements Richard model [45]. The proposed circuit model is created by connecting a 50Ω input impedance RF source in series with a (R-L-C) parallel branch, as shown in Figure 3.11. The main transmission line was distinguished by an inductive section LT and capacitive air gaps Cgap, which were previously depicted in Figure 3.11. The suggested circuit model S-parameters are examined and compared to those derived using CST MWS. According to the mentioned lumped parts, which are modeled in Advanced Devices Simulator (ADS). The evaluated RLC components are listed in Table 3.2.
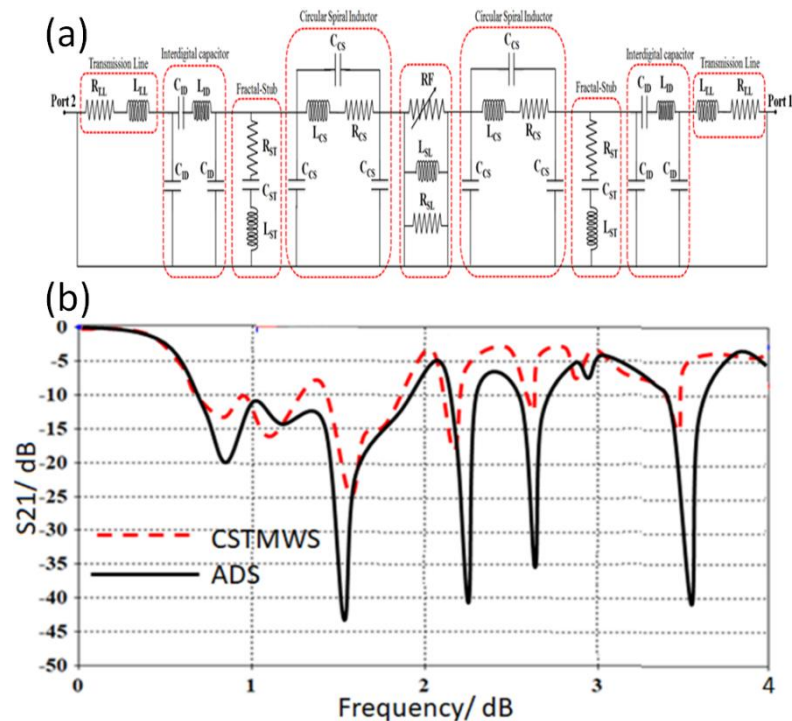
Figure 3.11. Circuit model of the proposed MTM structure: (a) Equivalent circuit and (b) S_{12} results.

44

Table 3.2. Equivalent circuit model lumped elements.

Element	Value
Resistance of the left hand (RLH)	12.2 Ω
Resistance of the right hand (RRH)	50 Ω
Conductance of the left hand (GLH)	0.1 S
Conductance of the right hand (GRH)	4 S
Capacitance of the left hand (CLH)	1.1pF
Capacitance of the right hand (CRH)	3.1pF
Inductance of the left hand (LLH)	3nH
Inductance of the right hand (LRH)	2.2nH

3.3.2.1 Design Methodology

Monopole antenna performance

In this section, the proposed monopole element performance in terms S11 spectra are investigated with respect to varying the separation distance between the monopole and the ground plane (Xg). Therefore, the considered distance Xg is changed from 1mm to 5mm with a step of 1mm with respect to monitoring S11 spectra as shown in Figure 3.12. It is observed from the obtained results, the antenna provides two frequency bands around 1.9GHz and 4.5GHz. Nevertheless, it is seen that the proposed antenna matching impedance is insignificantly changed with changing Xg at the first band, however, at the second band, the matching impedance is enhanced significantly at Xg=3mm; then, it returns back degraded due to increasing the distance. Also, it is observed that the frequency resonance location is not changed due to the fact of keeping the monopole length fixed to a certain length that has no effect on the current motion [37]. Moreover, it is observed that the generated frequency resonances are relative to the multiple constants of the halves of the wavelengths; which depends on the antenna's electrical lengths harmonics [46]. Consequently, the length of the proposed monopole is found to be relative to the physical length after the proposed CPW feeding structure. Such observation reveals

that the capacitive effects between the antenna ground plane and the monopole structure could accumulate the electrical charges significantly to increase the input impedance of the antenna over the source impedance [47]. For this, the authors considered Xg=2+1mm is the best chose to next design step; this is because the matching is found to be around -35dB at 4.35GHz.
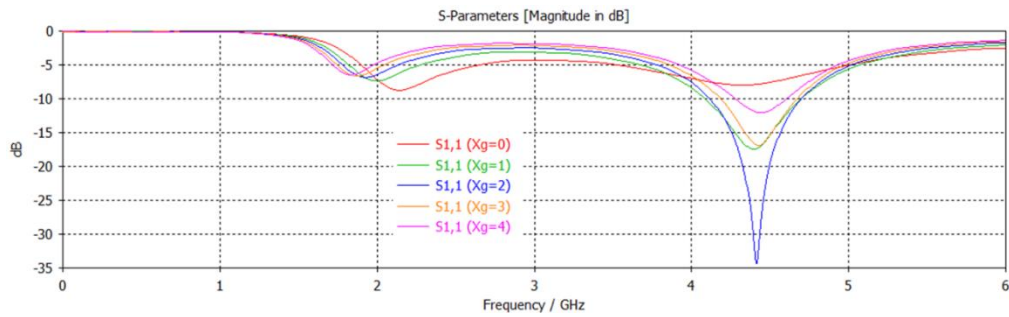
Figure 3.12. The obtained S_{11} spectra for the proposed antenna with changing X_g.

Now, to investigate the effects of increasing the ground plane length on the antenna frequency resonance, the authors considered Xg=3mm, but the ground plane length is changed from 8mm to 5mm with a step of 1mm. It is observed with decreasing the ground plane length, a significant decay in the antenna second mode frequency resonance. Therefore, it is concluded the ground plane length (Yg) is better to be 5mm for our applications. Reducing the length to less than 5mm is not very desired during the fabrication process of soldering limitations [48]. The calculated results are shown in Figure 3.13 in terms of S11 spectra with respect to varying the ground plane length (Yg).
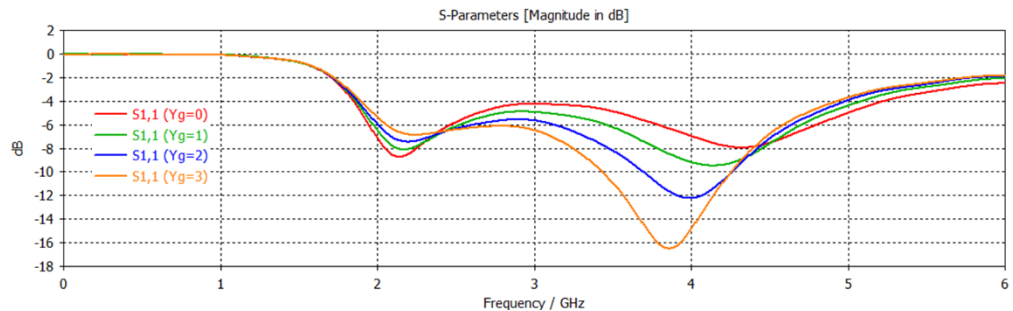
Figure 3.13. The obtained S_{11} spectra for the proposed antenna with changing Yg.

For further analysis, the authors applied a study to realize the effects of varying the monopole width on the antenna S_{11} spectra. Therefore, the monopole width (X_m) is changed from 1mm to 5mm. It is found that no significant variation in the S_{11} spectra in terms of bandwidth, matching, and frequency resonance as depicted in Figure 3.14.

This is attributed to the fact of current motion is usually on the antenna length that follows the dimension with more conduction area [37]. For this, it is well known such phenomena in different previous publications that discussed the current motion on the antenna maximum dimension [37].
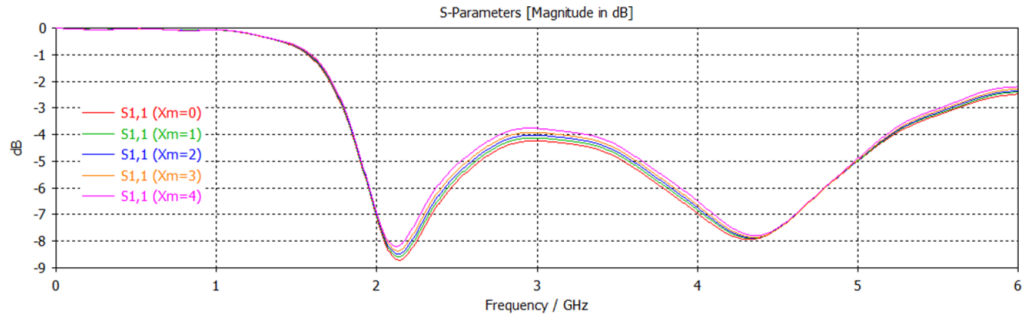
Figure 3.14. The obtained S_{11} spectra for the proposed antenna with changing X_m.

Interdigital Capacitor Effects

Since the introduction of IDC structure on the proposed antenna performance could realize a significant change, the authors applied a study to evaluate the antenna S11 and gain spectra. Therefore, the proposed IDC iteration number is changed from 1st to 4th degree. The effects of that on S11 and gain spectra are shown in Figure 3.15(a). We realized that the proposed antenna bandwidth of the second mode at 3.8GHz is significantly affected. Another mode is found to be generated at 5.8GHz due to the proposed IDC introduction as seen in Figure 3.14(b). An approximate expression for the interdigital capacitance is given by [49].

$$C = \frac{\epsilon_r + 1}{W'} l \left[(N-3)A_1 + A_2 \right] \qquad (1)$$

Where C is the capacitance per unit length (l) with respect to the finger width (W), A1 (the interior) and A2 (the two exteriors) are the capacitances per unit length of the

fingers, N is the number of fingers and can be expressed in microns. For infinite substrate thickness (or no ground plane), A1=4.409×10-6pF/mm and A2=9.92×10-6pF/mm.

Now, the antenna gain spectra over the entire frequency band of interest are discussed with respect to the same IDC iteration variation as shown in Figure 3.15(b). It is found that the proposed antenna gain is enhanced significantly by increasing the proposed IDC iteration increase. Such a fact is attributed to the effects of the proposed IDC on the inherent inductive behavior of the proposed monopole [47]. This, the introduction of the proposed IDC minimizes the stored energy by the induction part in the monopole [50].
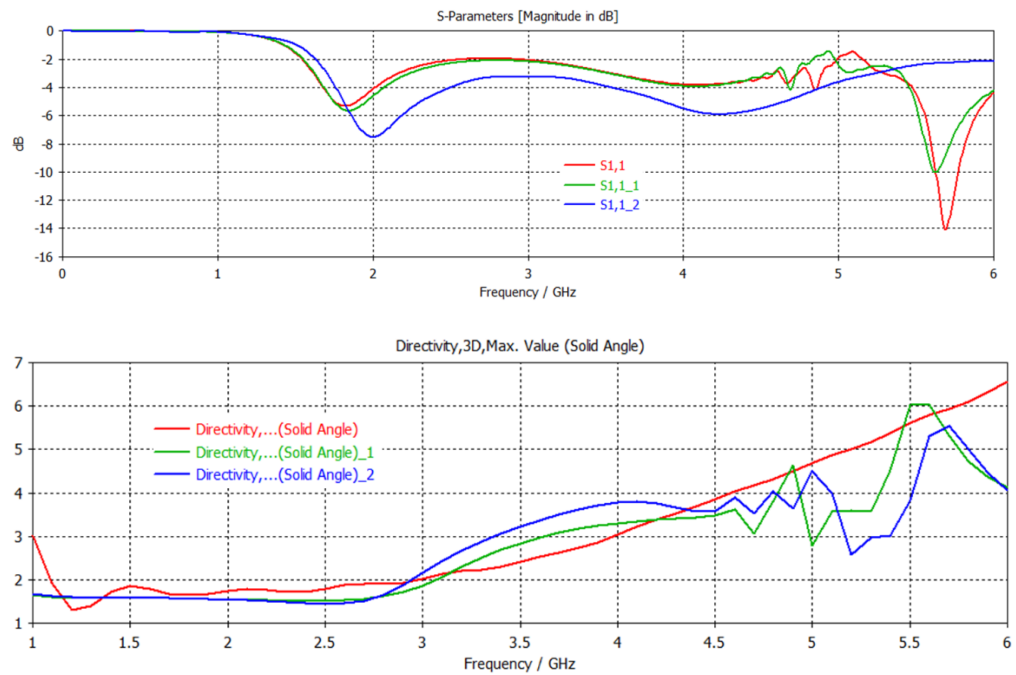
Figure 3.15. Obtained antenna performance variation with changing IDC iteration: (a) S_{11} and (b) gain spectra.

Mender Line Effects

The authors introduced a meander line to element the effects of coupling between the ground plane and the antenna parts. Such coupling is due to the effects of the electrical field fringing from the antenna edges [37]. The effects of such fringing could realize a further loss in the antenna performance specifically in terms of gain

[46]. We decided to apply a parametric study on the proposed meander line by changing the turn number from 1 turn to 5 turns with respect to S11 and gain spectra variation. As shown in Figure 3.16(a), it is found that the proposed antenna operates over several frequency bands and they increased with increasing the turn number. Such observation is due to the fact of the current path is furtherly can be increased on a meander line [50]. Therefore, the introduction of the proposed meander line is found to be an excellent candidate to realize a significant enhancement in the antenna size reduction.

Now, the antenna gain is found to be increased with increasing the turn number as seen in Figure 3.16(b). This realizes a significant enhancement due to the reduction in storing losses. Such reduction is attributed to the negative effects of the induction part by the mender line on the capacitive behavior of the ground plane with respect to the other antenna parts. It is good to mention that the authors did not increase the turn number furtherly, because the effects of increasing the turn number on the antenna performance become very slow after the 3rd turn and the antenna size limitations.

(a)

(b)
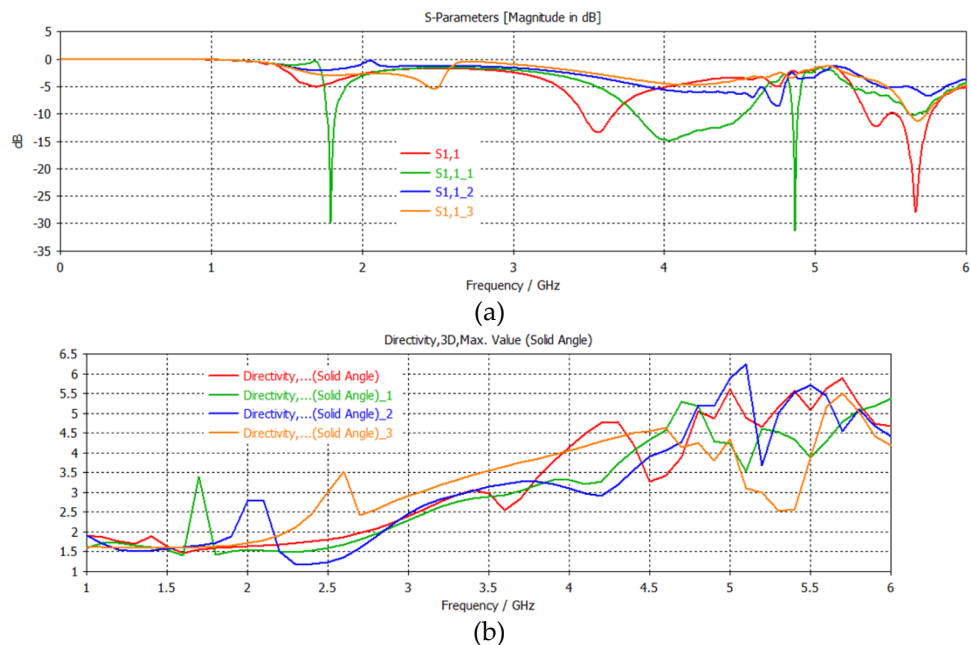
Figure 3.16. The obtained S_{11} and gain spectra for the proposed antenna with changing IDC iteration changing.

49

MIMO Array Performance

Now, the proposed antenna is designed to be configured as an array with two elements as shown in Figure 3.10. Therefore, to specify the effects of coupling on the proposed antenna performance, the separation distance (D) between the antenna elements is changed from 10mm to 25mm. As seen in Figure 3.17(a), the proposed antenna array S11 spectra are insignificantly affected by increasing D. This is a usual response because the fact of changing S11 spectra is relative to varying the antenna elements dimensions [37]. However, in the case of S12 spectra, the manner of the antenna mutual coupling variation is different; where it is increase with decreasing the distance between the antenna elements as shown in Figure 3.17(b).

Figure 3.17. The obtained S-parameters spectra for the proposed antenna array with changing D: (a) S_{11} and (b) S_{12} spectra.

Our philosophy in this research is to reduce the antenna element size within a miniaturized array configuration by adding MTM defects. Such addition can be invested to minimize the separation distance ultimately to 6mm with coupling effects in terms of S12 below -20dB as seen in Figure 3.18 Such performance is compared to the antenna array with and without MTM defects. The fact of reducing the mutual coupling with low separation distance is that such MTM defects apply a high surface impedance by producing a negative dielectric constant (-εr) over the frequency bands

50

of interest. Therefore, the propagated surface current towered the array center is decayed by a vancient mode with a significant attention factor [51].
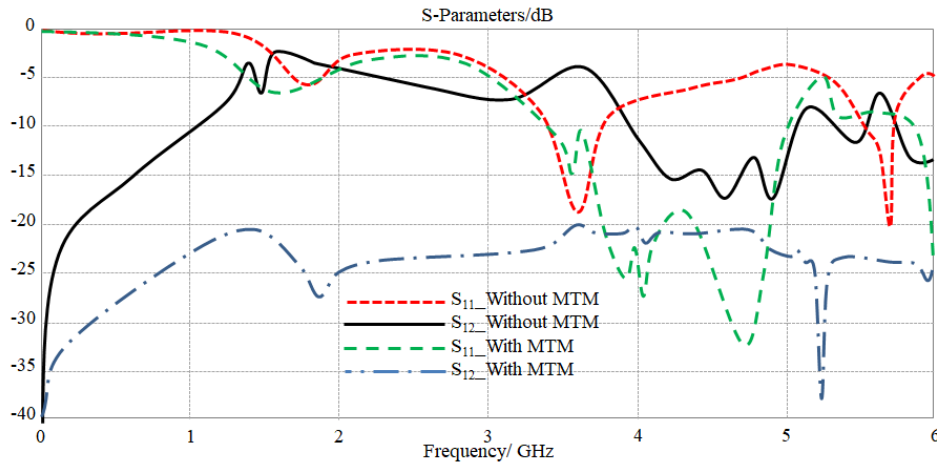
Figure 3.18. The obtained S-parameters spectra for the proposed antenna array with and without MTM defects.

Now, the proposed antenna array is introduced to a metamaterial unit cell column in the back panel to eliminate the mutual coupling between the antenna edges. In our design, we introduced the proposed unit cell parametrically, from one to four with the step of the one-unit cell, with the aim of minimizing the mutual coupling altimetry.

Therefore, it is observed from the evaluated S-parameters results, in Figure 3.18, significant enhancement in the antenna bandwidth is achieved after the proposed metamaterial introduction; see Figure 3.19(a), with increasing metamaterial unit cell number. Consequently, the antenna mutual coupling is found to be decreased with increasing the unit cell number that maintains the separation distance between the antenna elements about 0.1 λ at 3.5GHz. Therefore, we found from the proposed parametric study, the minimum S12 reduction is achieved when four-unit cells are introduced to the proposed array as seen in Figure 3.19(b). Such reduction, it is good to mention, is found to be overall the frequency band from 3.5GHz to 5.5GHz with S12 below -20 dB and S11 ≤ -10 dB. It is concluded from these results; the proposed metamaterial array behaves as a stop band filter to reject most of the frequencies within the frequency band of interest as discussed later.
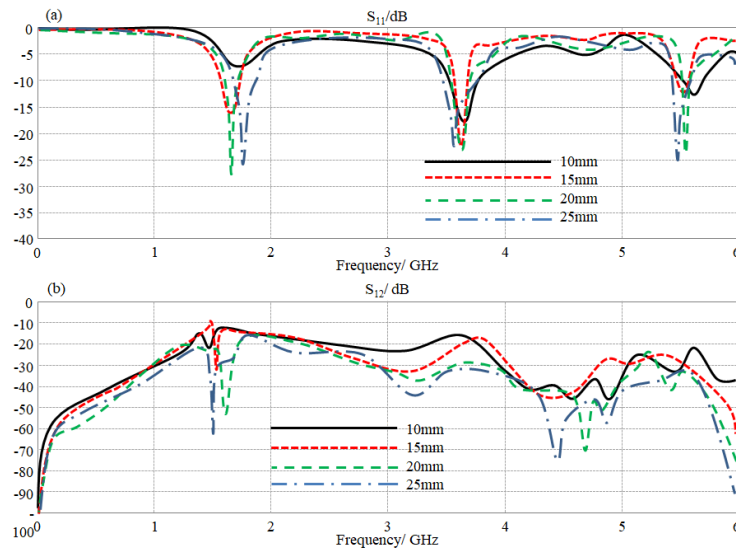
Figure 3.19. The obtained S-parameters spectra for the proposed antenna array with changing MTM defects number: (a) S_{11} and (b) S_{12} spectra.

3.3.2.2. Antenna Reconfiguration Study

The proposed antenna array is designed for reconfigurable MIMO systems based on sub-6GHz to suit the applications of 5G networks. Therefore, it is very obvious such systems require antenna terminals of configurable performance [52]. In our design, we introduced four LDR switches to control the antenna performance. The location of positioning the proposed LDR switches is selected to be between the meander line structure and the antenna ground plane. Such location is considered to reflect out of phase the surface wave, 90o phase difference, to cancel the capacitive part inductively; which realizes the frequency shift through imaginary part consolation [10].

Our target is to control the surface current on the antenna element by controlling the real impedance at a certain point; in which most of the charge accumulation could accrue [10]. It is well known from the literature that such accumulation of electric chargers happens at the meander lines corners [53]. Therefore, it is very wise to consider these locations for introducing the LDR switches. Nevertheless, the ground plane is a very saturated conductive surface that realizes an excellent phase reflection to obtain the imaginary part consolation for frequency reconfiguration [2]. In such a manner, each antenna element is introduced to four LDR switches to control the antenna performance in terms of frequency bandwidth and gain as listed in the antenna truth table 3.3. It is found from such a study a significant change could accrue when switching scenarios of the proposed LDR terminals change. Such variation in the antenna response is attributed to the fact of varying the surface current on the antenna path and the inductive/capacitive behaviors to realize a significant bandwidth variation. It is good to mention that the proposed work is conducted to only for cases due to the space limitations. For more details, the authors presented the variation in the S11 and S12 spectra in Figure 3.20; which found non-remarkable variation in the antenna mutual coupling. This is due to the fact that S12 spectra are usually a measure of coupling between the adjacent antennas that have no response to LDR switching scenarios. This observation was discussed earlier in [2].

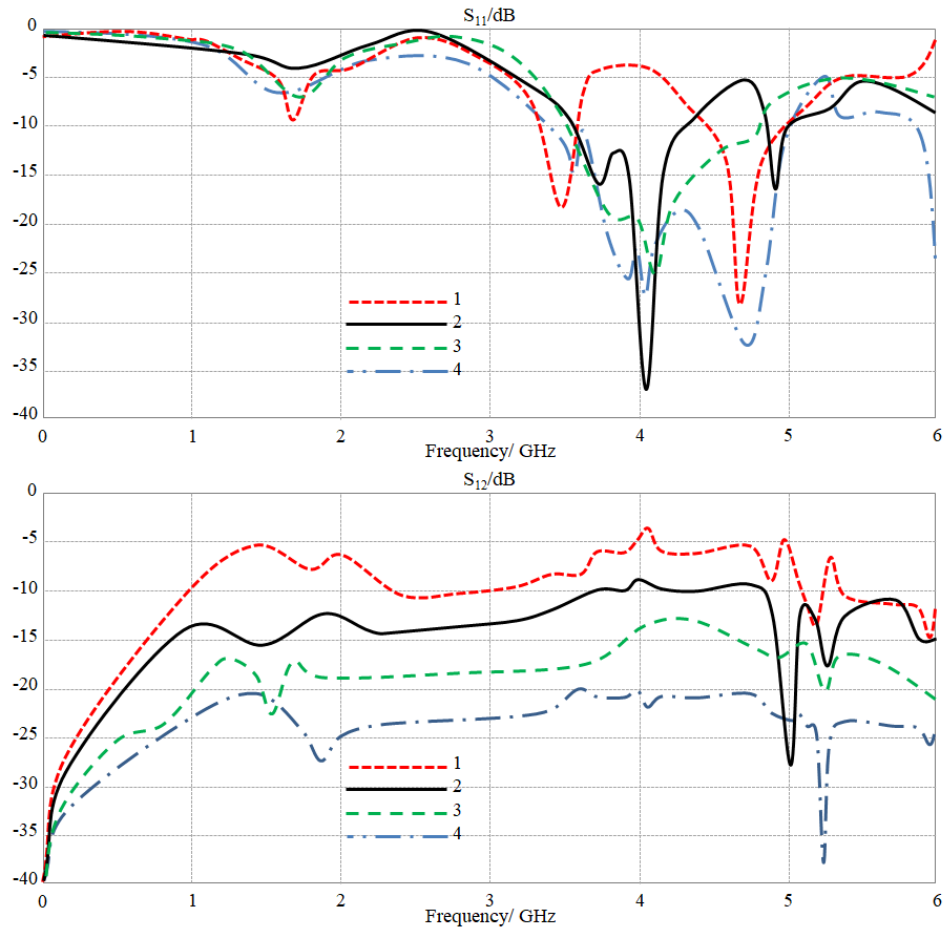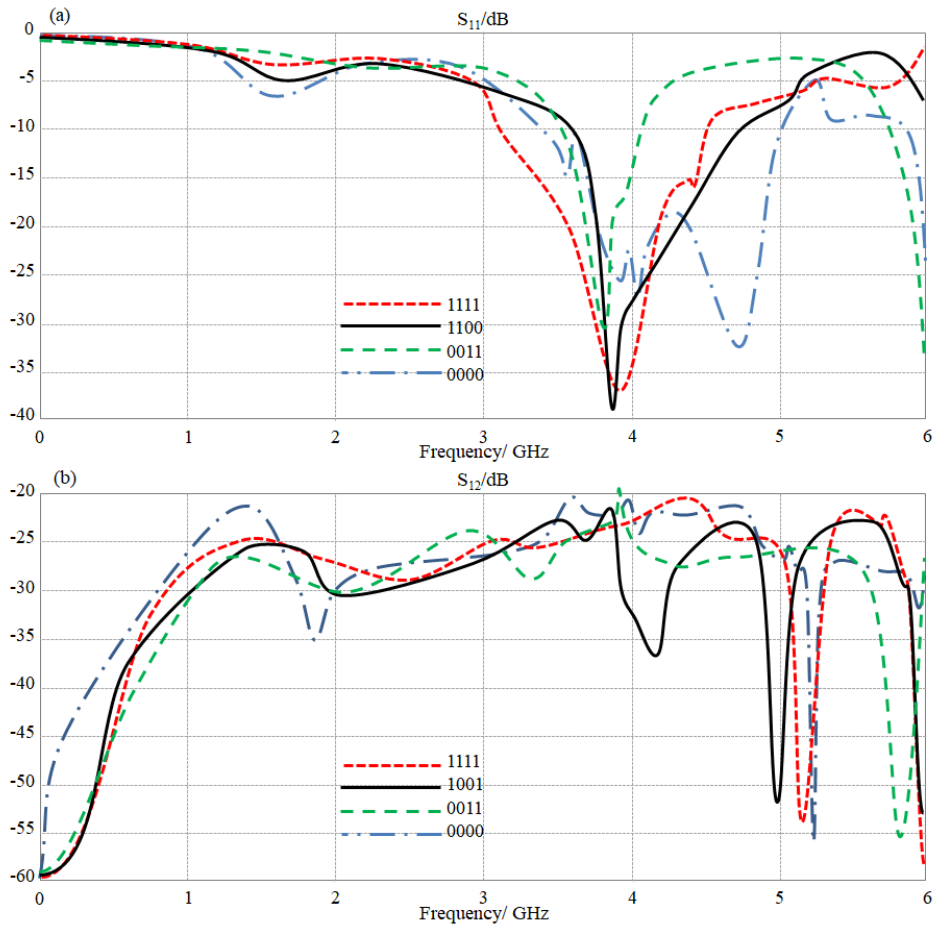Figure 3.20. The obtained S-parameters spectra for the proposed antenna array with changing switching scenarios: (a) S_{11} and (b) S_{12} spectra.

Table 3.3. Antenna performance with different switching scenarios.

Switching Scenario	Frequency/GHz	Gain/dBi
0	3-5.5	4.5
11	3.5-4.7	5.1
1100	3.4-4.1	6.2
1111	3.1-4.6	8.1

54

3.4. A NOVEL MIMO ANTENNA INTEGRATED WITH A SOLAR PANEL AND EMPLOYING AI-EQUALIZATION FOR 5G WIRELESS COMMUNICATION NETWORKS

3.4.1. MIMO Antenna Design

The proposed MIMO antenna system comprises four antenna elements strategically positioned around the sides of a cuboid structure, illustrated in Figure 3.21(a). Initially, the antenna specifications were determined in accordance with the application requirements. Fabrication was carried out on a substrate from the AD1000 family of Rogers, possessing a thickness of 1 mm, relative permittivity (ε_r) of 10.2, and loss tangent (tanδ) of 0.00021. The cuboid hosting the MIMO antenna had dimensions measuring 30×38×38 mm³.

Each of the four antennas forming the 4×1 MIMO array was energized via a common power divider. Structurally, each MIMO antenna consisted of a configuration of 3×5 radiation elements, with each radiating element comprised of four triangular-shaped radiators arranged to form a square shape with small gaps in between. These elements were framed within microstrip lines connected to a shared 50Ω feedline at the base of the antenna, as depicted in Figure 3.21(a). On the reverse side of the antenna, a truncated ground plane was employed, with each MIMO antenna being backed by a conductive reflector. Adjacent to each reflector were 2×6 conductive reflectors arranged in a configuration mirroring the triangular radiation elements.

The design parameters were tailored for operation within the sub-6 GHz frequency band (2.2 GHz to 6 GHz), with the requirement of $S_{11} \leq$-6 dB. Utilizing a 3D full-wave finite element method via CST Studio Suite, the antenna's performance was carefully designed and optimized. The final dimensions of the optimized antenna are presented in Figure. 3.21(a). Following fabrication, the proposed MIMO antenna in 3.21(b). underwent measurement for validation purposes. The design specifications ensure that the proposed MIMO antenna maintains isolation (S_{12}, S_{13}, and S_{14}) better than -15 dB across the entire frequency bands of interest. Furthermore, the antenna achieves a maximum gain of 7.4 dBi at 5.8 GHz, aligning with the demands of 5G systems, as well as LTE, GSM, WiMAX, and Bluetooth applications.
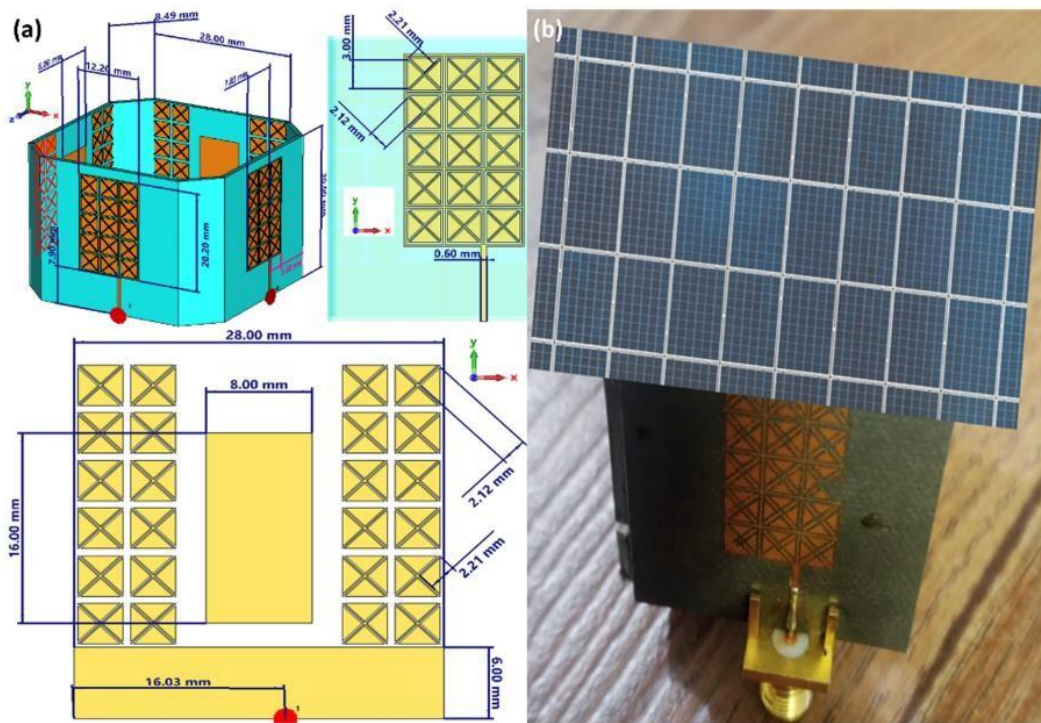
Figure 3.21. The proposed MIMO antenna, (a) 3D antenna structure, and (b) the fabricated prototype with solar panel.

3.4.2. Antenna Design Methodology and Analysis
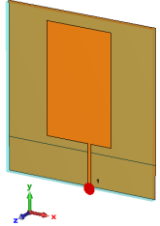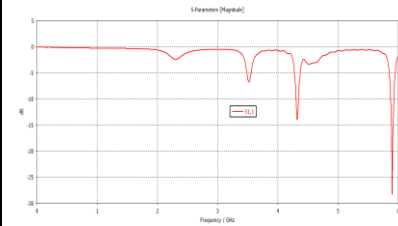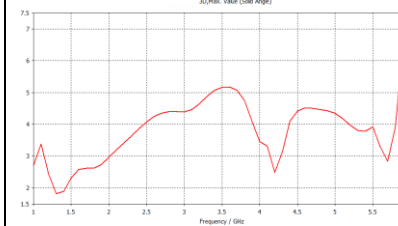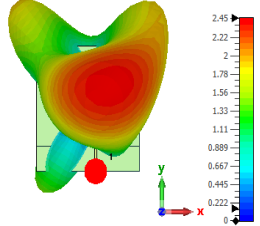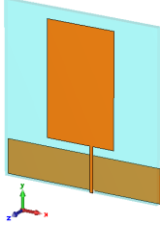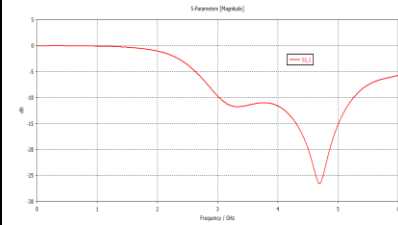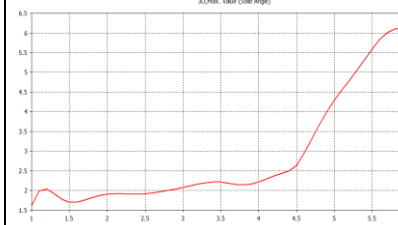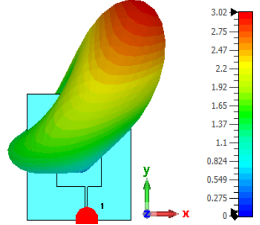
The proposed antenna design underwent simulation using CST Studio Suite, followed by a thorough performance analysis via a parametric study to achieve an optimal design. The design methodology employed is detailed in this section. The process for implementing the proposed antenna is illustrated in Table 3.4.

3.4.2.1 Single Antenna

Initially, the antenna geometry conforms to a standard microstrip patch configuration with a ground- plane, and it is edge-fed using a 50Ω feedline. In the first step, the antenna exhibits a narrow impedance bandwidth of more than -10 dB at 4.3 GHz and 5.9 GHz, with an average gain of approximately 4 dBi across the 2 GHz to 6 GHz range. To broaden the antenna's impedance bandwidth, the ground-plane is truncated in the second step. This adjustment extends the impedance bandwidth to better than -

10 dB between 3 GHz and 5.3 GHz, albeit with a slightly reduced average gain of around 3.5 dBi within the 2 GHz to 6 GHz range. Moving to the third step, the single patch antenna is partitioned into 3×5 elements, with each radiating element comprised of four triangular-shaped radiators arranged in a square configuration with small interstitial gaps. A single conductive reflector is etched onto the back of these radiating elements. Although this modification extends the impedance bandwidth, predominantly between 3 GHz and 5.5 GHz, the average gain diminishes to approximately 3.0 dBi across the 2 GHz to 6 GHz spectrum. In the fourth step, 2×6 conductive reflectors, designed to mirror the triangular radiation elements, are placed on the backside, effectively acting as metamaterial surfaces. While this adjustment contracts the impedance bandwidth to between 2.8 GHz and 4.2 GHz, the average gain experiences a modest increase to approximately 3.5 dBi within the 2 GHz to 6 GHz range.

Table 3.4. Design steps and associated antenna characteristics.

Step	Antenna Geometry	Reflection coefficient (S₁₁)	Gain (dBi)	Radiation Pattern
1				
2				
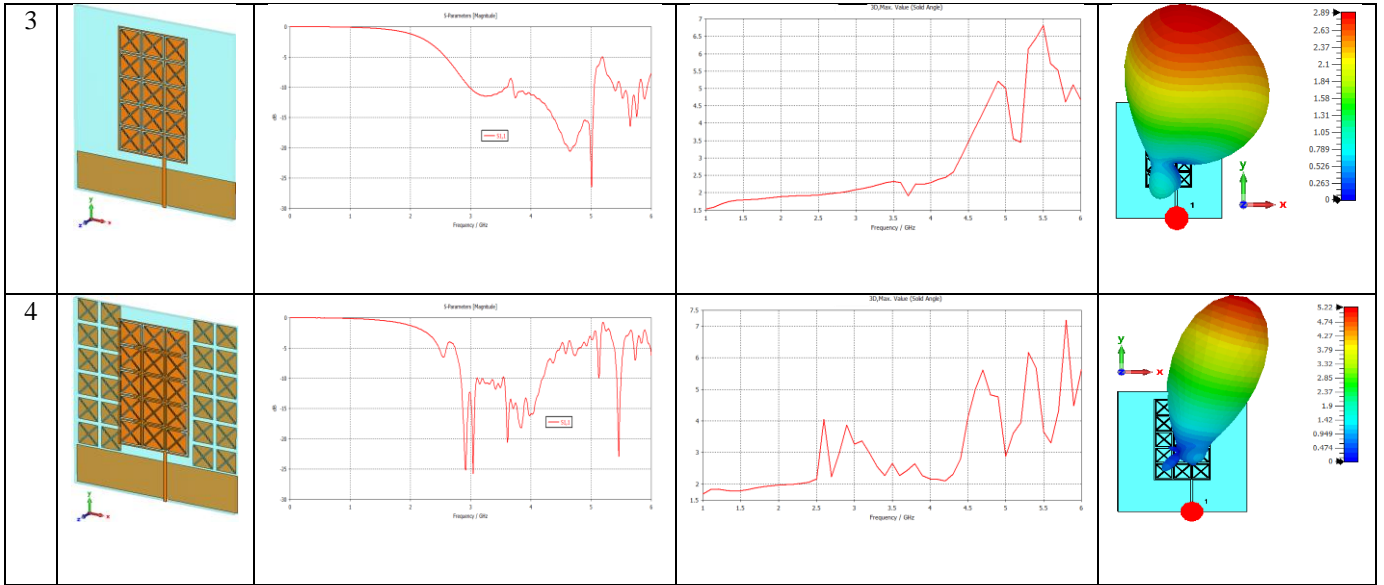
3.4.2.2 MIMO Antenna

In the depicted setup (Figure 3.21), antennas are positioned on each of the four sides of a cuboid structure. To determine the optimal distance between the antennas and the metamaterial-based reflective surface, a parametric study was conducted. Figure 3.22 shows the impact of varying this distance, ranging from 2 mm to 6 mm, on both the reflection coefficient (S_{11}) and the isolation between different ports (S_{12}, S_{13}, S_{14}). It is evident from the study that a gap of 6 mm yields significantly improved reflection coefficient compared to a 2 mm gap, especially when the electromagnetic coupling between the antennas and the reflective surfaces is weak. Furthermore, maintaining a 6 mm gap results in an average improvement of approximately 15 dB in isolation across the frequency range from 2 GHz to 6 GHz. This underscores the effectiveness of a larger 6 mm gap not only in optimizing the reflection coefficient but also in enhancing isolation, particularly within the specified frequency range.
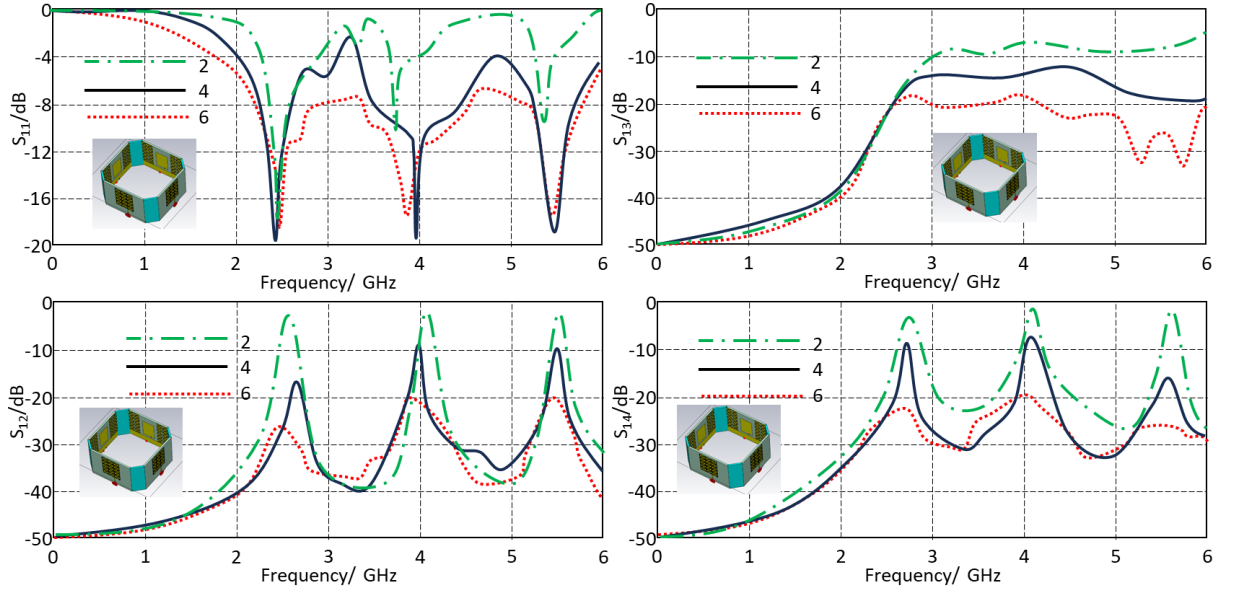
Figure 3.22. Spectra of reflection coefficient (S_{11}) and isolation between ports 2 to 1 (S_{12}), 3 to 1 (S_{13}), and 4 to 1 (S_{14}) of the proposed MIMO antenna array.

3.4.2.3. Solar Panel Introduction

In the proposed setup, a solar panel was integrated atop the MIMO antenna array. To explore the impact of the vertical distance between the solar panel and the array, a systematic parameter study was conducted, varying the distance from 1 mm to 4 mm in 1 mm increments. This investigation aimed to assess how these variations influenced the array's (S_{11}) and the isolation between different ports (S_{12}, S_{13}, S_{14}). Figure 3.23 shows that a vertical gap of 4 mm provides the most favorable reflection coefficient response, exhibiting an enhancement of approximately 4 dB across the frequency range from 2 GHz to 4 GHz. Correspondingly, the isolation between ports experiences a notable improvement of approximately 15 dB within the same frequency span when maintaining this 4 mm gap. This finding underscores the significance of optimizing the vertical distance between the solar panel and the antenna array to achieve optimal performance in both reflection coefficient and isolation metrics.
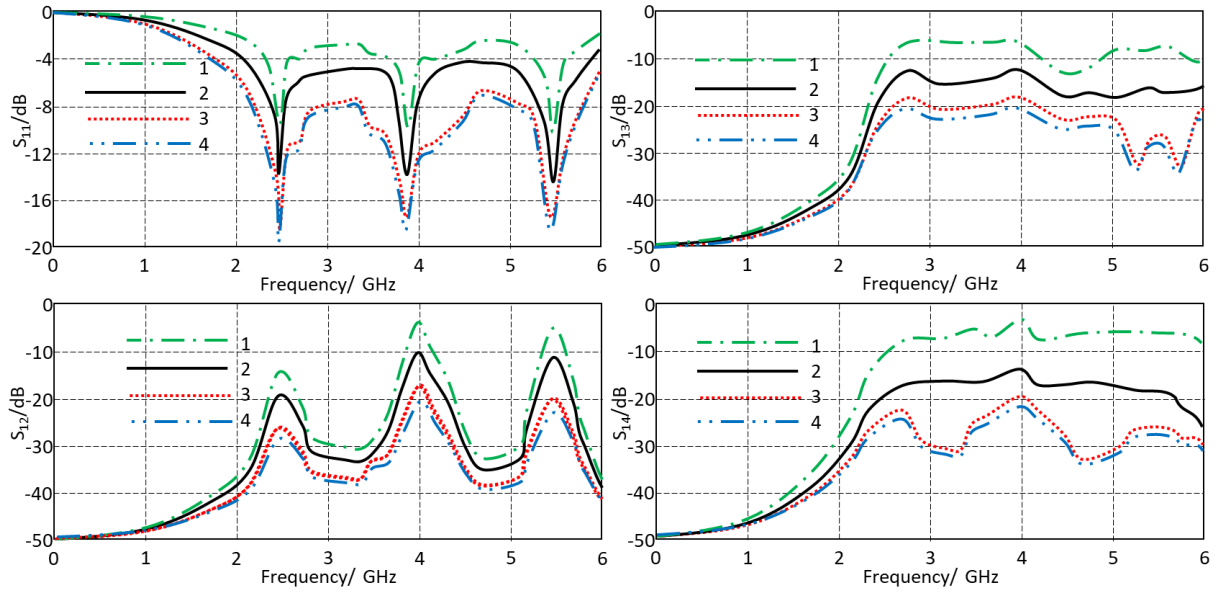
Figure 3.23. Spectra of reflection coefficient (S_{11}) and isolation between ports 2 to 1 (S_{12}), 3 to 1 (S_{13}), and 4 to 1 (S_{14}) of the proposed MIMO antenna array with a solar panel.

3.4.2.4. Configuration Scenarios

The proposed antenna has been engineered to exhibit adaptable radiation performance by influencing its surface currents. This feat was accomplished through the integration of five PIN diode switches connected between the antenna reflector and the partial ground plane. The efficacy of this design was assessed using the Mean Square Error (MSE) to ascertain path loss (γ) through an AI regression algorithm.

In the context of communication links, a power management system gauges if the received signal power falls below 70 dBm. Should this criterion be met, the system taps into solar panel reserves to amplify the incoming signal. Subsequently, an AI algorithm evaluates the channel's quality by analyzing channel capacity (CC) and bit error rate (BER). Should these parameters fall below acceptable thresholds, the algorithm orchestrates a modification in the antenna's radiation directionality. This adjustment is achieved by activating or deactivating the PIN diode switches as depicted in the flowchart illustrated in Figure 3.24.
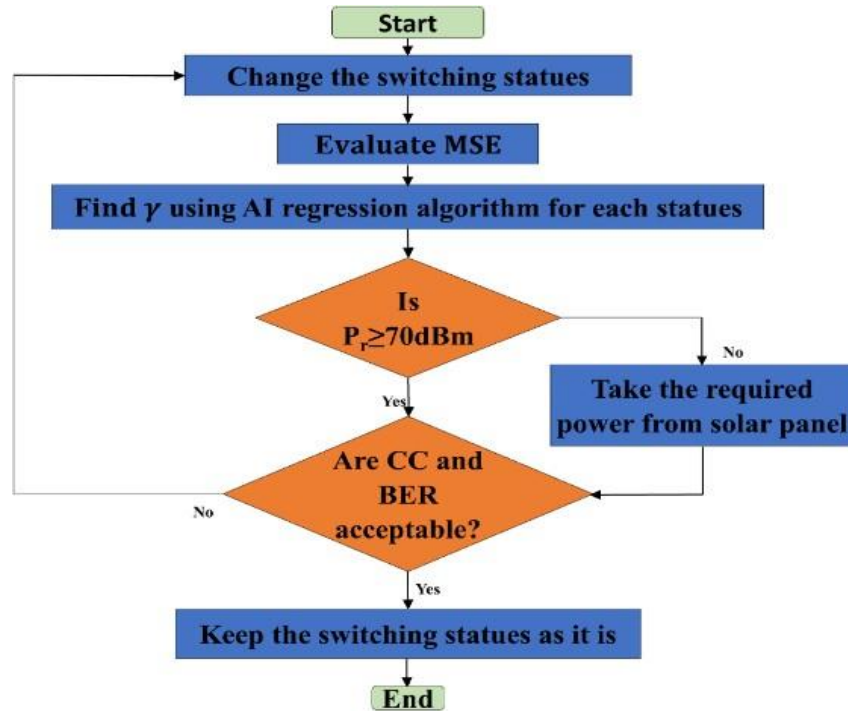
Figure 3.24. Flowchart followed to maintain acceptable channel capacity and bit error rate for effective and reliable communication link.

In our design of the MIMO antenna system tailored for Non-Orthogonal Multiple Access (NOMA) applications, we've implemented a mechanism to reconfigure the radiation direction. This functionality is essential for optimizing signal transmission efficiency in NOMA scenarios. The mechanism involves the incorporation of five PIN diode switches, strategically connected between the antenna reflector and a partial ground plane, as depicted in Figure 3.25. This figure demonstrates that activating any combination of these diodes has minimal impact on the array's reflection coefficient, ensuring stability in signal performance. However, by selectively switching these diodes, the surface currents on the antennas are altered, consequently influencing the radiation pattern, as visually represented in the figure. Of notable significance is the observation that when all diodes are switched from the off state, the radiation direction undergoes a distinct 90-degree change. This dynamic functionality enables precise control over the directionality of radiation, crucial for optimizing signal transmission in NOMA applications.
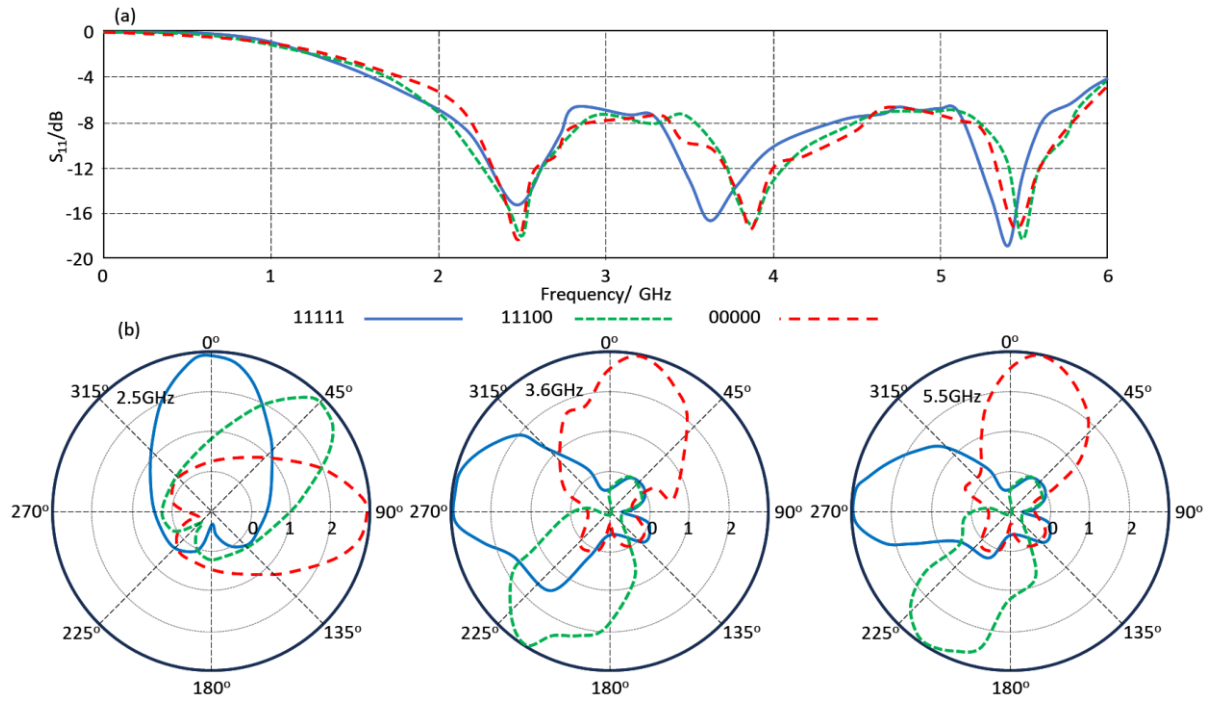
Figure 3.25. Performance of the proposed MIMO antenna array under different PIN diode switching scenarios: (a) S_{11} spectra, and (b) radiation patterns.

PART 4

RESULT AND DISCUSSION

4.1. A PRINTED MONOPOLE ANTENNA ARRAY INSPIRED BY HISTORICAL CITIES IN IRAQ

4.1.1. Result And Discussion Of First Design

To validate the obtained antenna results and ensure the quality of the performance in terms of S-parameter, gain, and radiation patterns, HFSS software package is invoked for that at the frequency bands of interest. The proposed antenna S11 and S_{12} spectra are presented in Figure 4.1(a). It is found that the proposed antenna realizes a frequency resonance at 3.45GHz and 5.8GHz with S_{11} magnitude below - 6dB to suite the applications of sub-6GHz of 5G wireless systems. The simulated results including the antenna gain spectra are shown in Figure 4.1(b). The antenna gain is found to be 2.34dBi and 2.6dBi, respectively, at 3.45GHz and 5.8GHz. Then, the simulated result in term of radiation patterns at 3.45GHz and 5.8GHz are presented in Figure 4.1(c). The radiation patterns are evaluated from CST MWS and HFSS software packages. It is seen that this antenna has radiation characteristics close to Omni-directional when Phi=0° at 3.45GHz. But, when Phi=90° the radiation characteristics achieves near bidirectional radiation pattern. At 5.5GHz, the radiation characteristics at both Phi=0° and Phi=90° achieves close to bidirectional radiation pattern.

In this research, a study was conducted on the results of previous studies, and the results obtained from those studies were compared with the results of this research. Table 4.1 presents the comparison of previous results with the current results in a simplified manner. We found that the proposed antenna array shows high size reduction with minimum mutual coupling effects with a neat shape that realizes an excellent candidate to 5G systems at sub-6GHz frequency bands. In [54], the antenna size was found smaller than our proposed design in this work with higher gain. However, their proposed design was implemented as a single antenna element not for

MIMO systems that limits their applications to sub-6GHz 5G networks. Our design is constructed as an antenna array based on two elements with maximum size of the single antenna element about 10×10mm2 to make our proposed design much smaller than all previous listed work in Table 4.1.

Table 4.1. Comparison between previous studies.

Ref.	Frequency/GHz	Gain/dBi	Size/mm^3	Substrate
[54]	3.5,5.7,8.8	4.1	25×22×1.6	FR-4
[55]	3.43	2	25×25×1.6	FR-4
[56]	0.915 , 1.575 , 2.4	/	89×87×0.762	RT5880
[57]	7	4.85	32×32×1.6	FR-4
[58]	1.8-8.1	5.5	50×50×0.8	FR-4
[59]	Narrow bands	-4.34	36×36×1.6	FR-4
[43]	9	1.6–6.4	38×35×1.57	Roger 5880
[60]	1.9,3.2	2.5-6	66×25×1.61	FR-4
[61]	2.26-8.54	-6.39	25×25×1.6	FR-4
[62]	2.26-8.54	-8.78	25×25×1.6	FR-4
[63]	2.4, 5.8	3.2,4.7	20×20×1.6	RO3210(tm)
This work	3.45, 5.5	2.34, 2.6	27×25×1.6	FR-4
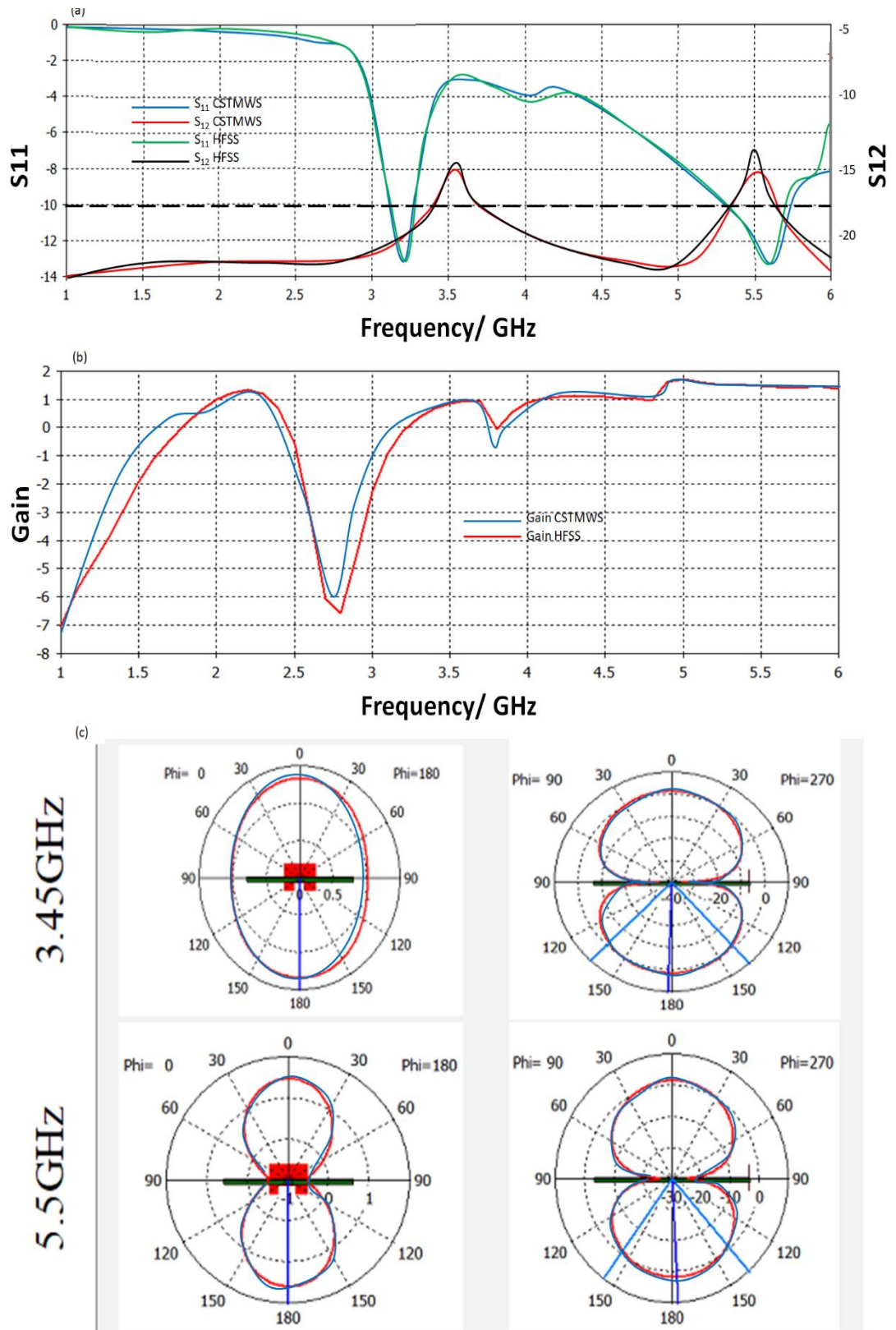
Figure 4.1. Antenna performance in terms of: (a) S-parameters, (b) gain, (c) radiation patterns.

4.2. ORIGAMI ANTENNA ARRAY IN THE SHAPED MOSQUE OF MUHAMMED AL-FATIH FOR VISUAL SIGHT ENHANCEMENT IN MODERN MIMO 5G NETWORKS

4.2.1. Result and Discussion of Second Design

4.2.1.1. MTM Characterizations:

To realize the proposed MTM unit cell performance is evaluated in terms of S-parameters spectra and dispersion diagram. Based on effective medium theory that was explained in [64], evaluated the effective constitutive parameters. These parameters describe the inherent characteristics of the proposed fractal structure at the resonance frequency band. Therefore, the permittivity, permeability, and intrinsic impedance are calculated. These calculations are applied to the proposed unit cell. In this analysis, the proposed unit cell is located inside a virtual wave guide structure to evaluate the unit cell basic characteristics. Therefore, the upper and lower walls are assumed to be perfect electric conductors (PEC). While, the other side walls are considered to be perfect magnetic conductors (PMC). Therefore, the generated waves inside such wave guides are excited from two wave guides ports to mimic TEM-like free space environment [64]. Thus, the unit cell S-parameters would be used to retrieve the basic constitutive electromagnetic properties as shown in Figure 4.2. It is found from the proposed results; the proposed unit cell provides band rejection at 3.5GHz frequency band. The obtained results from CST MWS are validated using HFSS software commercial package.
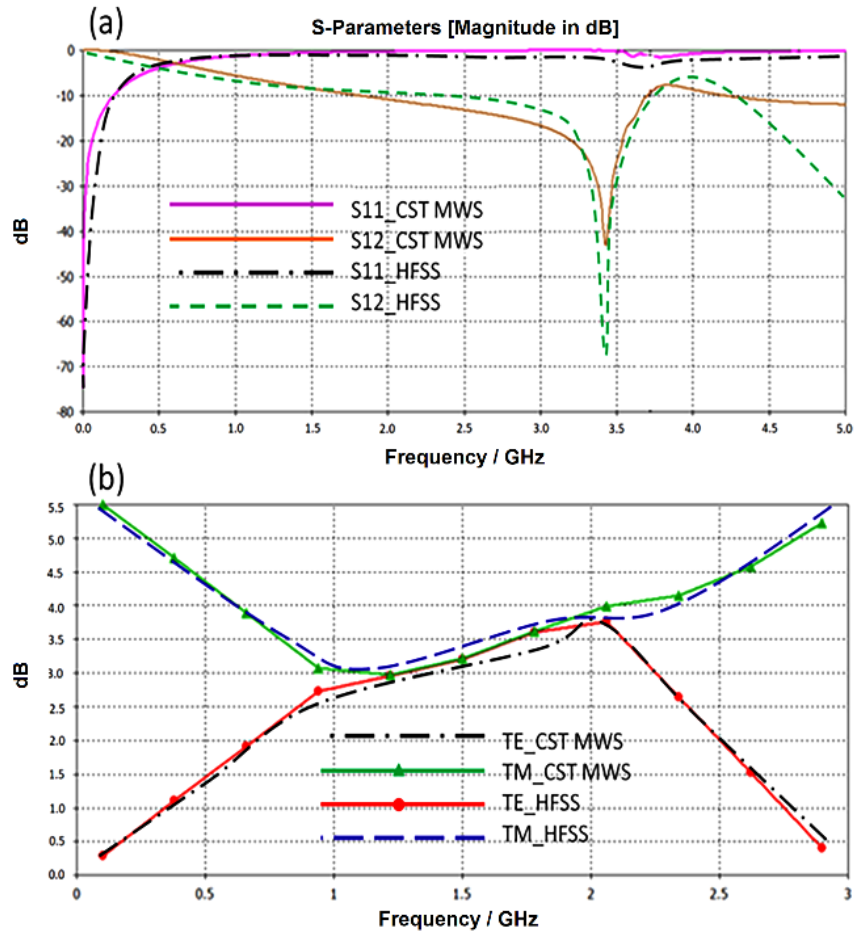
Figure 4.2. Unit cell performance: (a) S-parameters spectra and (b) Dispersion diagram.

4.2.1.2. Antenna Characterizations:

Next, the proposed antenna array performance in terms of S-parameters and radiation patterns are re-evaluated using both CST MS and HFSS software packages. An excellent agreement is found between the obtained results in terms of S-parameters, as seen in Figure 4.3.
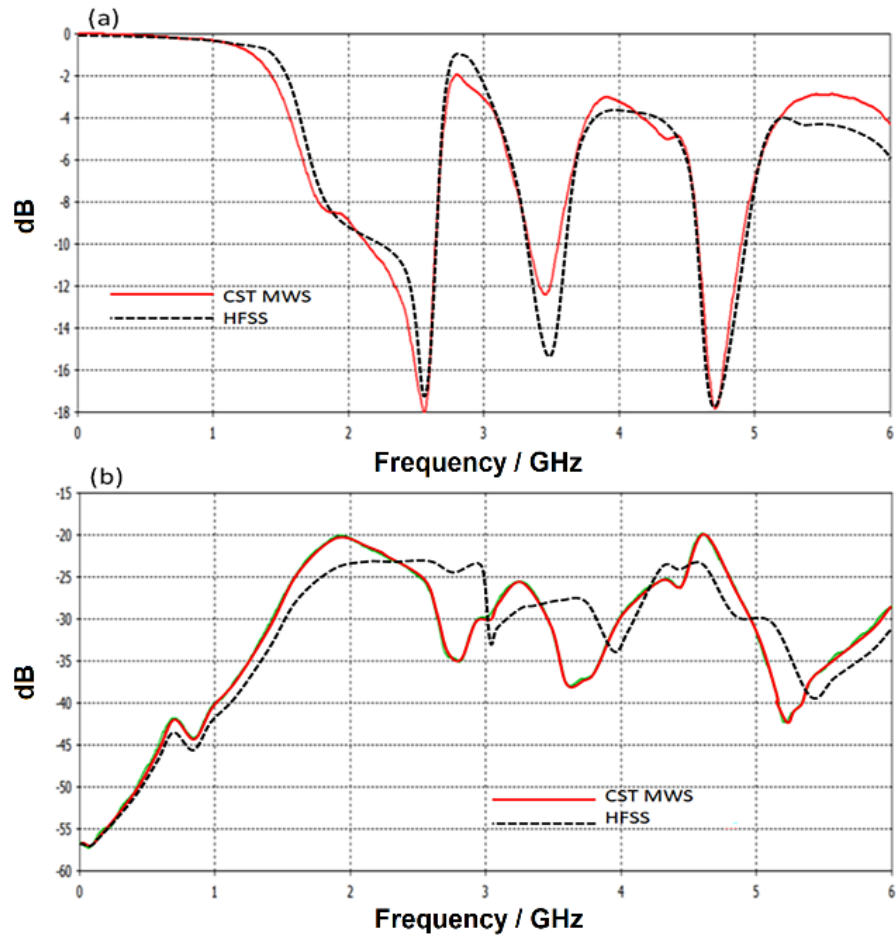
Figure 4.3. Validated S-parameters: (a) S_{11} and (b) S_{12} spectra.

However, insignificant discrepancy between the results in terms of radiation patterns due to the effect of boundary conditions differences between the two used software packages as shown in Figure 4.4. The evaluated radiation patterns are done at three frequency band of interest at 2.5GHZ, 3.5GHz, and 4.5GHz for 5G applications.
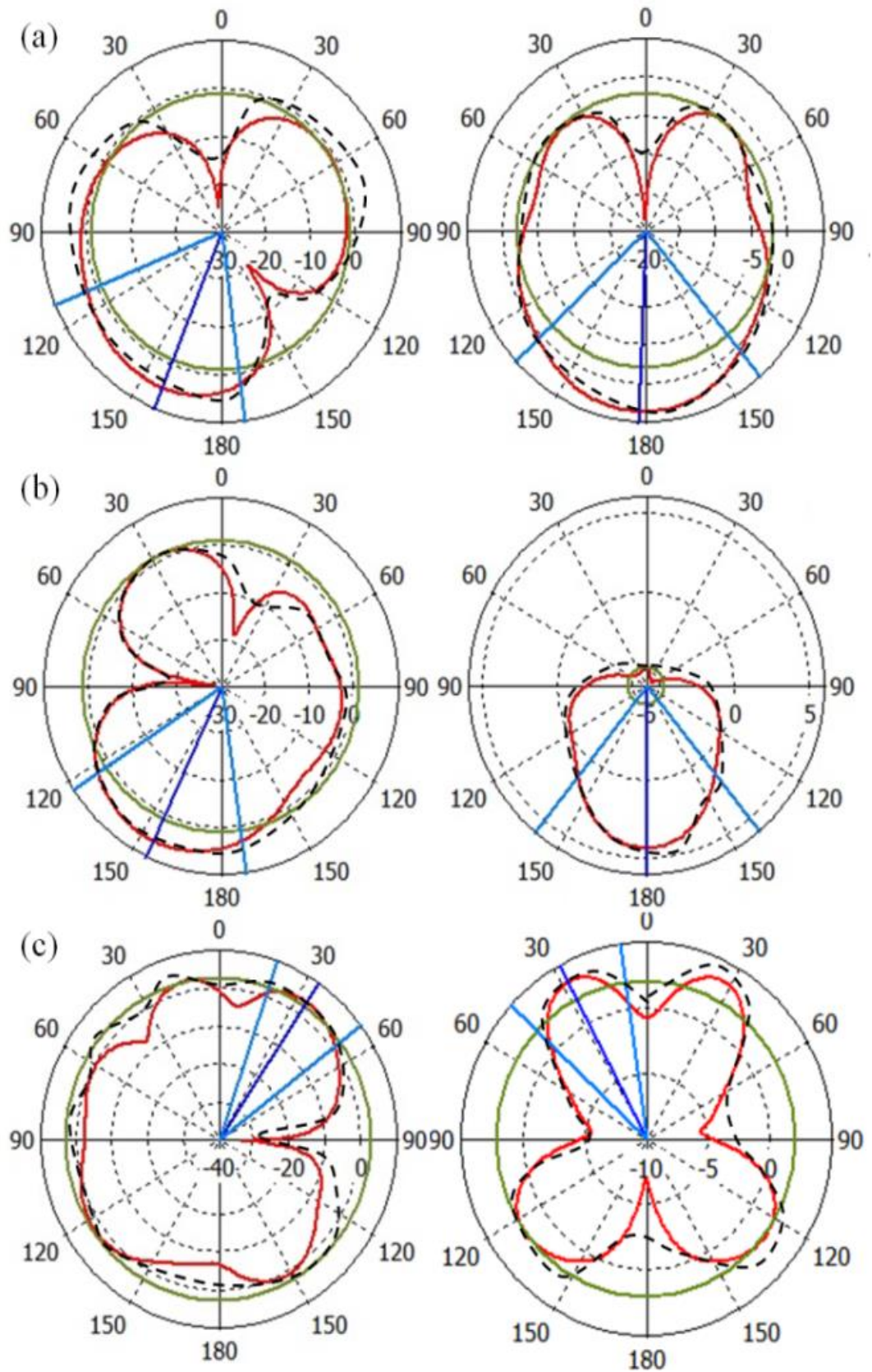
Figure 4.4. Validated radiation patterns at: (a) 2.5GHz, (b) 3.5GHz, and (c) 4.5GHz.

4.3. MINIATURIZED ANTENNA ARRAY BASED NOVEL METAMATERIAL TECHNOLOGY FOR RECONFIGURABLE MIMO SYSTEMS

4.3.1. Results And Discussion Of Third Design

Now, to validate the proposed antenna array performance experimentally, the proposed array is fabricated using a chemical wet etching process. As seen in Figure 4.5, the fabricated prototype is presented with maximum dimensions of $50\times30mm^2$. The proposed antenna S-parameters are measured using HP vector network analyzer.
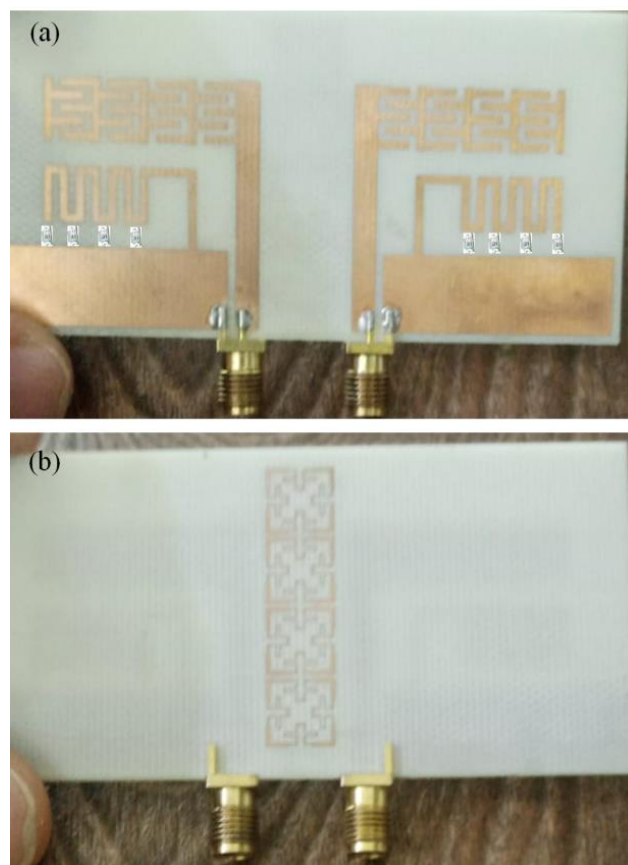
Figure 4.5. The proposed prototype: (a) front view and (b) back view.

The measured antenna radiation patterns in are considered at 3.5GHz, 4GHz, 4.5GHz, 5GHz, and 5.5GHz inside an RF chamber. This process is invoked after calibrating all processes in the channel using: Through calibration technique, open, short, and 50Ω load. The obtained result from the experimental measurements is evaluated for only two switching scenarios; when all LDR terminals are ON and OFF only. The obtained results are shown in Figure 4.6 for the two considered

scenarios in terms of S-parameters. It is found an excellent agreement between measured and simulated results.
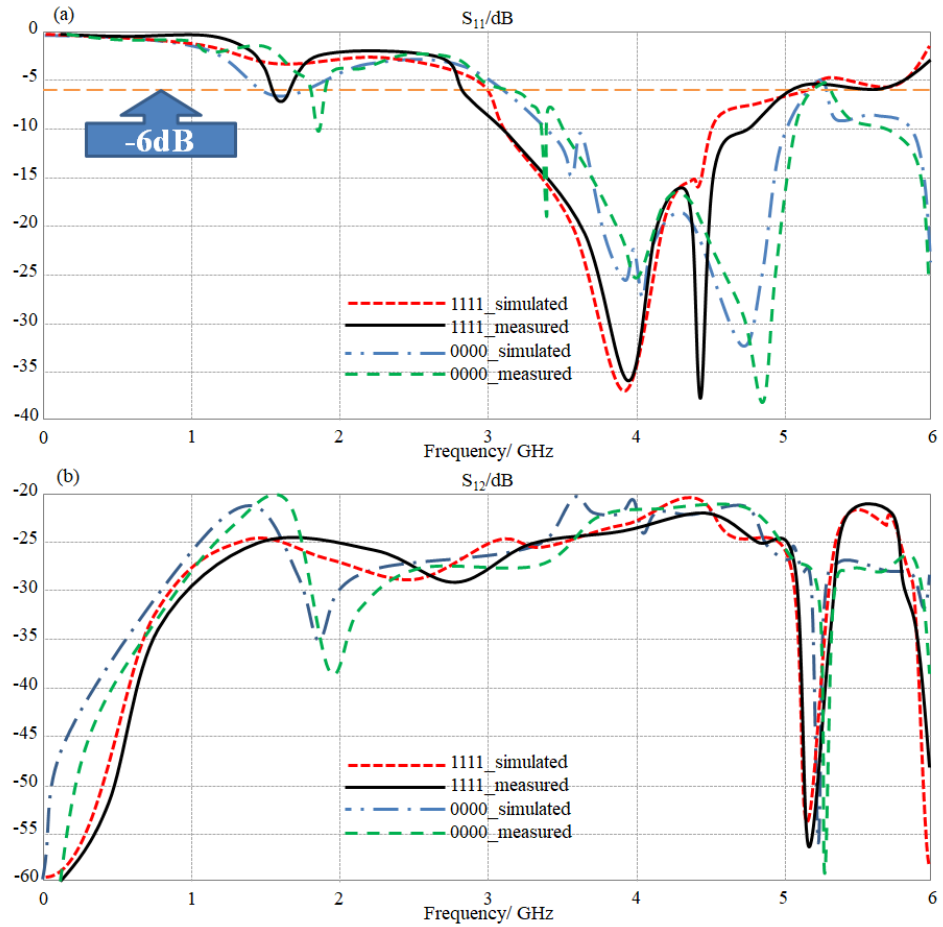
Figure 4.6. The measured S-parameters spectra for the proposed antenna array with changing switching scenarios: (a) S_{11} and (b) S_{12} spectra.

Later, the antenna radiation measurements are presented in Figure 4.7 at the frequency band of interest. The measurement reveals good agreement between simulated and measured results. It is good to mention that the presented results of the radiation patterns for the cases of all LDR switched ON and OFF only. From the obtained results it is found a variation accrues in the antenna directivity due to the surface current change as discussed later.

71
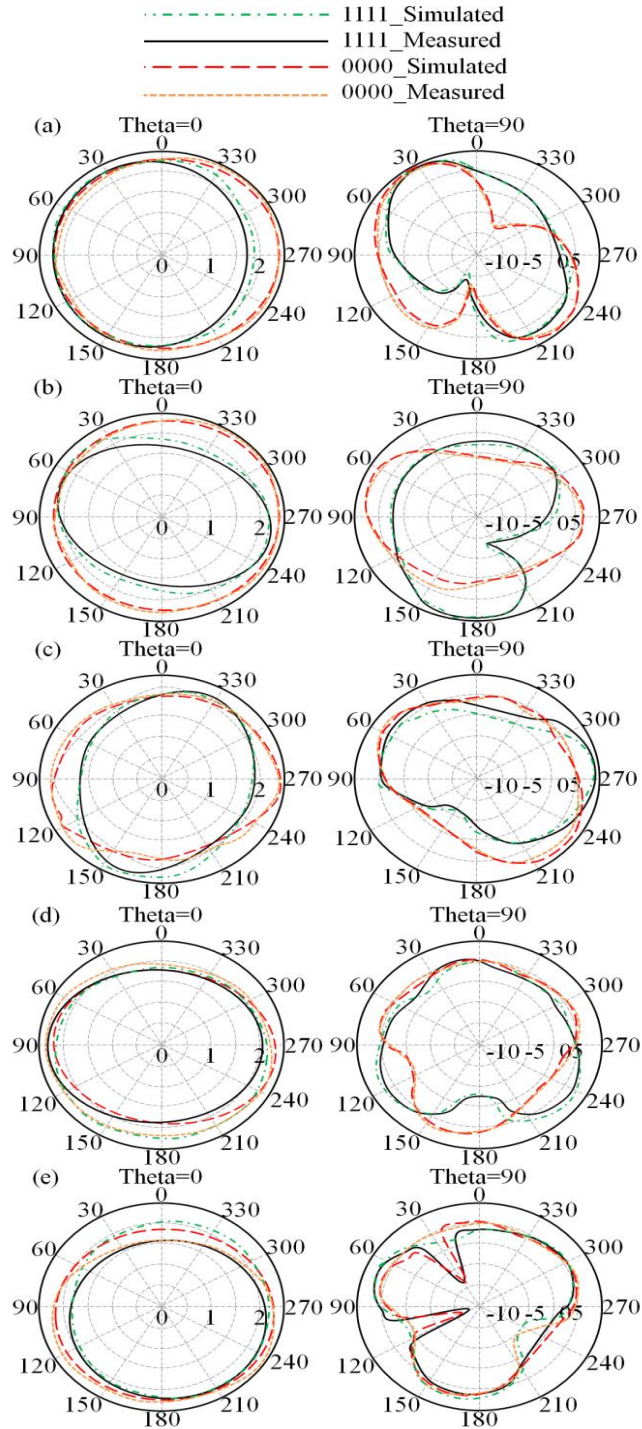
Figure 4.7. Measured antenna radiation patterns at different frequency bands: (a) 3.5GHz, (b) 4GHz, (c) 4.5GHz, (d) 5GHz, and (e) 5.5GHz.

The antenna performance in terms of correlation and diversity envelopes are evaluated experimentally to be compared with the simulated results in Figure 4.8. The achieved results show insignificant mutual coupling between the antenna elements to realize a maximum correlation factor below 1% with a high diversity of about 99% within the frequency band of interest. This is attributed to the effect of the

proposed MTM array reducing the mutual coupling significantly without effective separation distance. For further analysis, the authors applied a study to realize the MIMO antenna performance in terms of Envelop Correlation Coefficient (ECC), Diversity Gain (DG), Channel Capacity Loss (CCL), and Total active reflection coefficient (TARC) according to the process that was explained in [59]. As seen Figure 4.8, the proposed antenna system realizes a low value of ECC about 1% with high diversity of 10dB over the entire frequency band of interest. This is due to the introduction of the proposed filter design to achieve maximum effective mean gain MEG is about -5dBi; while, the maximum CCL value is about 0.06bps/Hz for the entire bandwidth. The measured TARC is found to be -15dB that show the capability of the proposed MTM inclusions to reduce the correlation factor between the antenna elements.
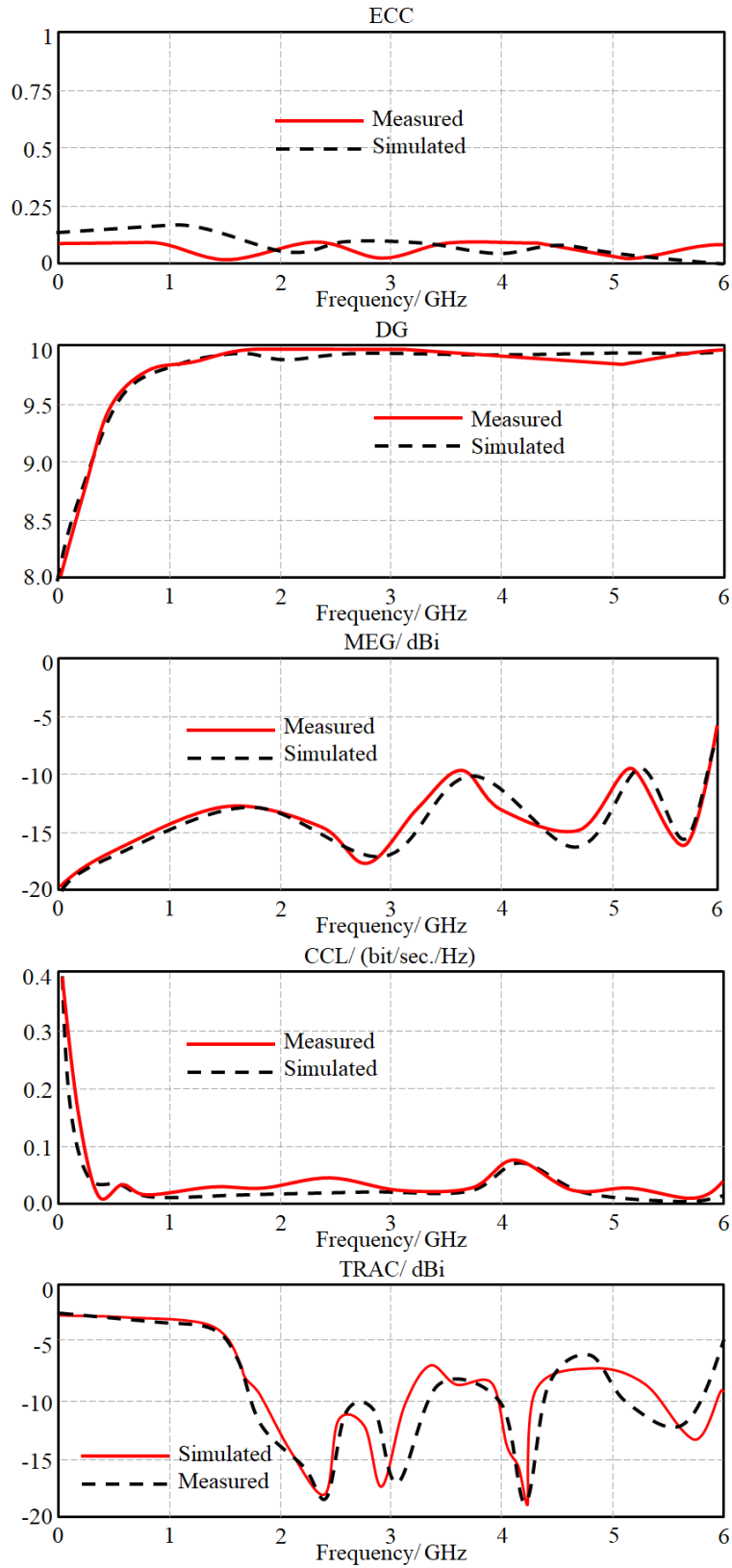
Figure 4.8. Antenna array performance in terms of: ECC, DG, MEG, CCL, and TRAC.

Now, to give a complete picture of the proposed antenna array performance, the authors evaluated the channel capacity (CC) and the bit error rate (BER) under the assumption of constructing an antenna array of 64×64 elements, theoretically only, for such assumption we tried to give an analytical validation of such antenna feasibility for massive MIMO systems. The calculated CC and BER are based on measured results from the antenna elements in terms of gain, bandwidth, and mutual coupling. The channel is affected by white Gaussian noise and the transmitted power is changed from -20 dBm to 20 dBm. In such circumstances, the maximum bit error rate is found to be about 0.15 the channel capacity is found to reach 2 Gbps. The obtained results are presented in Figure 4.9. In those calculations, a digital modulation schema based on Quadrature-Amplitude-Modulation (QAM) with an effective coverage is applied to indicate effects of that on BER. The considered BER in this case is defined as the number of acceptable errors at the prepared tolerates. In such case, typically, it is a number between 0.1 and 0.000001. This ratio is very affected by the Signal-to-Noise-Ratio (SNR) which is measured in dB. It is found from the results in Figure 4.9(a), a high SNR provide low BER, while, a low SNR would increase BER. It is obvious, frequency bands with higher gain are better than those with low gain to provide less chance of errors due to the noise effects. Later, the proposed antenna array CC spectra are evaluated and shown in Figure 4.9(b). It is found that the proposed antenna array CC capacity increases from 1.5Gbps to 4.5Gbps with frequency increase.
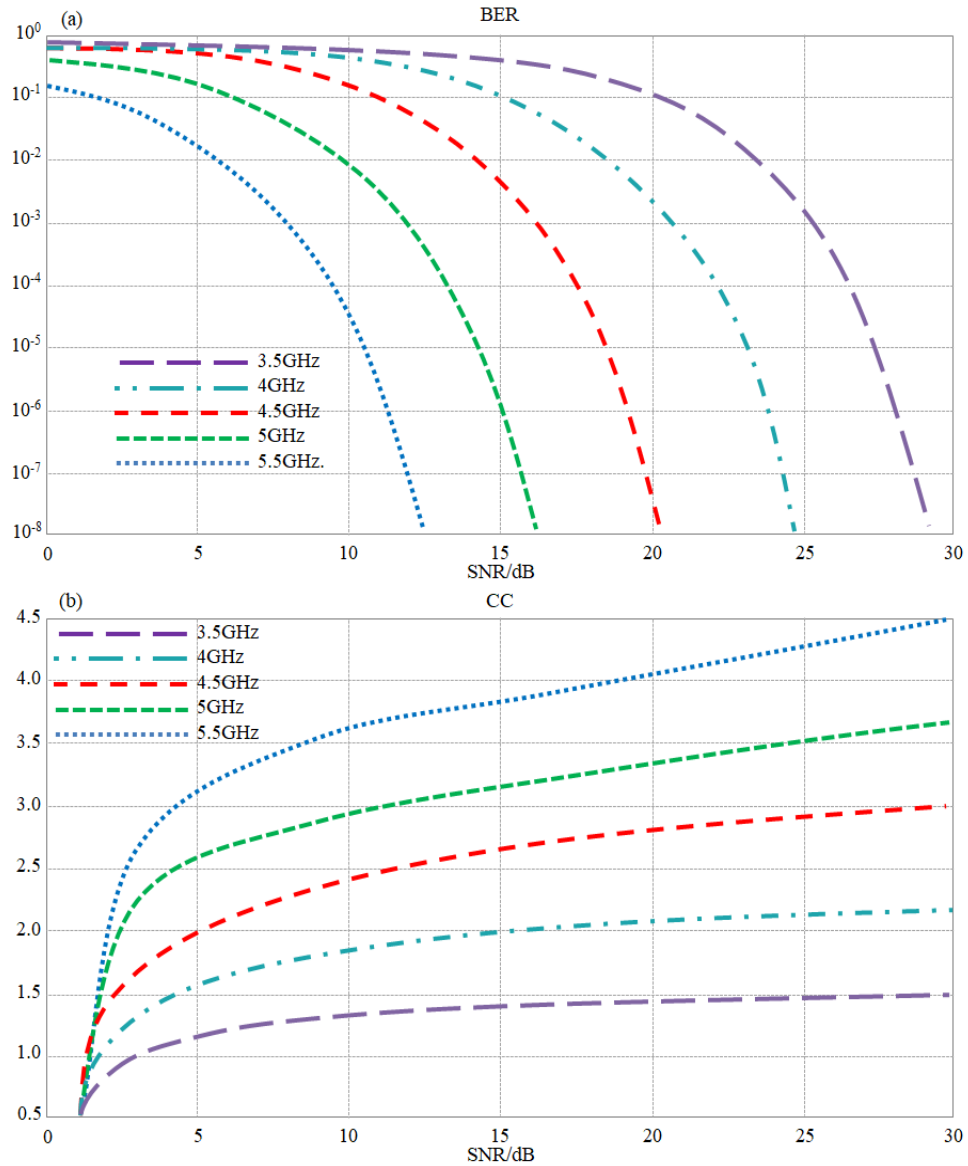
Figure 4.9. Channel performance calculations at different frequency bands: (a) BER and (b) CC.

Finally, the proposed antenna array performance is compared with respect to the published result in the literature in terms of antenna bandwidth, gain, size, re-configurability, and substrate type. It is observed that the proposed antenna array shows maximum size reduction with excellent configuration technique and performance in comparison with the previous one listed in table 4.2. Such a reconfiguration technique requires no biasing circuit or wiring system; while, the most of the old traditional techniques came up with high biasing complexity and wiring system.

76

Table 4.2. The proposed antenna performance in comparison to the published results.

Ref.	Size	Ports	BW/GHz	Gain/dBi	Coup/dB	DG	ECC	D	Rec.
[65]	130×100	8	5.1–5.9	2.1	-15	---	0.05	λ/1.9	Not
[52]	150×75	4	5.1–5.8	1.9	-14	9.8	0.06	λ/2	Not
[10]	136×60	8	5.1–5.9	1.9	-10	9.3	0.09	λ/2	Diode
[53]	150×75	12	4.8–5.1	2.6	-12	9.7	---	λ/2.1	Not
[2]	150×80	8	5.1–5.9	2.2	-10	9.2	0.11	λ/2.3	Not
[62]	133×133	4	3.3–5.8	1.1	-15	9.3	0.1	λ/2.1	Diode
[63]	160×70	2	5.6–5.6	12	-30	10	0.06	λ/1.4	Not
[66]	30×40	4	2-3, 3.4-3.9, 4.4-5.2	6.3	-20	10	0.01	λ/15	Not
This work	30×50	2	3-5.5	4.5	-20	10	0.01	0.08λ	LDR

4.4. A NOVEL MIMO ANTENNA DESIGN BASED DIRECT AI-EQUALIZATION FOR 5G-BAND SUB-6GHZ SIGNAL PROPAGATION

4.4.1. Antenna Performance Measurements

The MIMO antenna array we devised was manufactured using a standard chemical etching process. Subsequently, we evaluated the performance of the fabricated antennas by measuring their S-parameters and radiation patterns. Figure 4.10 compares the measured performance against the simulated results, revealing an excellent level of agreement between the two responses. Specifically, our proposed antenna exhibits optimal reflection coefficient performance, surpassing 15 dB at key frequencies of 2.3 GHz, 3.8 GHz, and 5.5 GHz. Correspondingly, the gains achieved at these frequencies are noteworthy, measuring at 5.2 dBi, 6.59 dBi, and 7.4 dBi, respectively. Additionally, the isolation between the antenna ports exceeds 20 dB, indicating robust signal separation capabilities. Moreover, our investigations into the radiation patterns under various PIN diode activation scenarios revealed a remarkable capability: a 90-degree alteration in radiation direction when all five PIN diodes transition from the 'OFF' to the 'ON' state. This dynamic functionality underscores the versatility and precision of our antenna design in adapting to diverse communication requirements.
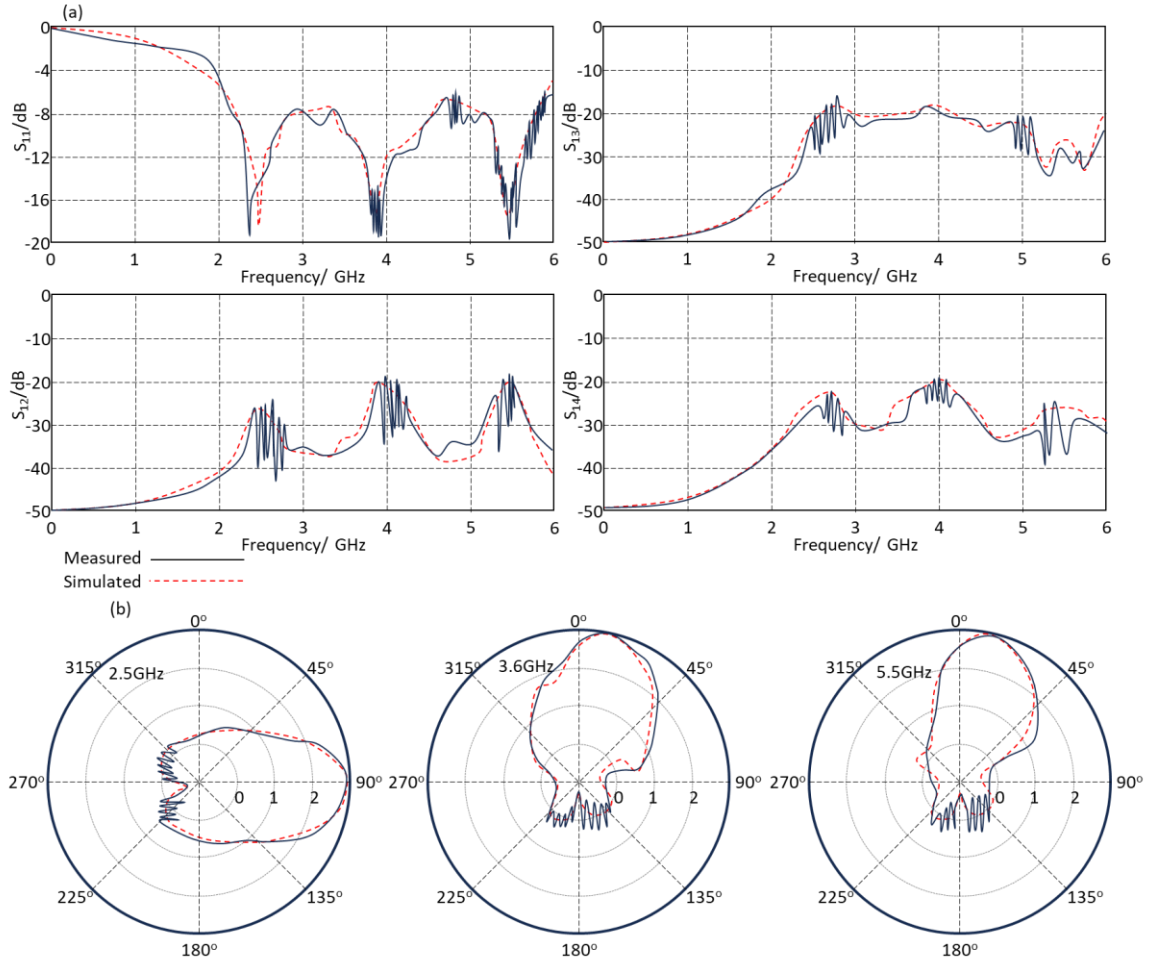
Figure 4.10. The measured antenna performance: (a) S-parameters, and (b) radiation patterns with different frequency resonance status: left 2.5GHz, middle 3.6GHz, right 5.5GHz.

4.4.2. Channel Performance

The performance evaluation of our proposed MIMO antenna array took place under real-world conditions in Baghdad, Iraq. The test location had three base-station towers, as shown in Figure 4.11. Tower 1 was approximately 19 m from the test location, while the other two towers were at distances of 49 m and 97 m. We collected empirical data specifically for the n79-band mobile network, comprising multiple cells, through driving tests conducted in urban and rural areas of the city. Figure 4.12(a) outlines the fundamental setup of our drive test scenario. In this setup, the mobile base-station tower, standing at a height of h_t, was positioned at a defined geographic latitude and longitude (φ_T, λ_T), transmitting with power P_t. Our MIMO antenna array was affixed atop a mast, situated within the base-station cell site at

coordinates (φ_i, λ_i), with a mast height of h_r. The diagonal distance (d_i) between the array and the base-station was computed, accounting for a 34 m difference in height between h_t and h_r. The base-station's coverage radius extended up to 600 m. To calculate the received power (P_r), we utilized Eqn. (1) [11].

$$P_r(d_i) = P_r(d_\circ) - 10\gamma \log\left(\frac{d_i}{d_\circ}\right) + X_\sigma \tag{1}$$

Here, $Pr(do)$ represents the measured power at $d_\circ$, a reference distance close to the base-station, ensuring di always exceeds $d_\circ$. The parameter γ denotes the rate of received power decay with distance, while $X\sigma$ accounts for fading, modeled as a zero-mean Gaussian- distributed random variable (in dB) with standard deviation σ. For our specific scenario, we determined γ at frequencies of 2.5 GHz, 3.6 GHz, and 5.5 GHz to be 2.2, 2.3, and 2.7, respectively, employing a regression analysis-based AI algorithm [67]. Figure 4.12(b) illustrates both the measured received power versus distance at the three spot frequencies and different Effective Received Power (ERP). Figure 4.13 shows how the PIN diode activation scenario affects the percentage of users as a function of distance from the array that receive signal strength greater than or equal to -70 dBm.

Figure 4.11. Testing location I Bagdad, Iraq
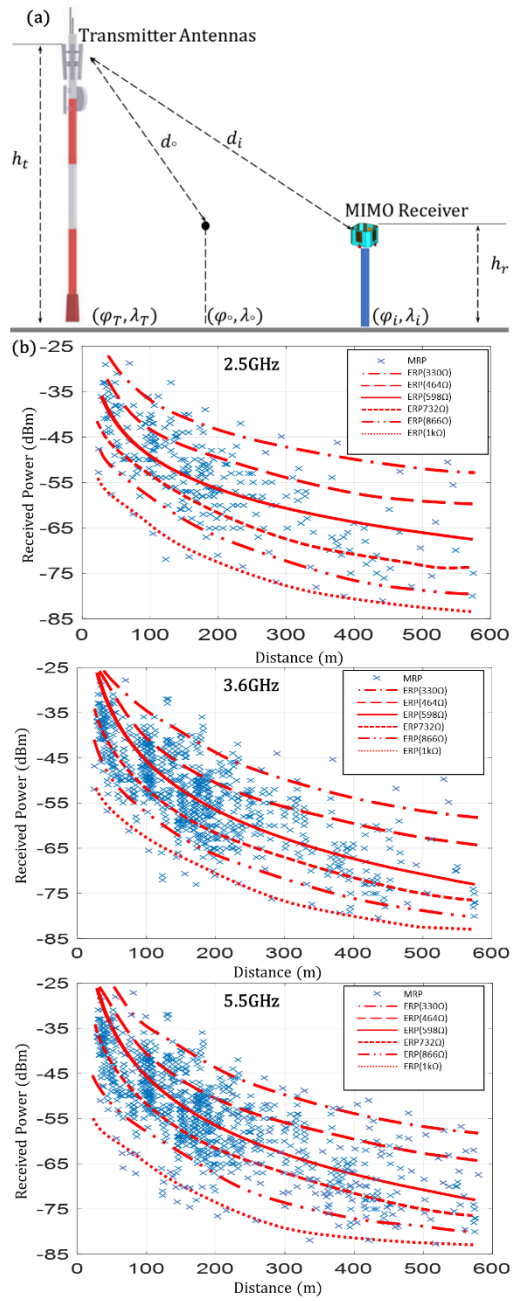
Figure 4.12. (a) Measuring setup, and (b) Regression estimation at the predefined spot frequencies.
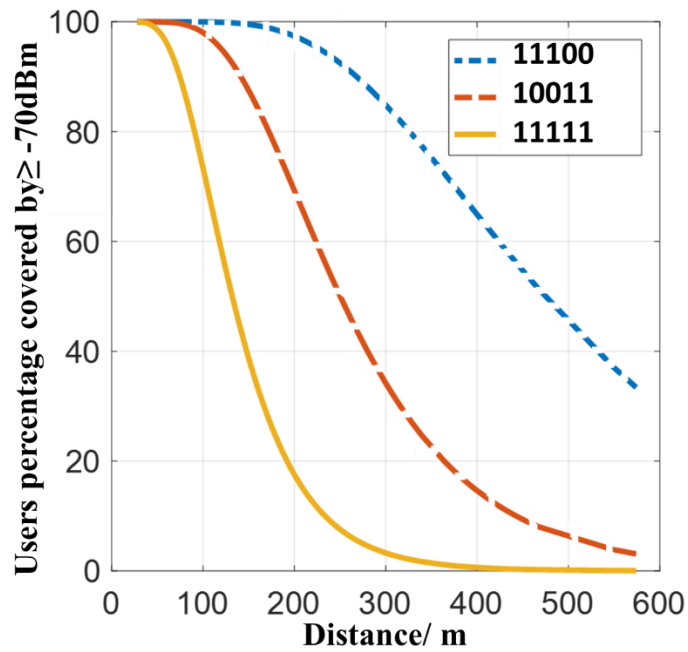
Figure 4.13. Percentage of users as a function of distance from the array that receive signal strength greater than or equal to - 70 dBm for different PIN diode switching combinations.

In Figure 4.14, we observe the effective channel diversity of the proposed MIMO antenna array, characterized by Gain Diversity (DG) and Envelope Correlation Coefficient (ECC) spectra. Notably, the array demonstrates a favorable combination of low ECC and high DG within the frequency band of interest, spanning from 2 GHz to 6 GHz. These findings position the proposed antenna as a highly promising candidate for various applications within 5G MIMO systems. Its ability to maintain low envelope correlation alongside high gain diversity suggests robust performance and suitability for diverse communication scenarios within this frequency range.
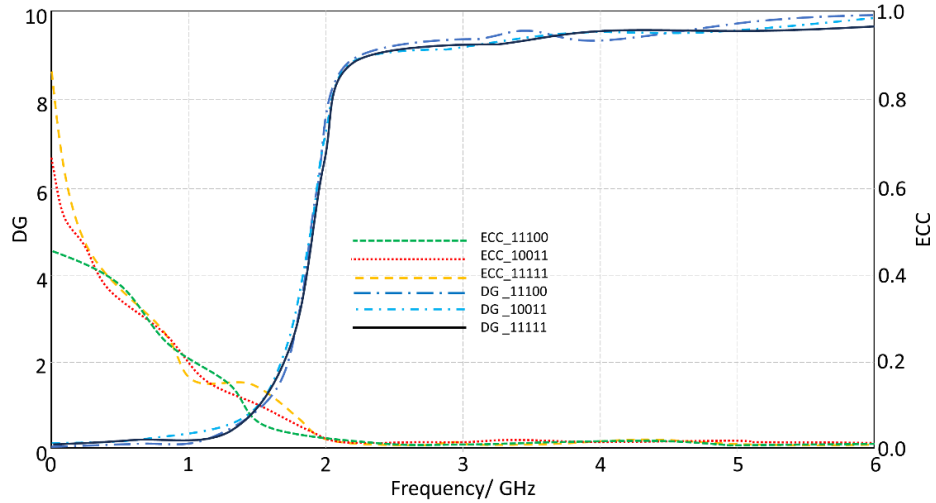
Figure 4.14. Gain diversity and envelope correlation coefficient of the proposed MIMO antenna array.

4.4.3. Impact of Solar Panel on the MIMO Antenna Array

In this work the solar panel was mounted on top of the proposed MIMO antenna array. The IV characteristics of the solar panel for load resistance (RL) change from 0 Ω to 1 MΩ as shown in Figure 4.15. It shows a sharp drop in output current for loads greater than 5 Ω.

The channel capacity represents the maximum rate at which information can be reliably transmitted over a communication channel. It is affected by various factors, including the distance from the base-station weather conditions. Channel capacity is given by

$$C = B. log_2 \left(1 + \frac{S}{N} \right) \qquad (2)$$

Where B is the channel bandwidth (Hz), S is the signal power (W) and N is noise power (W). Signal attenuation poses a significant challenge as it can diminish the signal-to-noise ratio (SNR) at the receiver, consequently affecting the quality of service. Additionally, the signal power received diminishes inversely with the distance between the transmitter and receiver, as described by the Friis transmission equation. To address this issue, an amplifier was employed to enhance the received signal power at the MIMO array, leveraging a solar panel for power supply. The efficiency of the solar panel is given by:

$$\eta = \left(\frac{P_0}{EA_c}\right) \times 100\% \qquad (3)$$

Where Po is the power output (W), E is incident solar radiation flux (W/m2) and Ac is area of panel (m^2).
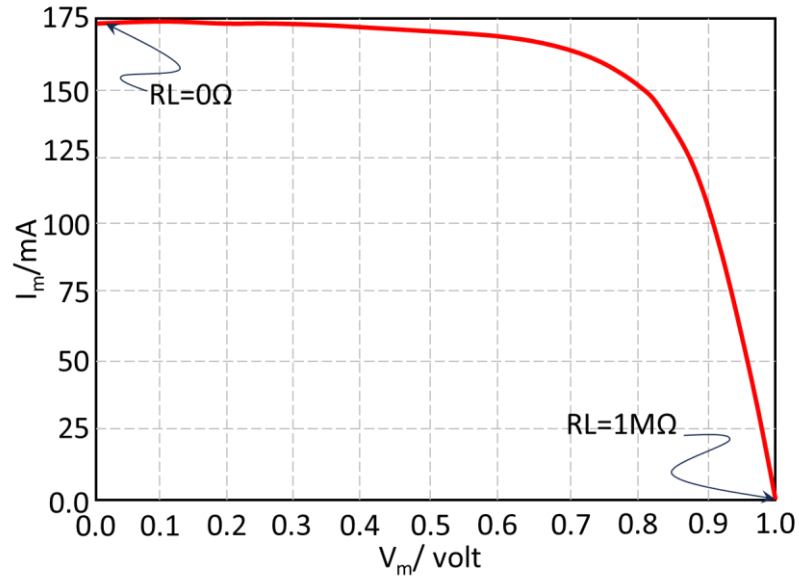
Figure 4.15. I-V characteristics measurements.

In Figure 4.16, the relationship between solar panel output voltage and channel capacity is depicted concerning the distance between the base-station and the MIMO antenna array. The empirical results clearly illustrate that as the voltage output to drive the amplifier increases, the achievable distance between the base-station and the array for a given channel capacity also increases.
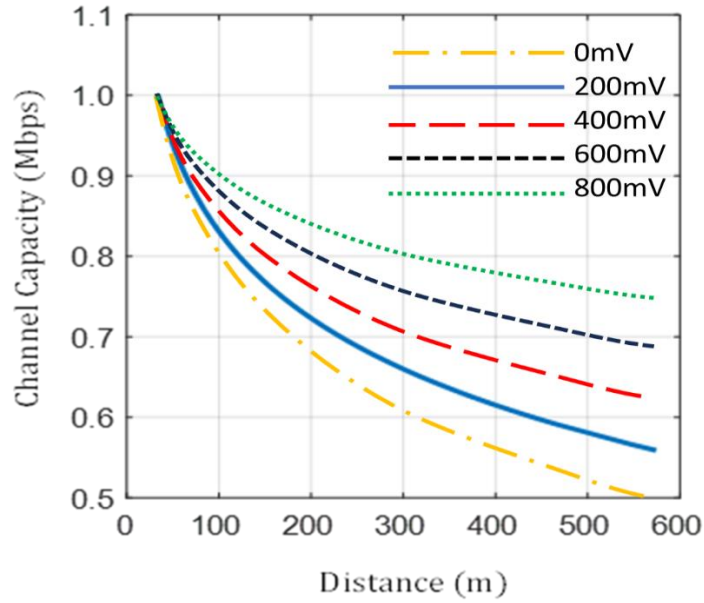
Figure 4.16. Channel capacity measurement using the proposed MIMO antenna array.

An AI equalizer was implemented alongside the proposed MIMO antenna array to enhance the channel capacity. Figure 4.17 illustrates the improvement in channel capacity as a function of the signal-to-noise ratio at frequencies of 2.5 GHz, 3.6 GHz, and 5.5 GHz. Generally, higher signal-to-noise ratios correspond to greater channel capacities. However, with AI equalization, a notable enhancement of 3 dB is achieved at a signal-to-noise ratio of 20 dBm.
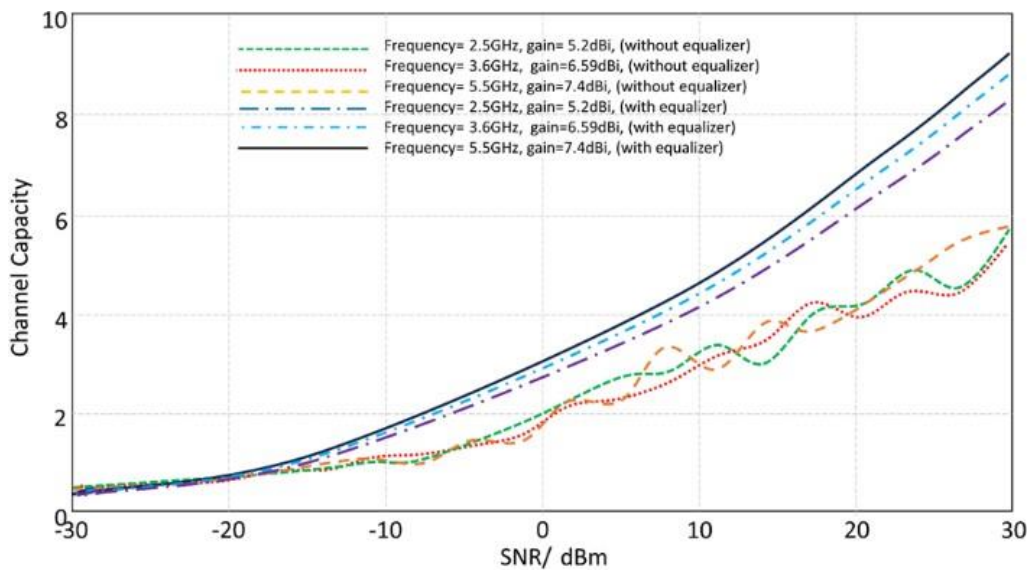
Figure 4.17. P_{amp} measurements, and (b) Channel capacity evaluation in Mbits/s.

The performance of the proposed antenna is evaluated by comparing it to similar antennas documented in the literature, as presented in Table 4.3. The comparison highlights significant advantages of the proposed antenna, notably its considerably smaller footprint and significantly higher gain, coupled with excellent coupling isolation.

Table 4.3. Comparison of the proposed design with respect to the literatures.

Ref.	Antenna size (mm^2)	Number of ports	Frequency bandwidth (GHz)	Maximum Gain (dBi)	Coupling isolation (dB)	DG (dB)	ECC
[67]	130×100	8	5.15-5.925	2.1	-15	---	0.05
[68]	150×75	4	5.15-5.85	1.9	-14	9.8	0.06
[69]	136×60	8	5.15-5925	1.9	-10	9.3	0.09
[70]	150×75	12	4.8-5.1	2.6	-12	9.7	---
[43]	150×80	8	5.147-5.95	2.2	-10	9.2	0.11
[71]	133×133	4	3.3-5.8	1.1	-15	9.3	0.10
[72]	160×70	2	5.6-5.67	12	-30	10	0.06
This work	38×38	4	2.3-2.6 3.6-4.1 5.3-5.6	7.4	-20	9.7	0.1

4.5. FABRICATION PROCESS AND MEASUREMENT SETUPS

Chemical etching, see Figure 4.18, is a sustainable method ECP Electronic volt that are usually involving the selective removal or cupper from a substrate to create the desired geometry. In this process, we invoked a design of our antennas from CST MS, next we adopted the desired material of the substrate to be the base of our design. A photoresistor is spread on top of the cupper layer. This layer acts as a mask to protect the desired geometry and remove the rest. After that, the board is exposed to Ultra vault (UV) light through a photo mask to harden the photoresist.

To develop the board, a solution based on $Na_2CO_3.H_2O$ is used to wash away the unwanted soft regions of the photoresistor. Later ferric chloride acid is used to dissolves the exposed cupper area leaving the wanted geometry. To remove the

hardened photoresistor, a solution based on strongcholic can be used for this purpose. Finally, the result geometry is the final design and can be soldered to the SMA port.
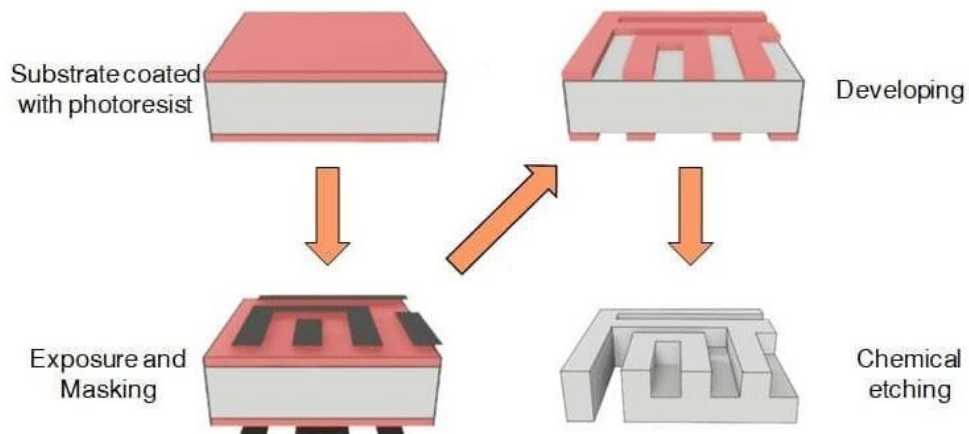
Figure 4.18. Basic Photochemical Etching Process [73].

Antenna measurements are essential requirements to characterize the gain, impedance, radiation patterns and bandwidth. For this, one of the main required facilities is the RF champers as seen in Figure 4.19. In these measurements the antenna under test is located in line with the site of a reference antenna, the distance between the antenna under test and the reference antenna must be in the far field to ensure minimum interference.

A mechanical rotary table is used to fit the antenna under test on the azimuth and zenith modes. A signal generator is connected to the antenna under test and a receiver of spectrum analyzer is connected to the standard antenna. Finally, the strength of the electromagnetic field in the magnitude and phase are recorded to plot the antenna radiation patterns.
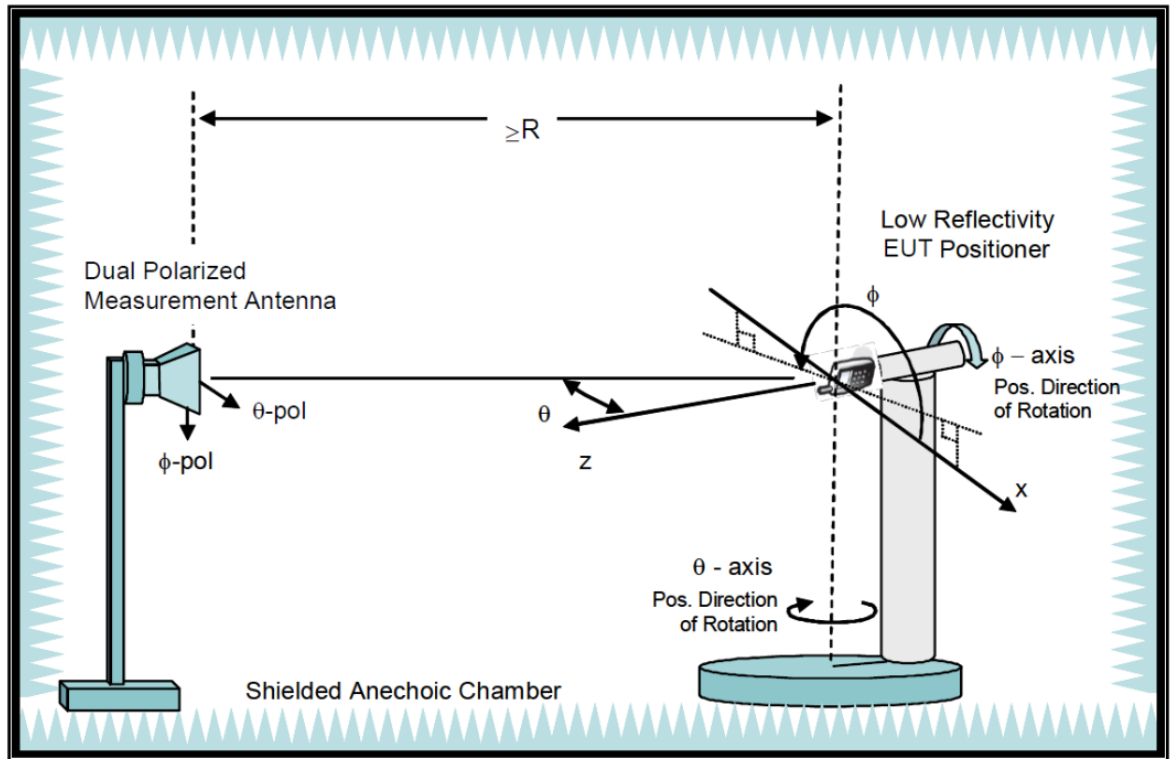
Figure 4.19. Antenna measurement setup inside RF champers [74].

PART 5

CONCLUSION

5.1 CONCLUSION

In conclusion, the researcher applied many designs. The first design consists of two antenna elements to achieve multi-frequency bands with an acceptable gain. The proposed antenna array was printed on an FR4 substrate with dimensions $33.6{\times}20{\times}1.6\text{mm}^3$. The obtained gain for this antenna array is found to be 2.34dBi and 2.6dBi at 3.45GHz and 5.5GHz, respectively. The suggested antenna array coupling was found to be about -15dB at maximum. Additionally, an antenna array was designed using origami technology that is shaped as Muhammad Al-Fatih Mosque. The antenna is printed on an FR-4 substrate to occupy a volume of $60{\times}136{\times}1$ mm^3. The antenna is designed to provide three main frequency bands around 2.5GHz, 3.5GHz, and 4.5GHz. The antenna elements were separated with five MTM unit cells to reach high size reduction and low mutual coupling. It was found that such bands show $|S_{11}|$ magnitude below -10dB with maximum coupling $|S_{12}|$ below -20dB. The antenna shows radiation patterns of omnidirectional around most of the frequency band of interest. On the other side, the researcher designed a minimized antenna array for MIMO applications. The proposed design parameters are optimized to fit the applications of Sub-6 5G. The proposed metamaterial is found to realize a significant mutual reduction of almost -20 dB over the frequency band from 3GHz up to 5.5GHz with a separation distance of 0.08λ. This antenna array is tested with different configuration scenarios by adding 4 LDR switches to each antenna element through the meander line and the ground plane. The researcher realizes such a reconfiguration process takes advantage of low complexity without including wiring or biasing systems. It is found that in the proposed antenna array when exposed to a massive MIMO environment, an acceptable BER and CC can be achieved after making the antenna size theoretically 64×64 elements. In the last design, the researcher integrated solar panels with a MIMO antenna array and high-

isolative walls offering a holistic approach to addressing the energy and performance requirements of modern 5G communication networks. It represents a significant step toward achieving a sustainable, efficient, and high-performing 5G infrastructure, which is crucial for meeting the ever-increasing demands of today's digital world while minimizing its environmental impact. This innovative solution offers a sustainable and environmentally friendly way to power base stations while simultaneously improving network capacity and signal quality, ultimately contributing to the advancement of 5G technology and reducing its environmental impact. Within the last design, three bands have been achieved at 2.5 GHz, 3.6 GHz and 5.5 GHz with S_{12}, S_{13} and S_{14} less than -20 dB over all interested bands. Finally, for validation, the researcher applies the antenna performance in terms of S-parameters and radiation patterns by CST and HFSS programs. The second and fourth designs have been fabricated, and experimental results have been compared with the simulated results.

5.2 FUTURE WORK

Reconfigurable MIMO metamaterial antenna arrays hold significant promise for advancing 5G and other modern wireless communication networks. The main potential future directions for research and development in this area are:

- ✓ Dynamic Beamforming and Beam Steering: Enhancing the re-configurability of antenna arrays to dynamically adjust beamforming and beam steering patterns in real-time. This can improve signal quality, coverage, and spectral efficiency in diverse environments, including urban, suburban, and indoor scenarios.
- ✓ Adaptive Frequency Reconfiguration: Developing techniques to dynamically reconfigure antenna arrays to operate across different frequency bands, including sub-6 GHz and millimeter-wave bands, to accommodate various 5G frequency requirements and support future frequency allocations.
- ✓ Intelligent Spectrum Sharing: Integrating intelligent spectrum sharing mechanisms with reconfigurable MIMO metamaterial antennas to enable

efficient utilization of scarce spectrum resources, including cognitive radio techniques and spectrum sensing algorithms.

✓ Cross-Layer Optimization: Investigating cross-layer optimization techniques to jointly optimize the physical layer characteristics of reconfigurable MIMO metamaterial antennas with higher-layer protocol parameters to improve overall network performance, including throughput, latency, and reliability.

✓ Energy Efficiency Enhancement: Developing energy-efficient reconfigurable MIMO metamaterial antennas by exploring advanced RF energy harvesting techniques, low-power circuit designs, and energy-aware antenna reconfiguration algorithms to prolong battery life and support sustainable wireless communication networks.

✓ Self-Healing and Fault Tolerance: Designing self-healing mechanisms for reconfigurable MIMO metamaterial antenna arrays to autonomously detect and mitigate faults or failures caused by environmental conditions, hardware defects, or malicious attacks, ensuring robust and reliable operation in dynamic wireless environments.

✓ Integration with AI and Machine Learning: Exploring the integration of artificial intelligence (AI) and machine learning (ML) techniques for autonomous optimization, adaptation, and self-learning in reconfigurable MIMO metamaterial antenna arrays, enabling adaptive beamforming, interference cancellation, and spectrum management.

✓ Compact and Low-Cost Designs: Researching novel fabrication techniques and materials to develop compact, low-cost, and scalable reconfigurable MIMO metamaterial antenna arrays suitable for mass deployment in 5G infrastructure, small cell networks, Internet of Things (IoT) devices, and wearable electronics.

✓ Security and Privacy Enhancements: Investigating security and privacy challenges associated with reconfigurable MIMO metamaterial antenna arrays, including authentication, encryption, and secure key exchange protocols, to protect against unauthorized access, eavesdropping, and cyber-attacks.

✓ Standardization and Commercialization: Contributing to standardization efforts within international standards organizations (e.g., IEEE, 3GPP) to

define interoperable interfaces, protocols, and performance metrics for reconfigurable MIMO metamaterial antenna arrays, facilitating their commercialization and widespread adoption in 5G and beyond.

5.3 RECOMMENDATIONS

To conduct research on reconfigurable MIMO metamaterial antenna arrays for 5G and modern wireless communication networks, there are some specific recommendations:

✓ Performance Evaluation in Real-world Environments: Conduct comprehensive field trials to evaluate the performance of reconfigurable MIMO metamaterial antenna arrays in real-world environments. Measure key performance metrics such as coverage, capacity, throughput, and latency in different deployment scenarios (urban, suburban, indoor) to assess their practical utility and effectiveness.

✓ Dynamic Beamforming Algorithms: Develop and evaluate novel algorithms for dynamic beamforming and beam steering in reconfigurable MIMO metamaterial antenna arrays. Investigate optimization techniques that can adaptively adjust antenna parameters based on changing channel conditions, user mobility, and network load to optimize signal quality and coverage.

✓ Frequency Reconfiguration Techniques: Research techniques for dynamic frequency reconfiguration of metamaterial antenna arrays to support multi-band and multi-standard operation in 5G networks. Explore methods for seamless transition between different frequency bands and polarization states to enhance spectrum utilization and compatibility with diverse communication standards.

✓ Machine Learning-Based Optimization: Explore the application of machine learning algorithms for optimizing the configuration and operation of reconfigurable MIMO metamaterial antenna arrays. Investigate how reinforcement learning, deep learning, and other ML techniques can be used to autonomously adapt antenna parameters to maximize network performance and efficiency.

- ✓ Energy-Efficient Designs: Investigate energy-efficient design principles for reconfigurable MIMO metamaterial antenna arrays, including low-power circuitry, energy harvesting, and sleep mode strategies. Evaluate the trade-offs between energy consumption, performance, and re-configurability to design antennas suitable for battery-operated devices and energy-constrained environments.

- ✓ Interference Mitigation Techniques: Develop interference mitigation techniques tailored for reconfigurable MIMO metamaterial antenna arrays to mitigate co-channel interference, adjacent channel interference, and multi-user interference. Investigate advanced signal processing algorithms, such as interference cancellation and precoding, to improve spectral efficiency and network capacity.

- ✓ Security and Privacy Considerations: Investigate security and privacy challenges associated with reconfigurable MIMO metamaterial antenna arrays, including potential vulnerabilities to jamming attacks, eavesdropping, and signal interception. Develop cryptographic techniques, authentication protocols, and intrusion detection mechanisms to enhance the security of wireless communication systems.

- ✓ Standardization and Prototyping: Contribute to standardization efforts by actively participating in relevant standardization bodies (e.g., IEEE, 3GPP) to help define interoperable interfaces, protocols, and performance benchmarks for reconfigurable MIMO metamaterial antenna arrays. Build prototype systems and conduct interoperability testing to validate compliance with emerging standards and facilitate commercialization.

- ✓ User-Centric Design and Optimization: Adopt a user-centric approach to design and optimize reconfigurable MIMO metamaterial antenna arrays, considering factors such as user experience, mobility patterns, and quality of service requirements. Conduct user studies and feedback surveys to understand user preferences and incorporate them into the antenna design process.

- ✓ Cross-Disciplinary Collaboration: Foster collaboration between researchers from diverse disciplines, including electrical engineering, materials science, signal processing, and communication theory, to address the

multidimensional challenges associated with reconfigurable MIMO metamaterial antenna arrays. Explore interdisciplinary research avenues to leverage insights and expertise from different fields and drive innovation in wireless communications.

REFERENCES

1. Z. A. A. Hassain, A. R. Azeez, M. M. Ali, and T. A. Elwi, "A modified compact bi-directional UWB tapered slot antenna with double band notch characteristics," Adv. Electromagn., vol. 8, no. 4, pp. 74–79, 2019.

2. Z. Al-Dulaimi, T. A. Elwi, and D. C. Atilla, "Design of a meander line monopole antenna array based hilbert-shaped reject band structure for MIMO applications," IETE J. Res., vol. 68, no. 4, pp. 2353–2362, 2022.

3. T. A. Elwi and A. M. Al-Saegh, "Further realization of a flexible metamaterial-based antenna on indium nickel oxide polymerized palm fiber substrates for RF energy harvesting," Int. J. Microw. Wirel. Technol., vol. 13, no. 1, pp. 67–75, 2021.

4. M. A. Jawad, M. A. Elwi, E. Y. Salih, T. A. Elwi, and Z. Abbas, "Monitoring the dielectric properties and propagation conditions of mortar for modern wireless mobile networks," Prog. Electromagn. Res. Lett., vol. 89, pp. 91–97, 2020.

5. Y. Al Naiemy, T. A. Elwi, and L. Nagy, "An end fire printed monopole antenna based on electromagnetic band gap structure," Automatika, vol. 61, no. 3, pp. 482–495, 2020.

6. [6] T. A. Elwi and S. G. Abdulqader, "Further investigation on solant–rectenna-based flexible Hilbert-shaped metamaterials," IET Nanodielectrics, vol. 3, no. 3, pp. 88–93, 2020.

7. A. I. Imran, T. A. Elwi, and A. J. Salim, "On the distortionless of uwb wearable hilbert-shaped metamaterial antenna for low energy applications," Prog. Electromagn. Res. M, vol. 101, pp. 219–239, 2021.

8. H. M. AlSabbagh, T. A. Elwi, Y. Al-Naiemy, and H. M. Al-Rizzo, "A compact triple-band metamaterial-inspired antenna for wearable applications," Microw. Opt. Technol. Lett., vol. 62, no. 2, pp. 763–777, 2020.

9. T. A. Elwi, D. A. Jassim, and H. H. Mohammed, "Novel miniaturized folded UWB microstrip antenna-based metamaterial for RF energy harvesting," Int. J. Commun. Syst., vol. 33, no. 6, p. e4305, 2020.

10. Y. Alnaiemy, T. A. Elwi, and L. Nagy, "Mutual coupling reduction in patch antenna array based on EBG structure for MIMO applications," Period. Polytech. Electr. Eng. Comput. Sci., vol. 63, no. 4, pp. 332–342, 2019.

11. S. M. Obaid, T. Elwi, and M. Ilyas, "Fractal Minkowski-shaped resonator for noninvasive biomedical measurements: Blood glucose test," 2021.

12. T. A. Elwi, "A further realization of a flexible metamaterial-based antenna on nickel oxide polymerized palm fiber substrates for RF energy harvesting," Wirel. Pers. Commun., vol. 115, no. 2, pp. 1623–1634, 2020.

13. T. A. Elwi, "Remotely controlled reconfigurable antenna for modern 5G networks applications," Microw. Opt. Technol. Lett., vol. 63, no. 8, pp. 2018–2023, 2021.

14. A. M. Al-Saegh and T. A. Elwi, "Direct extraction of rain-induced impairments on satellite communication channel in subtropical climate at K and Ka bands," Telecommun. Syst., vol. 74, no. 1, pp. 15–25, 2020.

15. T. A. Elwi, A. J. Salim, A. N. Alkhafaji, J. K. Ali, and A. S. A. Jalal, "Complex constitutive characterizations of materials in the X-band using a non-destructive technique," in Special Issue of the 8th International Advances in Applied Physics and Materials Science Congress (APMAS 2018), ACTA Physica Polonica A, 2019, pp. 567–570.

16. T. A. Elwi, Z. A. Abdul Hassain, and O. A. Tawfeeq, "Hilbert metamaterial printed antenna based on organic substrates for energy harvesting," IET Microwaves, Antennas Propag., vol. 13, no. 12, pp. 2185–2192, 2019.

17. H. S. Ahmed and T. A. Elwi, "On the design of a reject band filter for antennas mutual coupling reduction," Int. J. RF Microw. Comput. Eng., vol. 29, no. 8, p. e21797, 2019.

18. G. M. Hatem, A. J. Salim, T. A. Elwi, H. T. Ziboon, J. H. Majeed, and J. K. Ali, "Wunderlich curve fractal dipole antenna for dual-band wearable RFID applications," J. Eng. Appl. Sci., vol. 14, no. 4, pp. 1093–1099, 2019, doi: 10.3923/jeasci.2019.1093.1099.

19. B. I. Halim and A. Boutejdar, "Design and improvement a novel microstrip antenna using array of composite right/left handed transmission line (CRLH-TL) technique for multiband applications," in 2019 IEEE International Symposium on Phased Array System & Technology (PAST), IEEE, 2019, pp. 1–5.

20. S. Xie, J. Li, G. Deng, J. Feng, and S. Xiao, "A wide-angle scanning leaky-wave antenna based on a composite right/left-handed transmission line," Appl. Sci., vol. 10, no. 6, p. 1927, 2020.

21. M. Alibakhshikenari et al., "Bandwidth and gain enhancement of composite right left handed metamaterial transmission line planar antenna employing a non foster impedance matching circuit board," Sci. Rep., vol. 11, no. 1, p. 7472, 2021.

22. M. Comisso and R. Vescovo, "Fast 3D pattern synthesis with polarization and dynamic range ratio control for conformal antenna arrays," Int. J. Antennas Propag., vol. 2014, 2014.

23. M. H. Dahri et al., "A novel asymmetric patch reflectarray antenna with ground ring slots for 5G communication systems," Electronics, vol. 9, no. 9, p. 1450, 2020.

24.   P. Mei, S. Zhang, and G. F. Pedersen, "A low-cost, high-efficiency and full-metal reflectarray antenna with mechanically 2-D beam-steerable capabilities for 5G applications," IEEE Trans. Antennas Propag., vol. 68, no. 10, pp. 6997–7006, 2020.

25.   S. Kumar, A. S. Dixit, R. R. Malekar, H. D. Raut, and L. K. Shevada, "Fifth generation antennas: A comprehensive review of design and performance enhancement techniques," IEEE Access, vol. 8, pp. 163568–163593, 2020.

26.   N. Ojaroudi Parchin, H. Jahanbakhsh Basherlou, Y. I. A. Al-Yasir, A. M. Abdulkhaleq, and R. A. Abd-Alhameed, "Reconfigurable antennas: Switching techniques—A survey," Electronics, vol. 9, no. 2, p. 336, 2020.

27.   H. T. Chattha, "4-port 2-element MIMO antenna for 5G portable applications," IEEE Access, vol. 7, pp. 96516–96520, 2019.

28.   K. R. Jha, Z. A. P. Jibran, C. Singh, and S. K. Sharma, "4-port MIMO antenna using common radiator on a flexible substrate for sub-1GHz, sub-6GHz 5G NR, and Wi-Fi 6 applications," IEEE Open J. Antennas Propag., vol. 2, pp. 689–701, 2021.

29.   A. Biswas and V. R. Gupta, "Design and development of low profile MIMO antenna for 5G new radio smartphone applications," Wirel. Pers. Commun., vol. 111, no. 3, pp. 1695–1706, 2020.

30.   J. Kulkarni, A. G. Alharbi, A. Desai, C.-Y.-D. Sim, and A. Poddar, "Design and analysis of wideband flexible self-isolating MIMO antennas for sub-6 GHz 5G and WLAN smartphone terminals," Electronics, vol. 10, no. 23, p. 3031, 2021.

31.   L. Sun, H. Feng, Y. Li, and Z. Zhang, "Compact 5G MIMO mobile phone antennas with tightly arranged orthogonal-mode pairs," IEEE Trans. Antennas Propag., vol. 66, no. 11, pp. 6364–6369, 2018.

32.   R. Ramanujam and M. Perumalsamy, "An ultra-thin flexible four port MIMO antenna for WBAN communications," Microw. Opt. Technol. Lett., vol. 64, no. 7, pp. 1245–1251, 2022.

33.   K. N. Paracha, S. K. A. Rahim, H. T. Chattha, S. S. Aljaafreh, S. ur Rehman, and Y. C. Lo, "Low-cost printed flexible antenna by using an office printer for conformal applications," Int. J. Antennas Propag., vol. 2018, pp. 1–7, 2018.

34.   M. A. Abdelghany, A. A. Ibrahim, H. A. Mohamed, and E. Tammam, "Compact Sub-6 GHz Four-Element Flexible Antenna for 5G Applications," Electronics, vol. 13, no. 3, p. 537, 2024.

35.   M. M. Ismail, T. A. Elwi, and A. J. Salim, "Antenna Gain-Bandwidth Enhancements Using CRLH Hilbert Fractal-based Structure," Eng. Technol. J., vol. 41, no. 2, pp. 397–406, 2023.

36. [36] N. Kaur, J. Kaur, and S. Sharma, "MIMO antenna system with self isolation characteristics for GSM and sub-6 GHz 5G applications," Wirel. Pers. Commun., vol. 120, pp. 989–1002, 2021.

37. [37] S. Lee et al., "Design and Characterization of VHF Band Small Antenna Using CRLH Transmission Line and Non-Foster Matching Circuit," Appl. Sci., vol. 10, no. 18, p. 6366, 2020.

38. B. S. Bashar, M. M. Ismail, and A.-S. M. Talib, "Optimize cellular network performance using phased arrays," in IOP Conference Series: Materials Science and Engineering, IOP Publishing, 2020, p. 12128.

39. A. Ghaffar, W. A. Awan, N. Hussain, S. Ahmad, and X. J. Li, "A compact dual-band flexible antenna for applications at 900 and 2450 mhz," Prog. Electromagn. Res. Lett., vol. 99, no. April 2022, pp. 83–91, 2021, doi: 10.2528/PIERL21060601.

40. W. A. Awan et al., "Design and realization of a frequency reconfigurable antenna with wide, dual, and single-band operations for compact sized wireless applications," Electronics, vol. 10, no. 11, p. 1321, 2021.

41. M. Alibakhshikenari et al., "A comprehensive survey of 'metamaterial transmission-line based antennas: Design, challenges, and applications,'" Ieee Access, vol. 8, pp. 144778–144808, 2020.

42. A. A. Althuwayb, "MTM-and SIW-inspired bowtie antenna loaded with AMC for 5G mm-wave applications," Int. J. Antennas Propag., vol. 2021, pp. 1–7, 2021.

43. T. A. Elwi, "A miniaturized folded antenna array for MIMO applications," Wirel. Pers. Commun., vol. 98, pp. 1871–1883, 2018.

44. W. A. Awan, A. Ghaffar, N. Hussain, and X. J. Li, "CPW-fed dual-band antenna for 2.45/5.8 GHz applications," in 2019 8th Asia-Pacific Conference on Antennas and Propagation (APCAP), IEEE, 2019, pp. 246–247.

45. M. Bayat, H. Shahi, and J. Mazloum, "Dual-band balanced-to-single-ended crossover based on composite right-and left-handed transmission lines," Electron. Lett., vol. 56, no. 8, pp. 380–382, 2020.

46. K. Song, F. Zhang, M. Fan, Y. Zhu, and Y. Fan, "Compact broadband bandstop filter based on composite right/left handed transmission line," Electromagnetics, vol. 37, no. 4, pp. 196–202, 2017.

47. M. Haleem and T. A. Elwi, "Circularly polarized metamaterial patch antenna circuitry for modern applications," Int. J. Emerg. Technol. Adv. Eng., vol. 12, no. 12, 2022.

48. [48] E. S. AHMED, "Design of CPW Fed Two Layered Rectangular Dielectric Resonator Antenna for 5G Mobile Communications," J. Duhok Univ., vol. 23, no. 2, pp. 754–766, 2020.

49. Y. S. Mezaal, S. F. Abdulkareem, and J. K. Ali, "A dual-band printed slot antenna for WiMAX and metrological wireless applications," Adv. Electromagn., vol. 7, no. 3, pp. 75–81, 2018.

50. S. H. Ghadeer et al., "An innovative fractal monopole MIMO antenna for modern 5G applications," AEU-International J. Electron. Commun., vol. 159, p. 154480, 2023.

51. H. H. Al-khaylani, T. A. Elwi, and A. A. Ibrahim, "Optically remote-controlled miniaturized 3D reconfigurable CRLH-printed MIMO antenna array for 5G applications," Microw. Opt. Technol. Lett., vol. 65, no. 2, pp. 603–610, 2023.

52. Z. Al-Dulaimi, T. A. Elwi, D. C. Atilla, and C. Aydin, "Design of fractal based monopole antenna array with ultra-mutual coupling reduction for MIMO applications," in 2018 18th Mediterranean Microwave Symposium (MMS), IEEE, 2018, pp. 39–42.

53. K. C. Ravi, J. Kumar, T. A. Elwi, and M. M. Ali, "Compact MIMO antenna for 5G Applications," in 2022 IEEE ANDESCON, IEEE, 2022, pp. 1–6.

54. A. P. S. Sengar and A. Dahiya, "Reconfigurable smart antenna for wireless communication devices," Int. J. Eng. Technol., vol. 7, no. 4, pp. 271–272, 2018.

55. S. Ahmad et al., "A jug-shaped CPW-fed ultra-wideband printed monopole antenna for wireless communications networks," Appl. Sci., vol. 12, no. 2, p. 821, 2022.

56. S. Mohandoss, R. R. Thipparaju, B. N. B. Reddy, S. K. Palaniswamy, and P. Marudappa, "Fractal based ultra-wideband antenna development for wireless personal area communication applications," AEU-International J. Electron. Commun., vol. 93, pp. 95–102, 2018.

57. D. N. Elsheakh and E. A. Abdallah, "Ultra-Wideband Log Periodic Dipole Antenna (LPDA) for Wireless Communication Applications," J. Electromagn. Anal. Appl., vol. 10, no. 06, p. 119, 2018.

58. Y. Faouri et al., "Compact super wideband frequency diversity hexagonal shaped monopole antenna with switchable rejection band," IEEE Access, vol. 10, pp. 42321–42333, 2022.

59. T. A. Elwi, Z. Abbas, M. Noori, Y. Al-Naiemy, E. Y. Salih, and M. M. Hamed, "Conformal antenna array for MIMO applications," J. Electromagn. Anal. Appl., vol. 6, no. 04, p. 43, 2014.

60.   N. Sharma and S. S. Bhatia, "Split ring resonator based multiband hybrid fractal antennas for wireless applications," AEU-International J. Electron. Commun., vol. 93, pp. 39–52, 2018.

61.   S. Manafi and H. Deng, "Design of a small modified Minkowski fractal antenna for passive deep brain stimulation implants," Int. J. Antennas Propag., vol. 2014, 2014.

62.   S. H. Ghadeer, S. K. A. Rahim, and T. As. P. I. 3D M. A. A. for M. C. S. Elwi, "Solar Panel Integrated 3D MIMO Antenna Array for Modern Communication Systems," in 2021 International Conference on Advanced Computer Applications (ACA), IEEE, 2021, pp. 112–115.

63.   H. S. Ahmed, Z. S. Ahmed, R. S. Zamel, and T. A. Elwi, "Compact MIMO Antenna Array for 5G Applications based Novel Hayder-Koch Fractal Geometry," in 2022 International Telecommunications Conference (ITC-Egypt), IEEE, 2022, pp. 1–5.

64.   H. S. Najim, M. F. Mosleh, and R. A. Abd-Alhameed, "Design a MIMO printed dipole antenna for 5G sub-band applications," Indones. J. Electr. Eng. Comput. Sci., vol. 27, no. 3, pp. 1649–1660, 2022, doi: 10.11591/ijeecs.v27.i3.pp1649-1660.

65.   M. M. Ismail, T. A. Elwi, and A. J. Salim, "A miniaturized printed circuit CRLH antenna-based Hilbert metamaterial array," J. Commun. Softw. Syst., vol. 18, no. 3, pp. 236–243, 2022.

66.   A. R. Al-tameemi et al., "A Novel Conformal MIMO Antenna Array based a Cylindrical Configuration for 5G Applications," in 2022 9th International Conference on Electrical Engineering, Computer Science and Informatics (EECSI), IEEE, 2022, pp. 446–451.

67.   T. A. Elwi, "Novel UWB printed metamaterial microstrip antenna based organic substrates for RF-energy harvesting applications," AEU-International J. Electron. Commun., vol. 101, pp. 44–53, 2019.

68.   T. A. Elwi, "A slotted lotus shaped microstrip antenna based an EBG structure," J. Mater. Sci. Eng., vol. 7, no. 2, pp. 1–23, 2018.

69.   T. A. Elwi, "A further investigation on the performance of the broadside coupled rectangular split ring resonators," Prog. Electromagn. Res. Lett., vol. 34, pp. 1–8, 2012.

70.   S. Y. A. Fatah et al., "Design of compact flexible UWB antenna using different substrate materials for WBAN applications," in 2023 Photonics & Electromagnetics Research Symposium (PIERS), IEEE, 2023, pp. 373–378.

71.	A. I. Imran and T. A. Elwi, "A cylindrical wideband slotted patch antenna loaded with frequency selective surface for MRI applications," Eng. Sci. Technol. an Int. J., vol. 20, no. 3, pp. 990–996, 2017.

72.	T. A. Elwi, "Electromagnetic band gap structures based on ultra wideband microstrip antenna," Microw. Opt. Technol. Lett., vol. 59, no. 4, pp. 827–834, 2017.

73.	Qing, X., Chen, Z.N. (2015). Antenna Measurement Setups: Introduction. In: Chen, Z. (eds) Handbook of Antenna Technologies. Springer, Singapore. https://doi.org/10.1007/978-981-4560-75-7_68-1.

74.	N. W. Street, "Certification Program Test Plan," 2019, [Online]. Available: http://www.ctia.org/certification

RESUME

Humam Neamah Hussein HUSSEIN in bachelor degree, he completed an undergraduate program in computer engineering from ALHADBAA University (Nineveh-Iraq) in 2015. and completed his master's degree in computer and electrical engineering from ALTINBAS University (Istanbul-Turkey) in 2019. He completed his PhD at KARABUK University in 2024.